by Havva TANER

A thesis submitted to the Faculty of
Graduate Studies and Research in partial
fulfillment of the requirements for the
degree of Master of Science

Department of Geological Sciences
McGill University, Montreal

© Havva TANER, 1989

Havva TANER

HYDROTHERMAL MO-BI MINERALIZATION IN THE CADILLAC AND PREISSAC DEPOSITS, QUEBEC

ABSTRACT

Mo-Pi mineralization subvertical occurs in subhorizontal quartz-K-feldspar-muscovite veins surrounded by early albitic and later K-feldspar alteration haloes leucoadamellite of the Archean Preissac batholith, Abitibi region, Quebec. Fluid inclusions were studied to investigate physicochemical factors responsible for the mineralization. The veins contain four main types of fluid inclusions: aqueous L, and LV inclusions, aqueous-carbonic LLV inclusions, carbonic LV inclusions, and solid-bearing aqueous L and LV inclusions. The carbonic phase in carbonic inclusions melts between -56.6°C and -58°C indicating that it consists largely of CO,.

Aqueous liquid-vapour inclusions display 3 distinct salinity groupings with modes at 5, 18, and 26 wt % NaCl equivalent, respectively. All three aqueous inclusion types and the aqueous phase in carbonic inclusions show low initial melting temperatures (as low as -70°C) indicating the presence of salts other than NaCl. Leachate analyses show that the bulk fluid contained varying quantities of Na, K, Ca, Mg, Li, Ni and Cl. The most abundant components are Na, Ca and Cl.

The following trapped phases or daughter minerals were identified by SEM-EDS analysis: calcite $(CaCO_3)$, hydrophillite $(CaCl_2)$, muscovite, millerite (NiS), barite $(BaSO_4)$ and halite (NaCl).

Most aqueous inclusions homogenize to liquid at temperatures between 250°C and 400°C with a mode at 375°C. Carbonic inclusions homogenize to liquid or vapour between 210°C and 330°C. Halite-bearing aqueous inclusions homogenize by halite disappearance at a temperature of approximately 170°C. Aqueous inclusions containing trapped solids exhibit liquid-vapour homogenization at temperatures similar to those of halite-bearing aqueous inclusions.

Quartz-muscovite isotopic temperatures range from 584°C to 342°C with a mean of 425°C. The corresponding oxygen isotopic composition of the aqueous fluid in equilibrium with these minerals ranged from 1.2 to 5.5 per mil with a mean of 3.85 per mil, irdicating a significant meteoric component for the ore-forming fluid.

Isochores for carbonic fluid inclusions intersect with the modal isochore for aqueous fluid inclusions at a temperature of approximately 425°C and pressures between 680 and 740 bars.

A model is proposed in which molybdenite was deposited as a consequence of decreasing temperature and/or pressure and/or decreasing pH from CO₂-bearing, high to moderate salinity fluids of mixed magmatic-meteoric origin that were in equilibrium with K-feldspar and muscovite. These fluids evolved through interaction with volcanic (komatiitic) and sedimentary country rocks which yielded moderately high Ca/Na ratios (0.88), high Ni and CO₂.

SOMMAIRE

La leucoadamellite du batholite archéen de Preissac contient de la minéralisation de Mo-Bi dans des veines subverticales et subhorizontales riches en quartz, feldspath potassique et muscovite entourées par des halos d'altération albitique précoces et de feldspath potassique tardifs. Les inclusions fluides ont été étudiées pour investiguer les facteurs physicochimiques responsables de la minéralisation. Les veines contiennent quatre principaux types d'inclusions fluides: inclusions aqueuses L et LV; inclusions aqueuses-carboniques LLV; inclusions carboniques LV; et inclusions aqueuses L et LV contenant des solides. La phase carbonique dans les solutions des inclusions carboniques est constituée surtout de CO,

Les inclusions aqueuses, liquide-vapeur, exposent trois groupes distincts de salinité avec leur médiane à 5, 18, et 26 % poids de NaCl équivalent. Tous les trois types d'inclusions aqueuses et la phase aqueuse dans les inclusions carboniques montrent des températures de fusion initiales basses (jusqu'à -70°C) indiquant la présence de sels autre que NaCl. Les analyses par lessivage montrent que 12 fluide dominant lessivé renferme du Na, Ca, K, Mg, Li, Ni et Cl, et que les plus abondants sont Na, Ca et Cl. Les minéraux piéges suivants ont été identifiés par des analyses de SEM-EDS: calcite (CaCO₃), hydrophyllite (CaCl₂), muscovite, millérite, barytine (BaSO4) et halite (NaCl). La plupart des inclusions aqueuses deviennent un liquide homogène à des tempéatures entre 250°C et 400°C avec une médiane à 375°C. Les inclusions carboniques sont sous forme liquide ou vapeur homogène entre 210°C et 330°C. Les inclusions aqueuses contenant de la halite deviennent s'homogénéisent par la disparition de la halite à une température d'environ 170°C. Les inclusions aqueuses contenant des solides piégés montrent une homogénéisation des phases liquide-vapeur à des températures similaires à celles inclusions aqueuses contenant de la halite. températures isotopiques des assemblages quartz-muscovite varient de 584°C à 342°C avec une moyenne de 425°C. Les valeurs isotopiques δ^{18} 0 correspondant au fluide aqueux en équilibre avec les minéraux varient de 1.2 à 5.5 p.p.m avec une moyenne de 3.85 p.p.m. Ces valeurs suggérent constituant météorique significatif pour le fluide formant le aîte.

Les inclusions fluides carboniques possident des isochores que intersectent avec l'isochore modal pour les inclusions fluides aqueuses à une température d'environ 425°C et à des pressions variant entre 680 et 740 bars.

Un modèle est proposé selon lequel la molybdénite était déposée à la suite de la diminution de la température et/ou de la pression et/ou encore de la diminution de pH à partir de fluides, de salinité élevée à modérée, riches en CO₂. Ces fluides d'origine magmatique-météorique étaient en équilibre

avec le feldspath potassique et la muscovite. La composition de ces fluides a évolué à travers l'interaction avec des roches encaissantes volcaniques (komatiitiques) et sédimentaires, produisant des rapport de Ca/Na relativement élévés (0.88), et des valeurs élévés de Ni et de CO₂.

ACKNOWLEDGMENT

I am grateful to my thesis supervisors, Dr. A.E., Williams-Jones and Dr. S.A., Wood for their helpful guidance, advice and support, without which this work would not have been possible.

I offer my sincere thanks to G. Keating for performing the atomic absorption spectroscopy and whole-rock analysis, Dr. H.P., Schwarcz for performing the oxygen isotopic analysis, P. Stewart for performing the ICP analysis, and R. Yates for developing and printing the photographs.

Special thanks to my officemates S. Khositanont, F. Heinritzi, and J. Mungall for their friendly discussions on technical, academic, and social aspects. I wish to express my sincere thanks to my other fellow Graduate Students R. Linnen for his guidance with the fluid inclusion microthermometry at the beginning of this study, S. McCauley for his help on computer modeling, and B. Mountain for his technical assistance on many aspects.

I would also like to recognize all other members of the Department of Geological Sciences with whom I have collaborated on the technical, academic, administrative and friendship level.

Finally, I wish to thank to my husband Dr. M. F. Taner, for his support and encouragement during this study.

TABLE OF CONTENTS

	Page
ABSTRACT	i
SOMMAIRE	ii
ACKNOWLEDGEMENTS	iv
Table of Contents	v
List of Figures	ix
List of Plates	xiii
List of Tables	xv
CHAPTER 1. INTRODUCTION	1
CHAPTER 2. GEOLOGICAL SETTING	5
2.1 Geology of the rocks surrounding the Preissa	c-
Lacorne batholith	5
2.1.1 Introduction	5
2.1.2 Regional tectonic setting	6
2.1.3 Meta-volcanic rocks	7
2.1.4 Meta-sedimentary rocks	7
2.1.5 Meta-peridotite	8
2.1.6 Gabbro	8
2.2 Geology of the batholith	9
2.2.1 Dykes	10
2.2.2 Origin of the granitic rocks	11
2.3 Geology of the Cadillac Molybdenum deposit	12
2.3.1 Petrography of the wall rock	15
CHAPTER 3. HYDROTHERMAL MINERALIZATION AND ALTERATION	17
3.1 Mineralization	17

TABLE OF CONTENTS (continued)

	Page
3.1.1 Introduction	17
3.2 Alteration	24
3.2.1 Introduction	24
3.2.2 Early albitic alteration	24
3.2.3 K-feldspar alteration	26
3.2.4 Hematitization	28
3.2.5 Geochemistry of the host rock	30
CHAPTER 4. FLUID INCLUSION STUDIES	38
4.1 Introduction	38
4.2 Methodology	39
4.3 Classification and description of inclusions	40
4.3.1 Type 1 inclusions	41
4.3.2 Type 2 inclusions	43
4.3.3 Type 3 inclusions	44
4.4 Distribution of fluid inclusion types	50
4.5 Low temperature phase relationships	53
4.5.1 Aqueous inclusions	53
4.5.2 Carbonic inclusions	54
4.5.3 Solid-bearing aqueous inclusions	55
4.6 High temperature phase relationships	56
4.6.1 Aqueous inclusions	56
4.6.2 Carbonic inclusions	60
4.6.3 Solid-bearing aqueous inclusions	62
4.7 Salinity estimates	64

TABLE OF CONTENTS (continued)

	Page
4.7.1 Aqueous inclusions (Type 1)	64
4.7.2 Carbonic inclusions (Type 2)	67
4.7.3 Solid-bearing aqueous inclusions (Type 3)	69
4.8 Composition of the fluids	71
4.8.1 Nature of the species dissolved in the	
aqueous type 1 and type 3 inclusions	71
4.8.2 Fluid inclusion leachate analyses	73
4.8.2.1 Introduction	73
4.8.2.2 Method	74
4.8.2.3 Results	75
4.8.2.4 pH calculation	76
4.8.3 Composition of the carbonic inclusions	79
4.8.4 Scanning electron microscopy of minerals	
in fluid inclusions	81
4.8.4.1 Method	81
4.8.4.2 Results	81
CHAPTER 5. STABLE ISOTOPE STUDY	89
5.1 Introduction	89
5.2 Results	90
CHAPTER 6. INTERPRETATIONS	92
6.1 P-T conditions of entrapment	92
6.2 Source of hydrothermal fluids	94
6.3 Fluids and alteration	103
6.4 Solubility of molybdenite	104

TABLE OF CONTENTS (continued)

	Page
6.4.1 Solubility of nickel	110
6.5 Comparison of the Cadillac and Preissac	
molybdenum deposits to other molybdenum	
deposits	111
6.6 Genetic model	113
CHAPTER 7. CONCLUSIONS	115
REFERENCES	117
APPENDIX I Microprobe analyses	125
APPENDIX II Fluid inclusions leachate analyses	130
APPENDIX III pH calculation	133
APPENDIX IV Calculation of the bulk composition and	
bulk densities of inclusions	135

LIST OF FIGURES

		Page
1.1	A simplified geological map, showing the location and the geology of the Preissac-Lacorne batholith	3
1.2	A geological map of the Preissac massif, showing the location of the principal molybdenum mineralization	4
2.1	Sketch map of the Cadillac open pit, showing location of samples.	14
3.1	The paragenesis of vein minerals in the Cadillac and Preissac molybdenum deposits	. 21
3.2	Plots of wt % Na_2O , K_2O , versus SiO_2 diagram	32
3.3	Plots of wt % Al ₂ O ₃ , TiO ₂ versus SiO ₂ diagram	33
3.4	Plots of wt % Fe ₂ O ₃ , CaO versus SiO ₂ diagram	34
3.5	Plots of wt % P ₂ O ₅ , MgO versus SiO ₂ diagram	35
3.6	Q-Ab+An-Or diagram, showing the classification of intrusive rocks	36

		Page
4.1	Histograms, showing homogenization temperature	
	versus frequency for aqueous Type 1 inclusions	
	in the Cadillac and Preissac molybdenum deposits	
	as well as for albitic and K-feldspar alteration	
	in the Cadillac molybdenum deposit	58
4.2	Histograms, showing frequency distribution of	
	homogenization temperatures for Type 1 aqueous	
	inclusions in subvertical and subhorizontal veins	
	and in fluorite	59
4.3	Histograms, showing homogenization/decrepitation	
	temperature versus frequency for Type 2 carbonic	
	inclusions from the Cadillac and Preissac molybder	num
	deposits	61
4.4	Distribution of halite dissolution and vapour	
	disappearance temperatures in Type 3a inclusions,	
	and vapour disappearance temperatures in Type 3b	
	inclusions	63
4.5	Salinity versus frequency histograms for Type 1	
	aqueous inclusions in the Cadillac and Preissac	
	molybdenum deposits	65

		Page
4.6	Salinity versus frequency histogram for Type 1	
	aqueous inclusions in subvertical and	
	subhorizontal veins and in fluorite from	
	the Cadillac deposit	66
4.7	Salinity histogram for carbonic inclusions in the	
	Cadillac and Preissac molybdenum deposits	68
4.8	Salinity histogram for Type 3 halite and trapped	
	mineral-bearing aqueous inclusions in the Cadillac	
	and Preissac molybdenum deposits	70
4.9	Diagram, showing the compositions of Type 3a	
:	halite-bearing aqueous inclusions	72
4.10	Diagrams, showing the Carbonic phase homogenization	
	temperature versus final melting temperature of	
	carbonic ice in carbonic inclusions in the Cadillac	
	and Preissac molybdenum deposits	80
4.11	An inclusion cavity, containing halite,	
	and the X-ray spectra of the mineral	83

	Page
4.12 An inclusion cavity, containing calcite,	
and the X-ray spectra of the mineral and	
its matrix	84
4.13 An inclusion cavity, containing calcite and	
muscovite, and X-ray spectra of muscovite	
and its matrix	85
4.14 An inclusion cavity, containing a calcium	
chloride mineral, and X-ray spectra of the	
mineral and its matrix	86
4.15 An inclusion cavity, containing a nickel mineral,	
and X-ray spectra of the mineral and its matrix	87
4.16 An inclusion cavity, containing barite, and	
X-ray spectra of the mineral	88
6.1 P-T diagram, showing isochores for non aqueous	
carbonic inclusions intersecting the isochore	
for the modal homogenization temperature and	
salinity of Type 1 aqueous inclusions	93

		Page
6.2	A plot of salinity versus homogenization	
	temperature diagram of type 1 and 3 inclusions	101
6.3	Homogenization/decrepitation temperature	
	versus mole fraction of CO ₂ for carbonic inclusions	102
	LIST OF PLATES	
3.1	A subvertical quartz+muscovite vein surrounded	
	by an albitic alteration halo	18
3.2	A subvertical quartz+muscovite+K-feldspar vein	
	surrounded by a K-feldspar alteration halo	18
3.3	A thin section, showing molybdenite intergrown with	
	muscovite	21
3.4	A thin section, showing the development of	
	bismuthinite after molybdenite	22
3.5	A thin section, showing the development of	
	native bismuth after bismuthinite	22

LIST OF PLATES (continued)

		Page
3.6	A quartz-muscovite-molybdenite vein, surrounded	
	by leucoadamellite. Adjacent to the vein	
	plagioclase and K-feldspar have been replaced	
	by albite	25
3.7	A thin section of altered leucoadamellite,	
	showing the replacement of secondary albite	
	by K-feldspar	26
3.8	A K-feldspar alteration envelope, developed	
	around a quartz-K-feldspar-muscovite-molybdenite	
	vein in leucoadamellite	27
3.9	Hematitization	29
4.1	High to moderate salinity two phase Type la	
	aqueous inclusions	45
4.2	A moderate salinity two phase Type 1b aqueous	
	inclusion	45
4.3	Moderate to low salinity one phase Type 1b	
	aqueous inclusions	46
4.4	A low salinity two phase Type 1c aqueous inclusion	46

LIST OF PLATES (continued)

		Page
4.5	A three phase Type 2 carbonic inclusion	47
4.6	One phase (liquid) Type 2b carbonic inclusions	47
4.7	Vapour-rich, two phase Type 2c carbonic inclusions	48
4.8	Halite-bearing Type 3a aqueous inclusions	48
4.9	Trapped mineral-bearing Type 3b aqueous inclusions	49
4.10	Formation of hydrohalite in Type 3a inclusions	49
	LIST OF TABLES	
3.1	Whole rock analyses of leucoadamellite	37
4.1	Distribution of the inclusion types with the	
	corresponding vein and wall rock mineralogy in the	
	cadillac and Preissac molybdenum deposits	52
5.1	Results of oxygen isotopic analyses	91

CHAPTER 1

INTRODUCTION

Molybdenum mineralization was first discovered in the Preissac-Lacorne Batholith in 1901 (Leduc 1980), and was economically exploited between 1942 and 1972. The total production was 19,000 tons of molybdenite and bismuthinite, and came from three mines: Molybdenite Corporation of Canada, Preissac Molybdenite, and Cadillac Molybdenite (Fig. 1.1). The only other molybdenum deposit in the batholith of possible economic interest is Moly Hill (Fig. 1.1 and 1.2) which contains 272,400 tonnes of ore with 0.13 percent Mo and 0.079 percent Bi.

Additional metals of possible economic significance occurring in or adjacent to the Preissac - Lacorne batholith include lead (northwest of the Preissac massif), beryllium (southeast of the La Motte massif), lithium (mainly in the Lacorne massif), niobium (south of the La Motte massif), and nickel (to the west of the La Motte massif).

This study has been devoted to the Cadillac and Preissac molybdenum deposits both of which are located in the Preissac massif (Fig. 1.2). The aim of the study was to investigate the nature and origin of the hydrothermal fluids which deposited the molybdenite-bismuthinite in the batholith. Fluid inclusion, alteration and various geochemical studies were

undertaken for this purpose. Samples were collected from the Cadillac, and Preissac Molybdenum deposits during the summers of 1986 and 1987. Sixty-eight samples were examined during the course of the investigation, of which 42 were used in the fluid inclusion study. These and the remaining samples were also studied petrographically or geochemically.

Microscopic observations of the fluid inclusions in quartz and fluorite were used to clarify the various inclusion and establish their frequency distribution. Homogenization temperature, and microthermometrically-based estimates of composition were used to construct isochores to establish the pressure-temperature conditions of mineralization. Fluid inclusion leachate analyses were used in conjunction with the microthermometric measurements to establish the composition of the fluids. SEM-EDS analyses of daughter and trapped minerals were used as a complementary approach to qualitatively establishing the fluids. Major element analyses were used to investigate the chemical changes that occurred during wall-rock alteration. Oxygen isotope data were used to estimate vein formation temperatures and interpret the origin of the fluids.

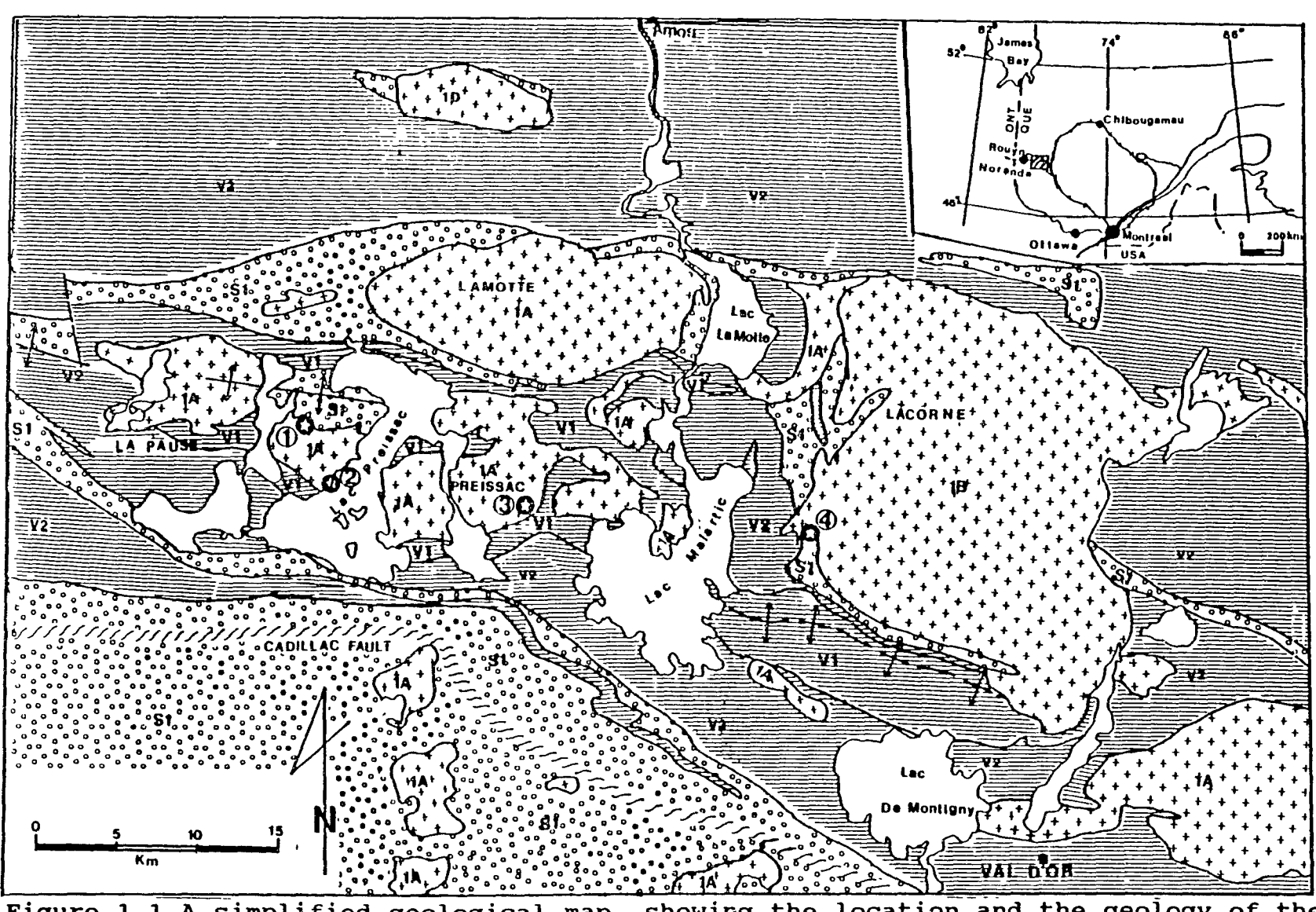


Figure 1.1 A simplified geological map, showing the location and the geology of the Preissac-Lacorne batholith. 1A granitoid rocks, 1B and 1D granodiorite, V1 ultramafic volcanic rocks, S1 meta-sedimentary rocks. Numbers in circles represent molybdenum deposits: 1 Preissac molybdenum, 2- Cadillac molybdenum, 3- Moly Hill, 4- Molybdenite Corporation of Canada (modified from compilation of the MERQ).

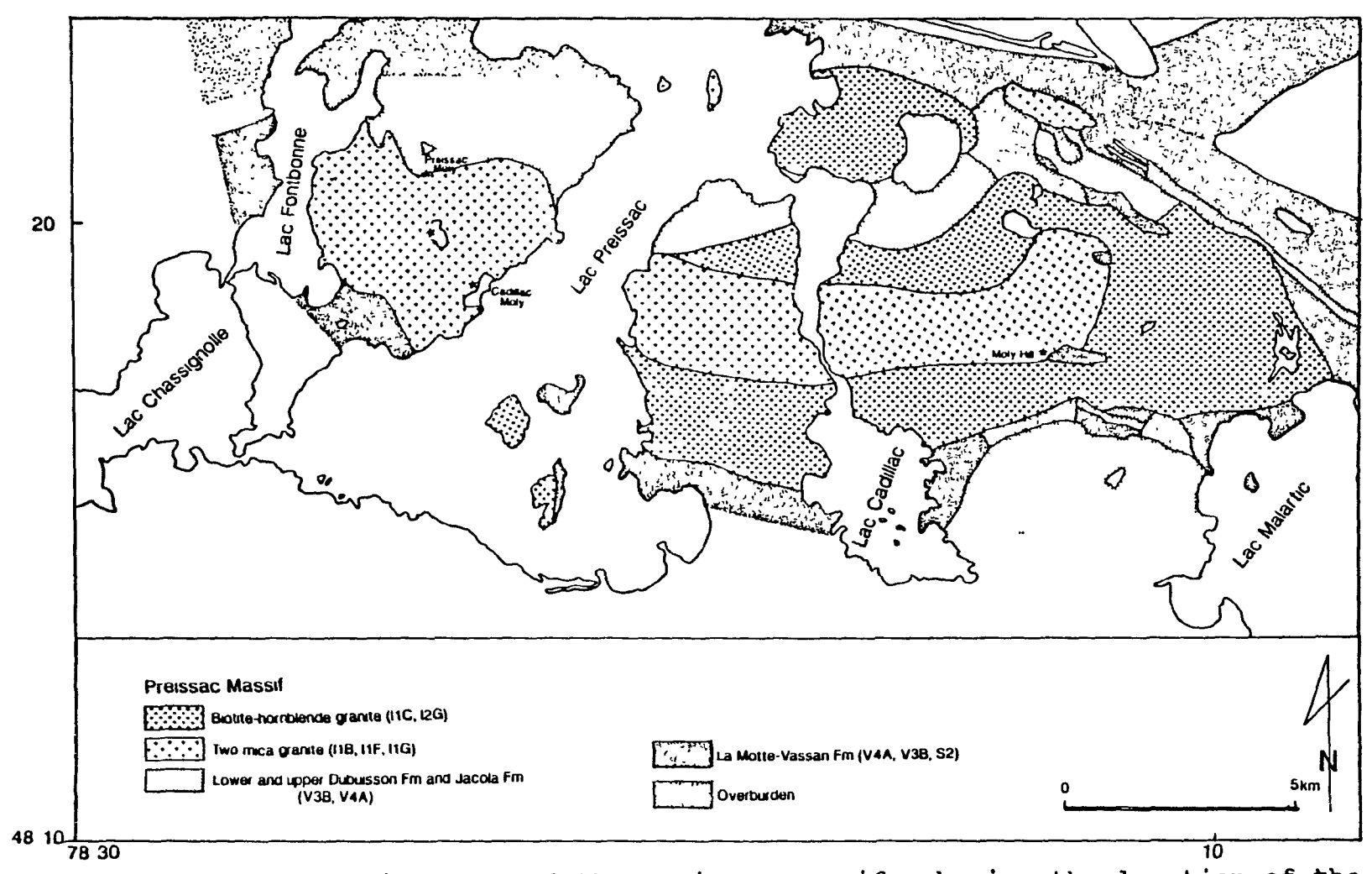


Figure 1.2 A geological map of the Preissac massif, showing the location of the principal molybdenum mineralization (After Boily 1989).

CHAPTER 2

GEOLOGICAL SETTING

2.1 GEOLOGY OF THE ROCKS SURROUNDING THE PREISSAC-LACORNE BATHOLITH:

2.1.1 Introduction

The Preissac-Lacorne batholith intrudes the Abitibi greenstone belt, Quebec, and outcrops within an anticline that strikes east from La Pause township (Fig. 1.1) (Ambrose 1941). The batholith is a continuous body that shallows to the east (Dawson 1966), and is bounded on the south by the Cadillac fault (Fig. 1.1). It is about 64 km long and 15 km wide and consists of three principal massifs (Preissac, Lacorne, and La Motte) (Fig. 1.1), and associated smaller stocks.

divided The rocks in the area can be into pre-batholithic, batholithic, and post-batholithic types with respect to the Preissac-Lacorne batholith (Dawson 1966). The pre-batholithic rocks include basic to intermediate metavolcanic rocks (Kinojevis and Malartic Groups), biotite schist (Kewagama Group), and meta-peridotite. Some pre-batholithic; most is post-batholithic. The metavolcanic rocks (lavas), which are the most widespread of the country rocks, and the biotite schist outcrop in a thin zone near the margins of the batholith. They have been intruded by gabbro, meta-peridotite, and granitic rocks. All rocks in the batholith are Archean in age except for the gabbro-diabase dykes, which are Proterozoic (Latulippe 1953).

The Preissac massif has been radiometrically dated at 2697±40 Ma using the U-Pb method on zircon (Gariepy 1985).

2.1.2 Regional Tectonic Setting

The east-trending Abitibi orogen is the largest (764 km long by 201 km wide) Archean belt of its type in the Canadian Shield (Goodwin 1970), and is thought to have formed either by rifting of sial-based volcanic basins (e.g Ludden and Hubert 1986), or through island arc style subduction (Dimroth 1983). Ludden and Hubert (1986) have divided the belt into a northern and a southern volcanic zone, based on structural, geochemical, sedimentological, and geochronological differences. The Preissac-Lacorne batholith is a late to post kinematic intrusive located in the southern volcanic zone.

The Preissac-Lacorne batholith is dominated by the east-west trending Cadillac (in the south) and Porcupine-Destor (in the north) faults. The Mo-Bi mineralization is believed to be related to hydrothermal activity along the Cadillac fault which is interpreted to have been active contemporaneously with and subsequent to the volcanic activity and sedimentation

in the Abitibi orogen (Dimroth et al. 1982).

2.1.3 Meta-Volcanic Rocks

Volcanic rocks outcrop along the north sides of the La Motte and Lacorne massifs, on the south and east sides of the Lacorne massif, and between the Preissac massif and the Kapitagama Stock (Fig. 1.1). The volcanic rocks are massive but locally exhibit such structures as pillows, flow - breccias, and/or amygdules, and include some thin tuffaceous beds. Regional metamorphism of the volcanic rocks (basalt, pyroclastic rocks) has produced greenschist facies metamorphic mineral assemblages (Dawson 1966).

2.1.4 Meta-Sedimentary Rocks

Coarse clastic metasedimentary rocks (metagreywacke and metaconglomerate) are intercalated with the volcanic rocks (Dawson 1966). As a result of regional metamorphism these rocks have been transformed into biotite, or biotite - hornblende - plagioclase schists (Dawson 1966). Biotite schists outcrop on the west, north, and east sides of the Lacorne massif.

2.1.5 Meta-Peridotite

Meta - peridotite, which is interbanded with volcanic rocks, outcrops over an extensive area surrounding the Preissac massif, separating it from the La Motte and Lacorne massifs (Dawson 1966). It also outcrops in thin conformable lenses, in the volcanic rocks, and less commonly, in the biotite schists north and south of the Lacorne massif. Regional metamorphism has resulted in the replacement of primary olivine and/or pyroxenes with pseudomorphous aggregates of chlorite, serpentine, talc, magnetite, and carbonate.

2.1.6 Gabbro

Pre-and post-batholithic gabbro bodies outcrop near the Preissac-Lacorne batholith. The pre-batholithic gabbro is truncated by the east side of the Lacorne massif and forms a sill-like body within the lavas (Tremblay 1950). The post-batholithic gabbro occurs as dykes within the batholith. The older gabbro shows evidence of regional metamorphism and deformation whereas the younger dykes are characterized by autometamorphic effects and contact aureoles in their wall - rocks (Dawson 1966).

2.2 GEOLOGY OF THE BATHOLITH

The rocks of the batholith, in order of decreasing abundance are: leucoadamellite (33 percent), syenodiorite (31 percent), granodiorite (28 percent), monzonite (8 percent), and associated dykes of granodiorite, feldspar porphyry, aplite, and mineralized quartz veins (Dawson pegmatite, 1966). The leucoadamellite is believed to represent the parent magma for the rare-element pegmatites that are common in this batholith (Siroonion et al. 1958). The leucoadamellite outcrops in the core of the Preissac massif, over most of the La Motte massif, and in the northwestern part of the Lacorne massif. Granodiorite outcrops near the margins of the Preissac massif, at the east end of the La Motte massif, and in the periphery of the Lacorne massif. The monzonite syenodiorite are restricted to the Lacorne massif. Syenodiorite also occurs in small tabular bodies occupying tension fractures in the wall-rocks near the contact of the batholith (Dawson 1966).

The Preissac massif may be distinguished from the Lacorne and Lamotte massifs by the paucity of pegmatites, absence of exotic mineral-bearing varieties of pegmatites, and the abundance of molybdenum mineralization (Boily et al. 1989).

2.2.1 Dykes

Pegmatite dykes are most abundant in the leucoadamellite volume percent), and least abundant granodiorite. They are abundant at the east end of the Preissac massif, on the west and north side of the La Motte massif and on the north side of the Lacorne massif (Rowe 1953). The pegmatite dykes can be classified as either homogeneous, or heterogeneous (Cameron et al. 1949). The homogeneous pegmatites resemble the leucoadamellite mineralogically, and consist mainly of quartz, albite, microcline, and muscovite. The heterogeneous pegmatites, contain the same major mineral constituents as well accessory spodumene, beryl, lithium mica, niobium-tantalite, and red garnet.

Aplite dykes are abundant in the leucoadamellite. They are also a major component of some of the large heterogeneous pegmatite dykes.

Small feldspar porphyry dykes are sparsely distributed in tension fractures in the country rocks at the east end of the Lacorne massif.

The Preissac massif, which is part of the Preissac - Lacorne batholith, outcrops over an elliptical area of approximately 150 km² with its major axis striking east (Fig. 1.1). The leucoadamellite forms the core of the Preissac massif (Fig. 1.1, 1.2) and contains numerous quartz and

quartz pegmatite veins. The leucoadamellite outcrops are mineralogically homogeneous and free of xenoliths (Dawson 1966).

2.2.2 Origin of the Granitic Rocks

Various models have been proposed to explain the origin of the granitic rocks of the Preissac-Lacorne batholith. Dawson (1966), on the basis of field relationships and chemical analyses, suggested three possible mechanisms for generating the related magmas: partial melting of sedimentary or primary granitic layer; differentiation of a magma of granodioritic composition, and hybridization of the magma with wall-rock materials. He also proposed that the leucoadamellite, pegmatites, and quartz veins, represented advanced of fractional progressively more stages crystallization of a primary granodiorite magma, rather than granitization of wall-rocks. Other rocks, which are quartz poor and mafic, originated, according to his model, by contamination of granodiorite or digestion of metavolcanic rocks, whose xenoliths of which, are disseminated throughout these rock types. Card (1982) suggested that the leucogranite formed by anatexis of metasedimentary rocks (possibly Pontiac gneisses underlying the Abitibi belt). Danis (1985), and Bourne and Danis (1987) proposed that the peraluminous rocks (leucoadamellite) in the Lacorne batholith formed by mixing

of an anatectic peraluminous magma with basaltic magma, and proposed sidewall crystallization (Baker and McBirney 1985) to explain the origin of the reversely zoned metaluminous rocks. Gariepy and Allegre (1985) showed that the granitoid magma is a partial melt of continental crust, comprising juvenile, mantle-derived rocks and non negligible amounts of earlier formed sialic material. According to them the episode of crustal anatexis occurred as a consequence of orogenic events which resulted in the burial of altered crustal rocks.

2.3 GEOLOGY OF THE CADILLAC MOLYBDENUM DEPOSIT

The Cadillac molybdenum deposit is an open pit and hosted mainly by leucoadamellite, which varies from medium— to fine-grained, and from white to pink to grey in colour. The leucoadamellite is mineralogically homogeneous and in places is cut by aplite dykes. It consists mainly of quartz, feldspar and minor amounts of muscovite. In some samples minor biotite is also present. In the southern and eastern parts of the open pit, biotite schist overlies the leucoadamellite which is locally brecciated and filled by quartz.

Leucoadamellite within the mineralized zone is intensely fractured. Complex crosscutting relationships of older veins by younger ones indicate that fracturing and movement occurred during and after mineralization.

A majority of the veins are vertical to steeply dipping and strike 82°-110° at dips ranging from 73° S to 77° N (Fig. 2.1). Subhorizontal veins are common, particularly in the south and southwestern parts of the pit. They either strike 335-340° and dip 40-42°E, or strike 230° and dip 25°N (Fig. 2.1). Their temporal relationship to the subvertical veins is not clear.

The subvertical veins are parallel to the major fractures, some of which are coated with molybdenite + pyrite or fluorite. The branching of veins, and the variation in strike along individual veins indicate a tensional environment.

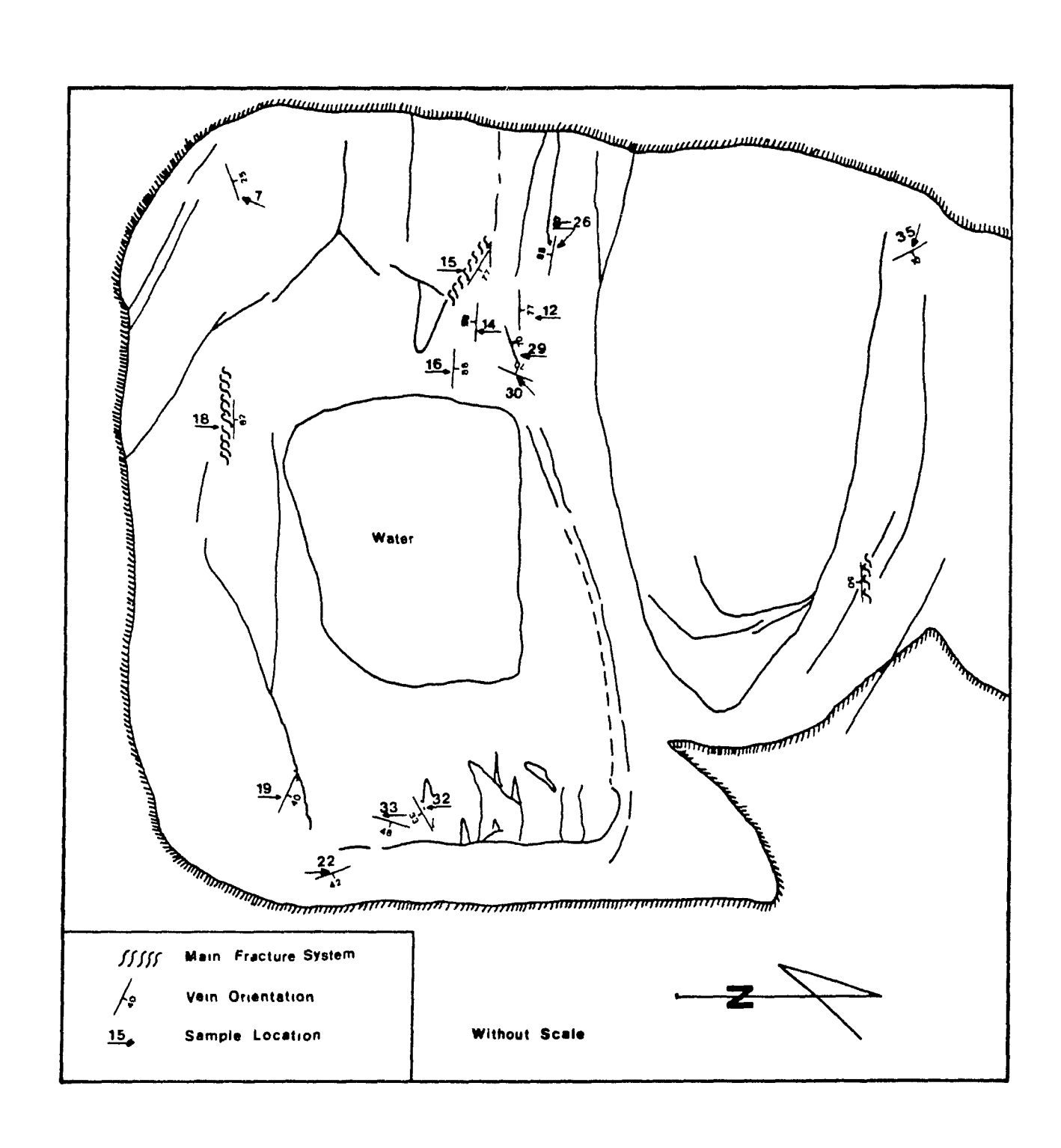


Figure 2.1 Sketch map of the Cadillac open pit, showing the location of samples.

2.3.1 Petrography of The Wall Rock

Twenty-five polished thin sections of the wall-rocks were studied (16 from the Cadillac, and 9 from the Preissac Molybdenum Deposits) using standard transmitted and reflected light microscopy. All samples, except one (biotite schist), were taken from the leucoadamellite.

Thin section examination shows that quartz is ubiquitous and is the most abundant mineral in almost all samples with an average of 55 volume percent.

Feldspar is the second most abundant phase with an average content of 40 volume percent: percent is plagioclase, and 16 percent is K-Feldspar. The K-feldspar includes microcline, orthoclase, and microperthite. It also occurs with quartz as microveinlets filling in fractures in primary rocks, and is therefore, in part, a secondary mineral. Microprobe analyses of feldspars from the wall-rock are given in Appendix I, Table 1. The composition of plagioclase varies from almost pure albite to oliqoclase. Some plagioclase appears cloudy owing to the presence of numerous disseminated dark crystals (hematite ?). Small sericite flakes are also present in many plagioclase crystals. Micrographic textures are seen in thin section and are locally well developed. Such textures are most commonly developed in water-rich magmas, generally in the presence of a separate aqueous phase (Jahns and Burnham 1969). Jahns and

Burnham (1969) showed that, in the presence of chloride-rich aqueous solutions, granitic melt crystallized to a graphically intergrown assemblage of alkali feldspar and quartz. These intergrowths may thus reflect zones of accumulation of a separate, chloride-rich aqueous phase. Myrmekitic textures are also seen in thin sections.

Muscovite is the third most abundant mineral. Garnet, biotite, apatite, calcite, zircon, and titanite are present in minor amounts. Calcite is present in almost all samples whereas the other minor minerals are present in some samples and absent in others. The garnet is red and occurs either in thin planar concentrations or in disseminations of small grains. Biotite is partially to completely altered to chlorite. In general, biotite is more common in samples from the Cadillac mine than the Preissac mine.

CHAPTER 3

HYDROTHERMAL MINERALIZATION AND ALTERATION

3.1 MINERALIZATION

3.1.1 Introduction

Molybdenum mineralization occurs in either subvertical subhorizontal veins occupying fractures within leucoadamellite. The majority of veins are subvertical and contain quartz + muscovite ± K-feldspar (Plates 3.1 and 3.2). The major part of the ore zone is in the western part of the open pit, and consists of intensely mineralized veins. The vein thickness varies from 0.5 mm to 1.5 m. In general, the thinner veins have proportionally wider alteration haloes than ones. This probably reflects the varying the thicker importance of diffusion and infiltration with fracture width. In the case of the thin veins, flow was probably impeded and thus there was more opportunity for the fluids to infiltrate the wall-rock and cause alteration. The mineralizing fluids probably flowed faster in the wider fractures than in the thinner ones and therefore infiltrated less into the country rocks. Mineralization in the eastern half of the open pit is in the form of a well developed stockwork.

National Library of Canada

Bibliothèque nationale du Canada

Canadian Theses Service Service des thèses canadiennes

NOTICE

AVIS

FOR MICROFILMING.

UNFORTUNATELY THE COLOURED ILLUSTRATIONS OF THIS THESIS CAN ONLY YIELD DIFFERENT TONES OF GREY.

THE QUALITY OF THIS MICROFICHE
IS HEAVILY DEPENDENT UPON THE
QUALITY OF THE THESIS SUBMITTED

LA QUALITE DE CETTE MICROFICHE
DEPEND GRANDEMENT DE LA QUALITE DE LA
THESE SOUMISE AU MICROFILMAGE.

MALHEUREUSEMENT, LES DIFFERENTES ILLUSTRATIONS EN COULEURS DE CETTE THESE NE PEUVENT DONNER QUE DES TEINTES DE GRIS.

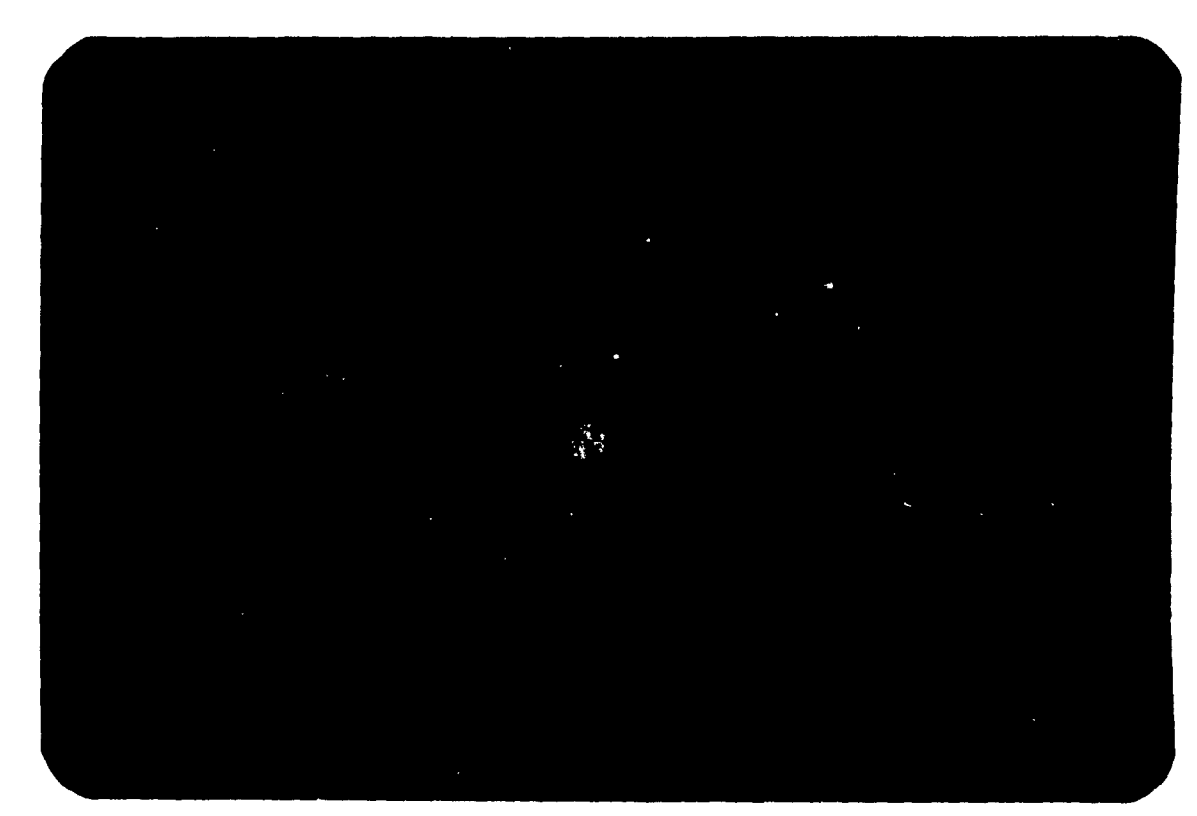


Plate 3.1 A subvertical quartz+muscovite vein surrounded by an albitic alteration halo.

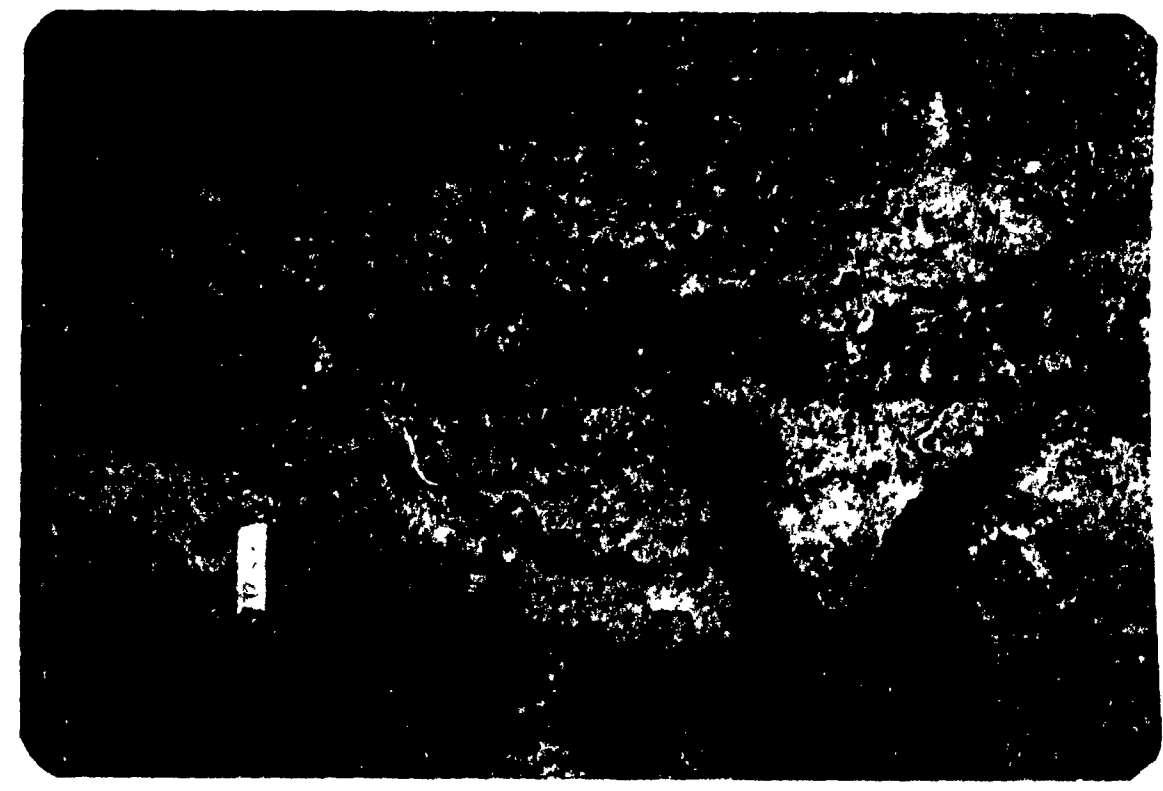


Plate 3.2 A quartz+muscovite+K-feldspar vein surrounded by a K-feldspar alteration halo.Molybdenite (in grey) is disseminated in the K-feldspar alteration halo.

Molybdenite is the most abundant primary ore mineral in the orebody. It is mainly intergrown with muscovite (plate 3.3) and shows a close spatial relationship with K-feldspar (plate 3.2.). Molybdenite also occurs as coatings on fractures and as disseminated crystals in the wall-rocks with other sulphide minerals.

Bismuthinite and native bismuth are the second and third most common minerals of economic interest in the Cadillac and Preissac molybdenum deposits. Microprobe analyses show that another bismuth mineral, gladite $(Bi_{5.2}.Cu_{1.3}.Pb_1.Fe_{.2}S_9)$, an intermediate member of a solid-solution series between bismuthinite and aikinite $(2PbS.Cu_2S.Bi_2S_3)$ is also present in the Preissac deposit (Appendix I, Table 3).

Pyrite is a ubiquitous sulphide mineral in the orebody. It occurs in molybdenite-bearing quartz veins, in barren veins, and as disseminations throughout the host rock. In some veins, pyrite forms euhedral crystals up to 2 cm long.

Minor chalcopyrite and sphalerite accompany molybdenite in the veins or occur with other accessory minerals in the host rock. Microprobe analyses show that sphalerite has a low iron content (Appendix I, Table 3) suggesting high fs₂ and/or high fo₂ in the fluid during its precipitation (Barton and Skinner 1979). There is also minor disseminated rutile, ilmenite and hematite in the host rock.

In veins containing molybdenite, bismuthinite, and native

bismuth, three stages of paragenesis are recognized on the basis of petrographic relationships: molybdenite is the earliest sulphide phase to have formed (Plate 3.4), followed by bismuthinite (Plate 3.4), and then by native bismuth (Plate 3.5). Presence of native bismuth may suggests lowering of fs₂ late in paragenesis. Alternatively, it could represent a lowering of fo₂, an increase in pH or an increase in temperature. The latter is the least likely. Their paragenetic relationship to sphalerite, and chalcopyrite are not known since no crosscutting relationships have been observed between Mo-Bi veins and those containing sphalerite and chalcopyrite in hand specimens or thin sections.

The barren quartz veins contain the same silicate minerals with traces of pyrite as the Mo-Bi mineralized veins.

Detailed field and laboratory study of barren and mineralized veins suggests that there were four separate pisodes of vein formation. These stages were established using subvertical veins. The paragenesis of the minerals and related stages are given in Figure 3.1.

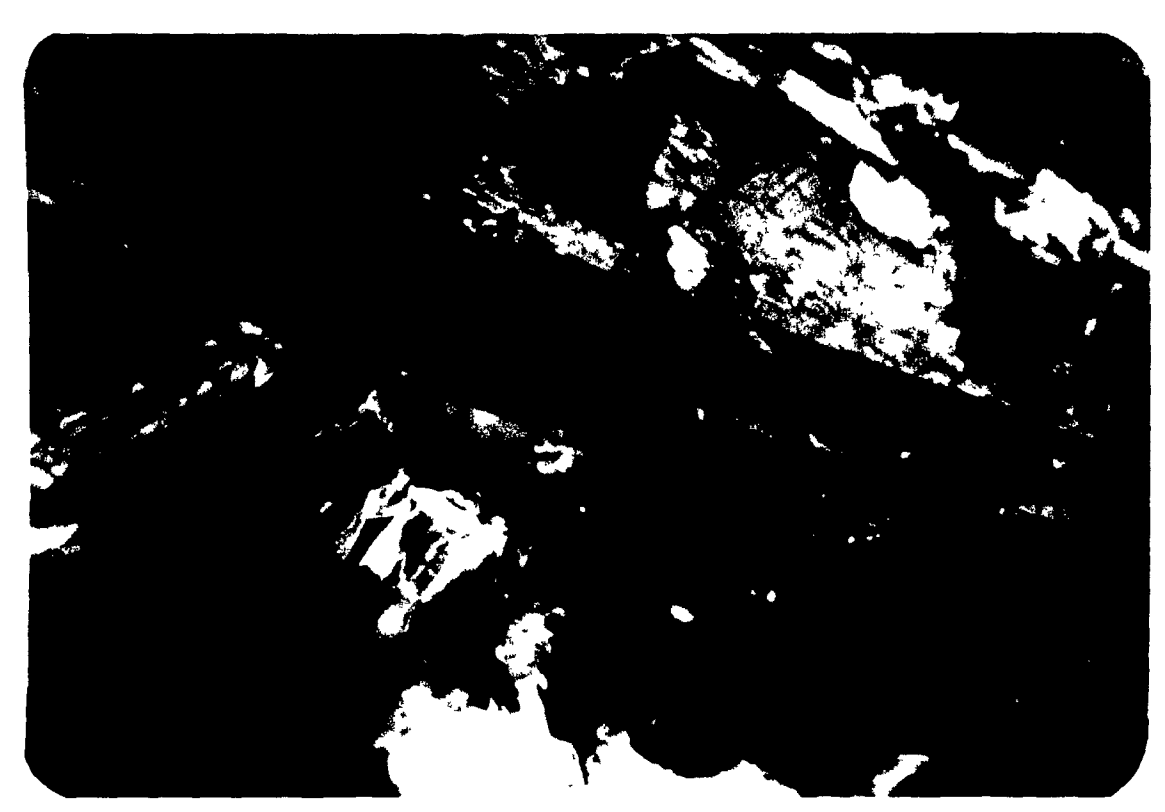
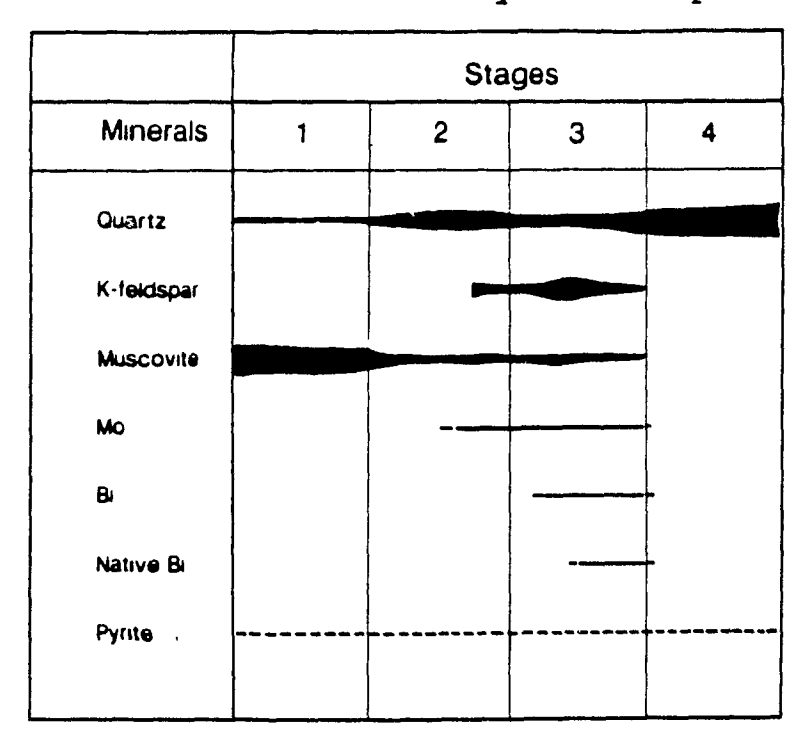


Plate 3.3 A thin section, showing a large crystal of molybdenite (in black) intergrown with muscovite.

Figure 3.1 The paragenesis of some vein minerals in the Cadillac and Preissac molybdenum deposits



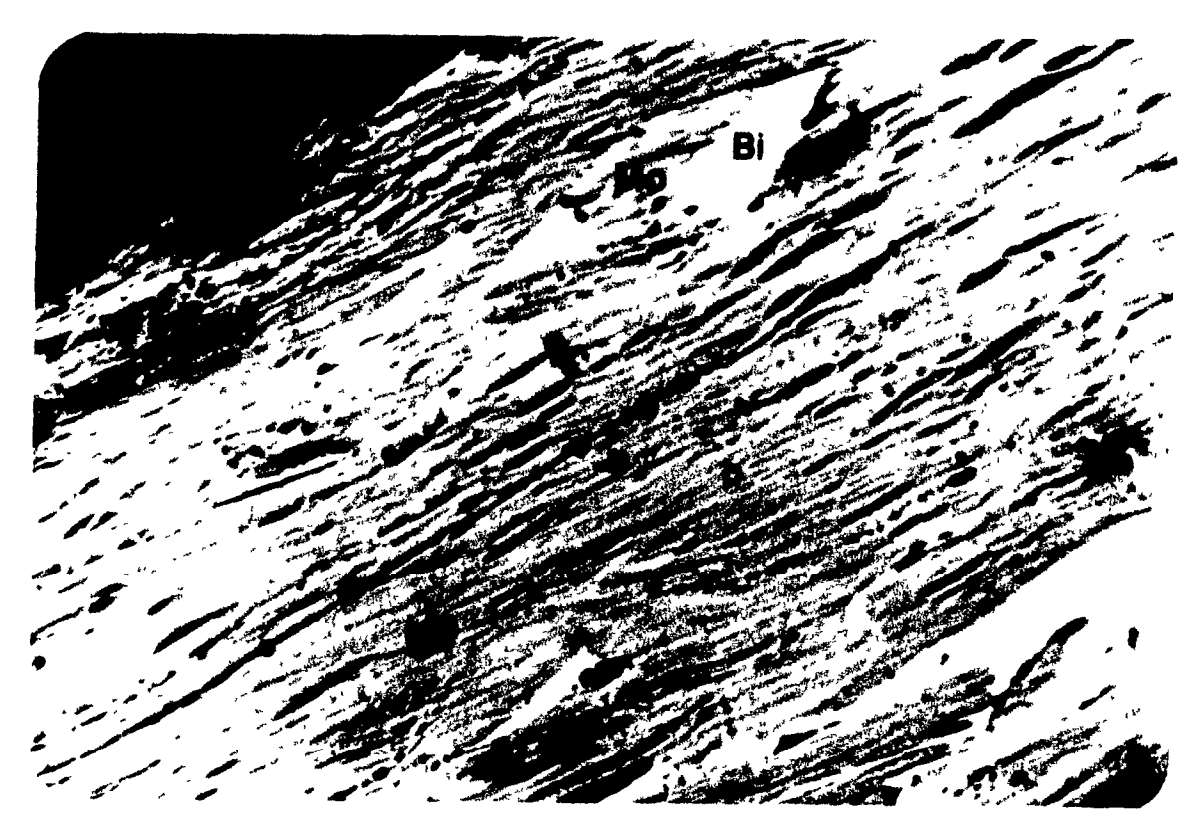


Plate 3.4 A polished thin section, showing the development of bismuthinite (Bi) after molybdenite (Mo).

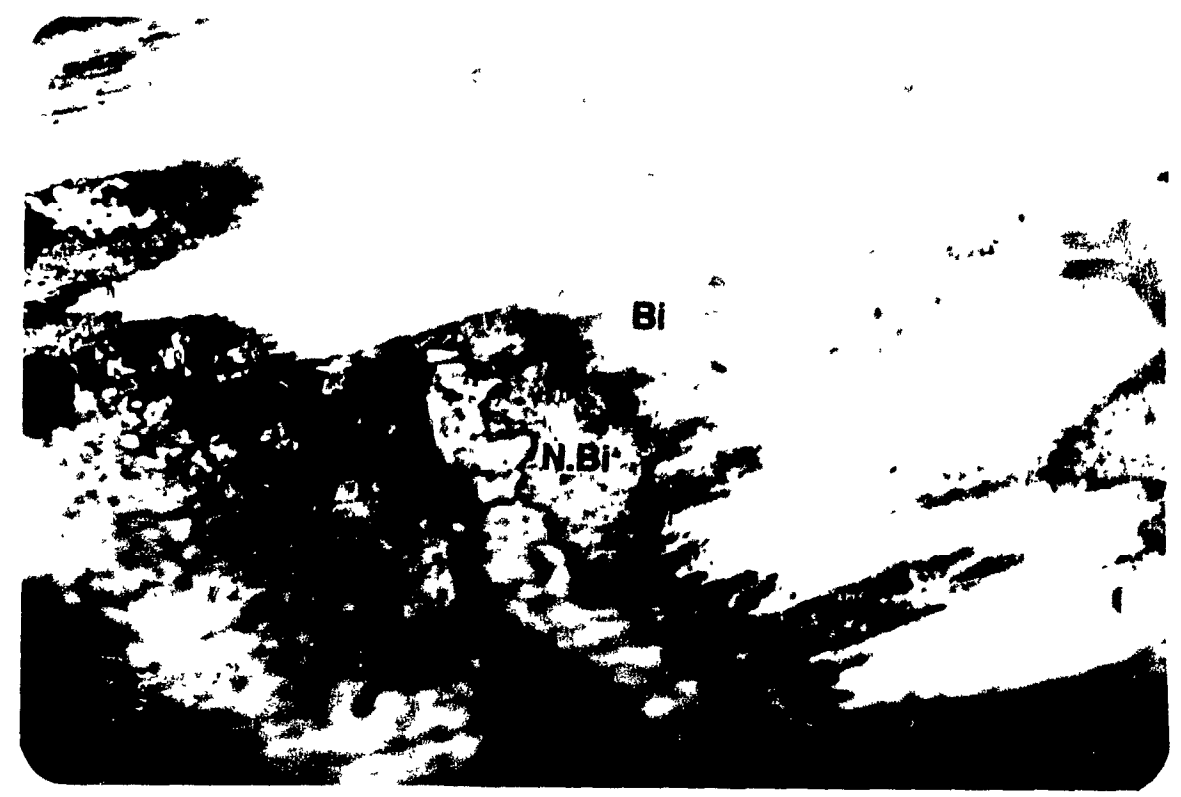


Plate 3.5 A polished thin section, showing the development of native bismuth (N.Bi) after bismuthinite (Bi).

Stage I veins contain 90% muscovite and 10% Quartz, and are very thin (≤3mm.). They are not mineralized, and are cut by all the other veins types. They may or may not contain pyrite.

Stage II veins contain 60-90% quartz, 5-20% muscovite, and up to 30% K-feldspar. They contain trace amounts of molybdenite, and may or may not contain pyrite.

Stage III veins contain 30-90% quartz, 5-60% K-feldspar, and 5-15% muscovite. These veins are distinguished from Stage II veins by their high contents of molybdenite. Traces of pyrite are also observed.

Stage IV veins contain quartz, and trace amounts of pyrite.

Subhorizontal veins belong to either stage II or stage III on the basis of their mineralogy.

Electron microprobe analyses suggest that muscovite in early non mineralized veins (LC-11-1, LC-11-31) may be depleted in potassium relative to muscovite in mineralized (LC-10-6) veins (Appendix I, Table 2).

Stage V veins comprise thin reddish coatings of hematite on open fractures. Hematite veins cut the vein types described above, and therefore represent latest stage of veining in the history of the Cadillac and Preissac molybdenum deposits.

Fluorite is deposited either as a coating of wall rock or in tensional fractures with molybdenite.

3.2 ALTERATION

3.2.1 Introduction

Wall-rock alteration was studied using a combination of microscopic, macroscopic and chemical techniques including staining for K-Feldspar and plagioclase (Bailey 1960). Three types of alteration are recognized in the Cadillac molybdenum deposit: 1- Early albitic alteration, 2- K-feldspar alteration and 3- Hematitization.

3.2.2 Early albitic alteration

Early quartz-molybdenite veins are surrounded by haloes in which feldspars have been destroyed and replaced by very cloudy albite. Plate 3.6 shows a slabbed specimen of the fresh wall rock containing a quartz vein surrounded by an albitic alteration halo, before (Plate 3.6 a), and after staining (Plate 3.6 b) with sodium cobaltinitrate. The absence of a yellow stain around the vein indicates that the halo adjacent to the vein does not contain K-feldspar. Further staining was conducted for plagioclase, using barium and rhodizonate. Lack of staining showed that the halo is albite (Bailey 1960) (Plate 3.6 b). This conclusion is supported by microprobe data which indicate that the plagioclase in the halo is almost pure albite.



Plate 3.6 A quartz-muscovite vein, surrounded by leucoadamellite. Adjacent to the vein plagioclase and K-feldspar have been replaced by albite. a) before staining, and b) after staining.

CENTIMETRES

3.2.3 K-feldspar alteration

Plagioclase including secondary albite adjacent to some quartz veins was locally replaced by secondary K-Feldspar (3.7). Thus, K-feldspathization took place after albitization of the primary feldspars. Pockets of K-feldspar are developed in the interiors and the borders of individual plagioclase crystals. Plate 3.8 shows an example of a hand specimen containing such a vein before (Plate 3.8 a), and after, (Plate 3.8 b) staining with sodium cobaltinitrate. It is clear from the plates that there is a strong concentration of K-feldspar around the vein.

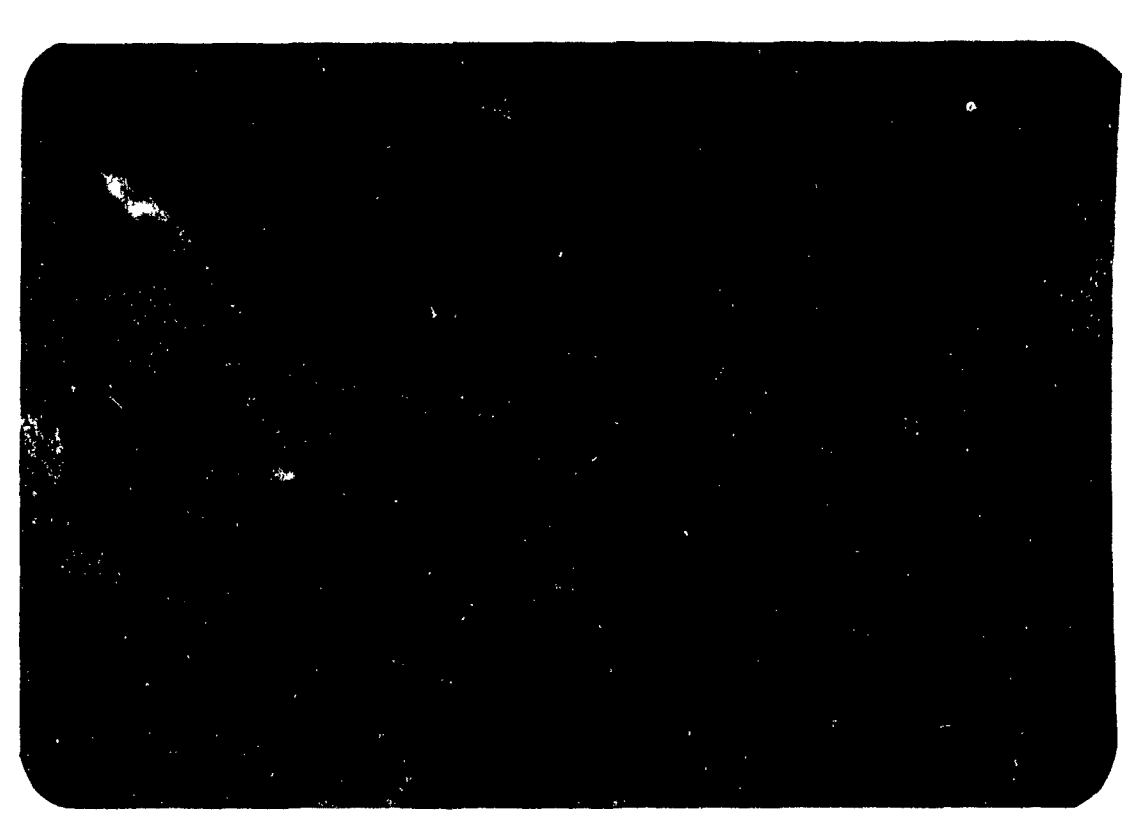


Plate 3.7 A thin section of altered leucoadamellite, showing the replacement of secondary albite by K-feldspar.



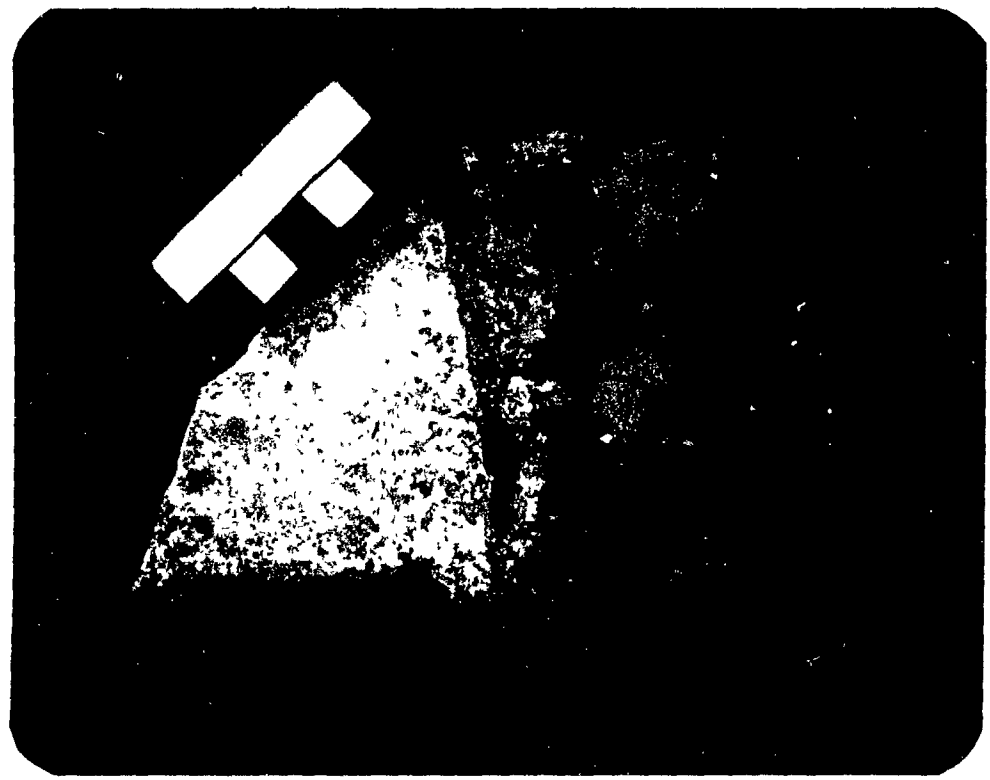


Plate 3.8 A K-feldspar alteration envelope, developed around a quartz-muscovite-K-feldspar-molybdenite vein. abefore staining, b- after staining.

3.2.4 Hematitization

The other interesting alteration is the hematitization of the rocks as coating (Plate 3.9 a), and associated K-feldspathization of pre-existing feldspar in the red hematitic zone (Plate 3.9 b). The replacement of plagioclase by K-feldspar probably proceeded in two steps. First, plagioclase was converted to very cloudy albite, and later reacted with a fluid to form K-feldspar. Plate 3.9 shows the sample before (Plate 3.9 a) and after staining with sodium cobaltinitrate (Plate 3.9 b).

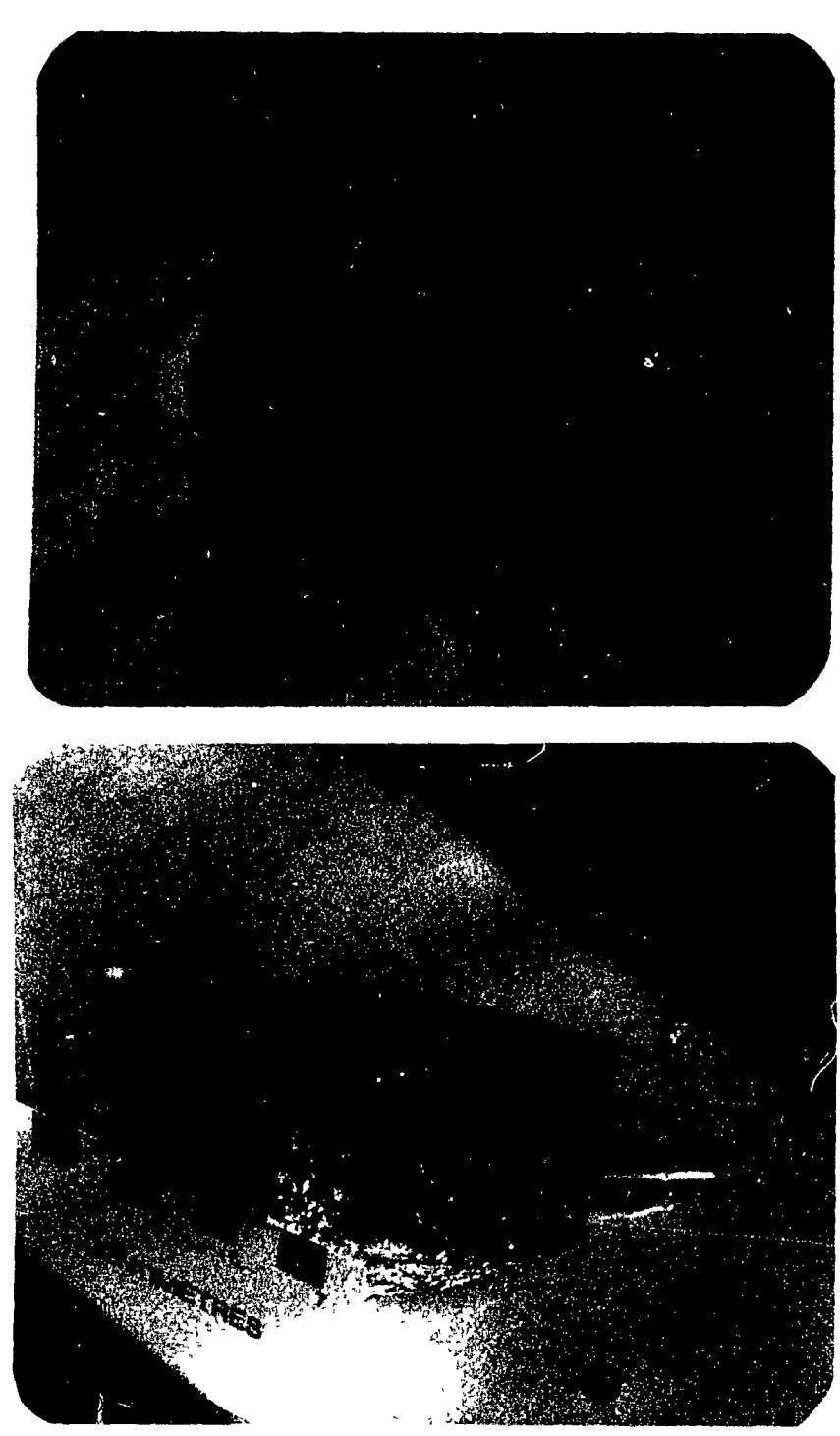


Plate 3.9 Hematitization and K-feldspar alteration. abefore staining, and b- after staining

3.2.5 Geochemistry of the Host Rock

Eleven samples from the altered and unaltered parts of the leucoadamellite have been analyzed for their major elements. The results of these analyses are given in Table 3.1 and Figures 3.2, 3.3, 3.4, 3.5 as plots of each oxide versus SiO₂.

The unaltered rocks form tight clusters on each of the oxide plots showing that the host rock to the mineralization is very uniform in composition. The fact that $Al_2O_3 > Na_2O + K_2O + CaO$ (Table 3.1) indicates that it is peraluminous. The normative composition corresponds to that of granite using the Streckeisen classification scheme (Fig. 3.6).

As expected, albitically altered samples, have slightly higher Na contents than the unaltered rock (Fig. 3.2). The Ca content is markedly lower reflecting replacement of Ca in plagioclase by Na during albitization. The contents of Fe₂O₃, TiO₂, and MgO are also lower in the albitized samples. The depletion in TiO₂ is particularly surprising given that Ti is considered to be an immobile element. This element has, however, been shown to be mobile in the presence of CO₂-bearing fluids (Murphy and Hynes 1986). These authers concluded that since Ti is a high-field-strength element, it could be transported by complexing it with carbonic species. Therefore its depletion here may reflect the fact that carbonic fluids were quite important in the evolution of the

Cadillac and Preissac molybdenum deposits. The content of SiO_2 , K, Al_2O_3 , and P_2O_5 are unchanged from those of the albitized samples.

As expected, K20 increased during K-feldspar alteration (Fig. 3.2). The major difference between albitization and potassic alteration is that the latter was accompanied by major depletions in SiO₂ (Fig. 3.2, 3.3, 3.4, 3.5 X's). The depletion of silica was accompanied by corresponding increases in Al₂O₃ that define an inverse linear correlation between the two oxides with a slope of approximately -1 (Fig. 3.3, as X's). This suggests that the SiO, depletion was accompanied by a volume loss leading to the concentration of Al,O, in the residual rock. The porosity that, it is proposed, was created by alteration would have permitted infiltration of the mineralizing solutions which may explain why molybdenite is commonly disseminated in the K-feldspar alteration haloes (Plate 3.2). TiO2, Fe2O3, and MgO decrease during Kfeldspathization. The Na₂O content of potassically altered rocks is similar to or, in some cases, higher than that of albitically altered rocks. However, as noted above, there may have been a volume loss associated with K-feldspathization, in which case Na,0 may have actually been removed or at least not added.

In summary, during albitization the major change was a sharp decrease in Ca whereas K-feldspathization was dominated mainly by loss of SiO_2 and additions of K_2O .

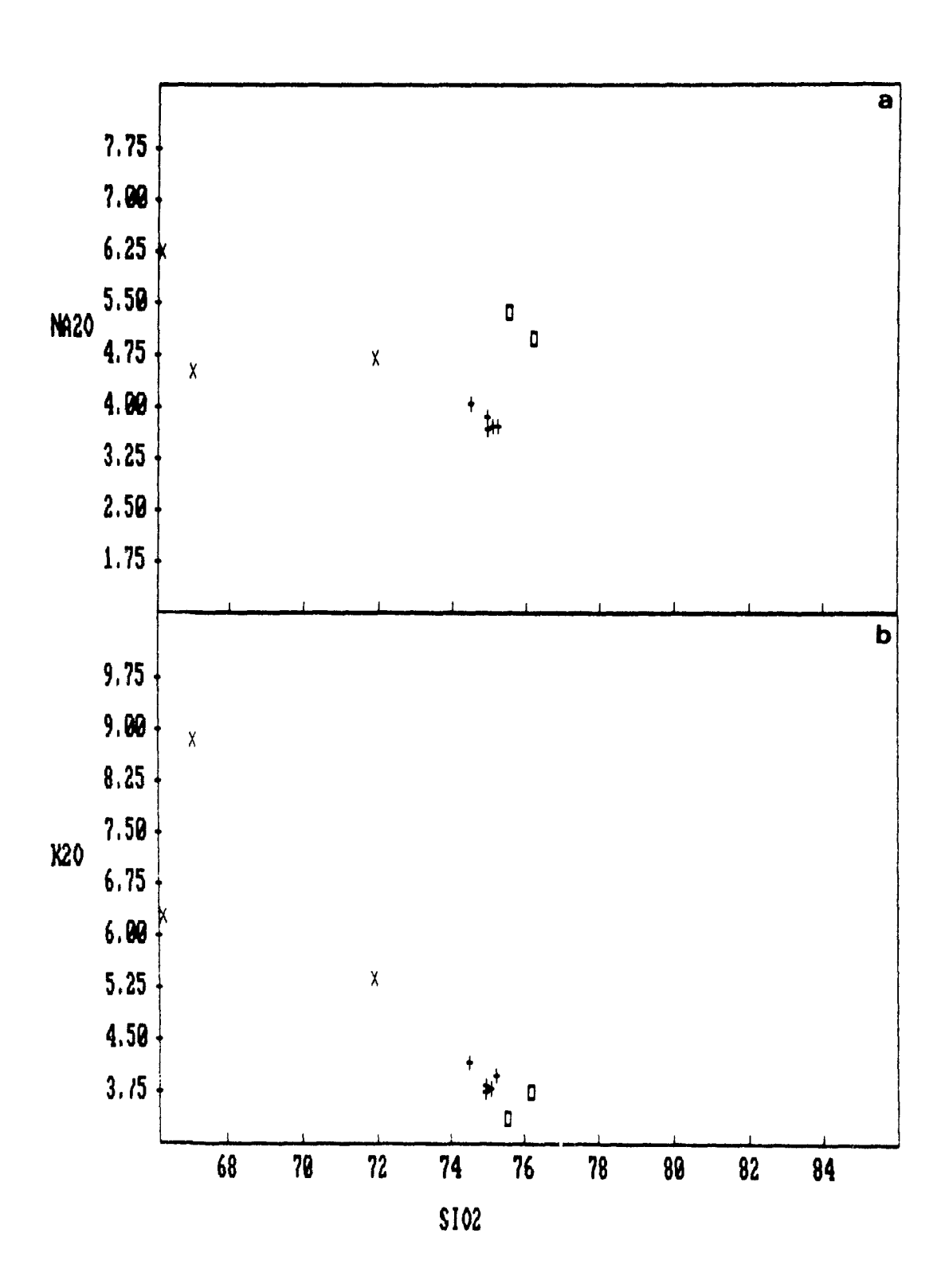


Figure 3.2 Plots of wt % Na₂O (a), K₂O (b) versus SiO₂ diagram. Crosses represent unaltered granite, X's represent K-feldspar alteration, open boxes represent albitic alteration.

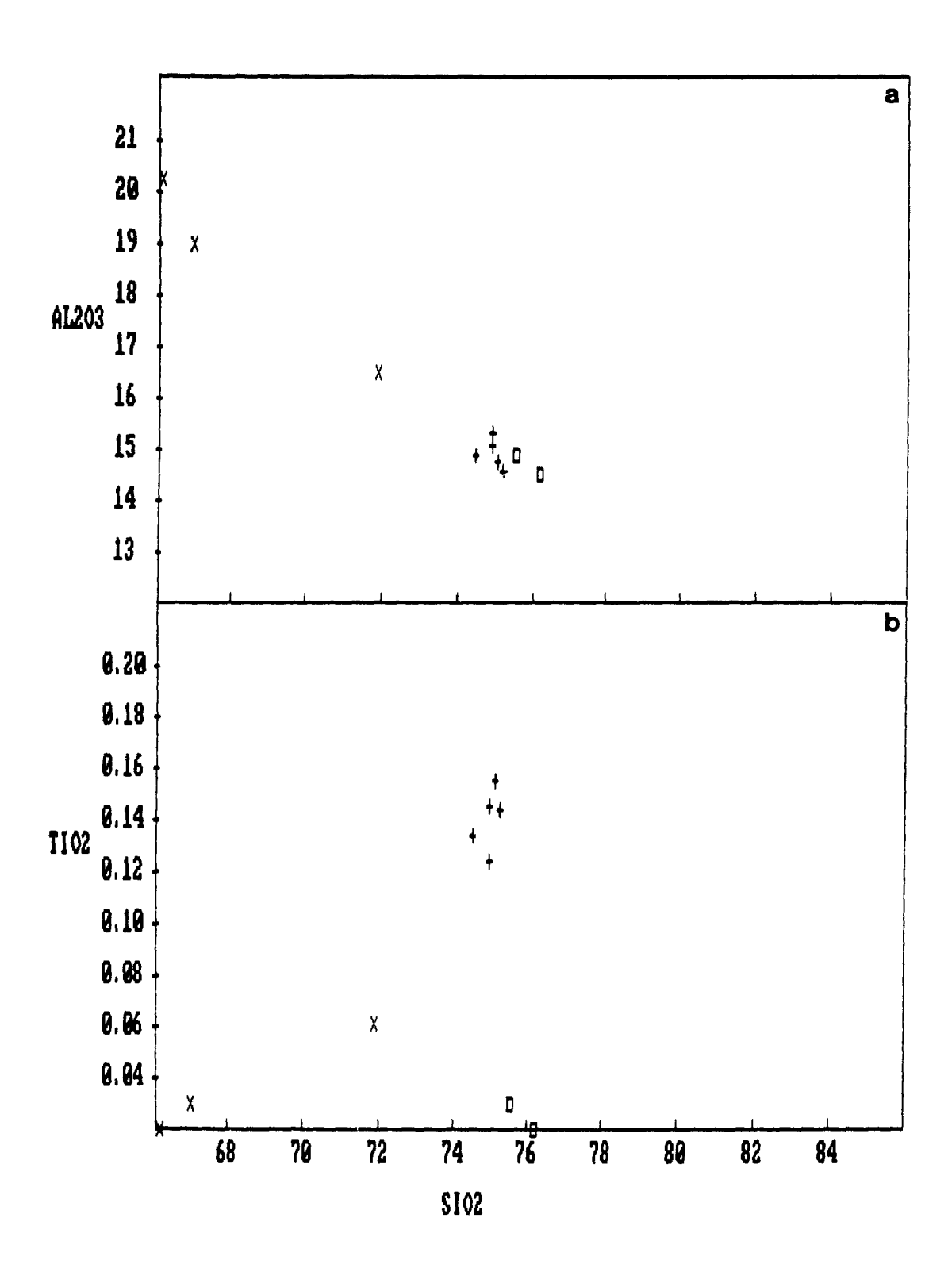


Figure 3.3 Plots of wt % Al₂O₃ (a), TiO₂ (b) versus SiO₂ diagram. Crosses represent unaltered granite, open boxes represent albitization, X's represent K-feldspathization.

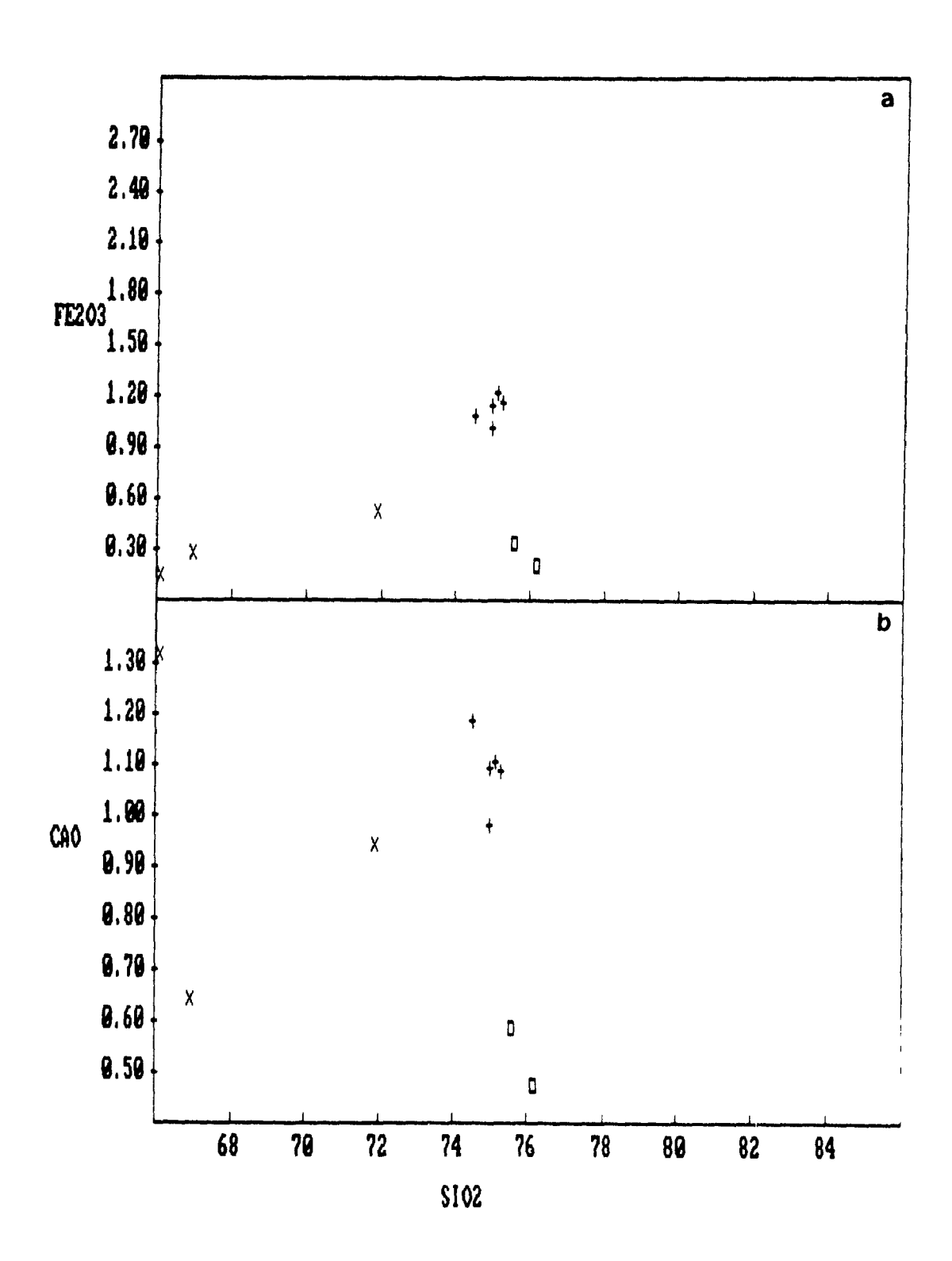


Figure 3.4 Plots of wt % Fe_2O_3 (a), CaO (b) versus SiO_2 diagram. Crosses represent unaltered granite, open boxes represent albitization, X's represent K-feldspathization.

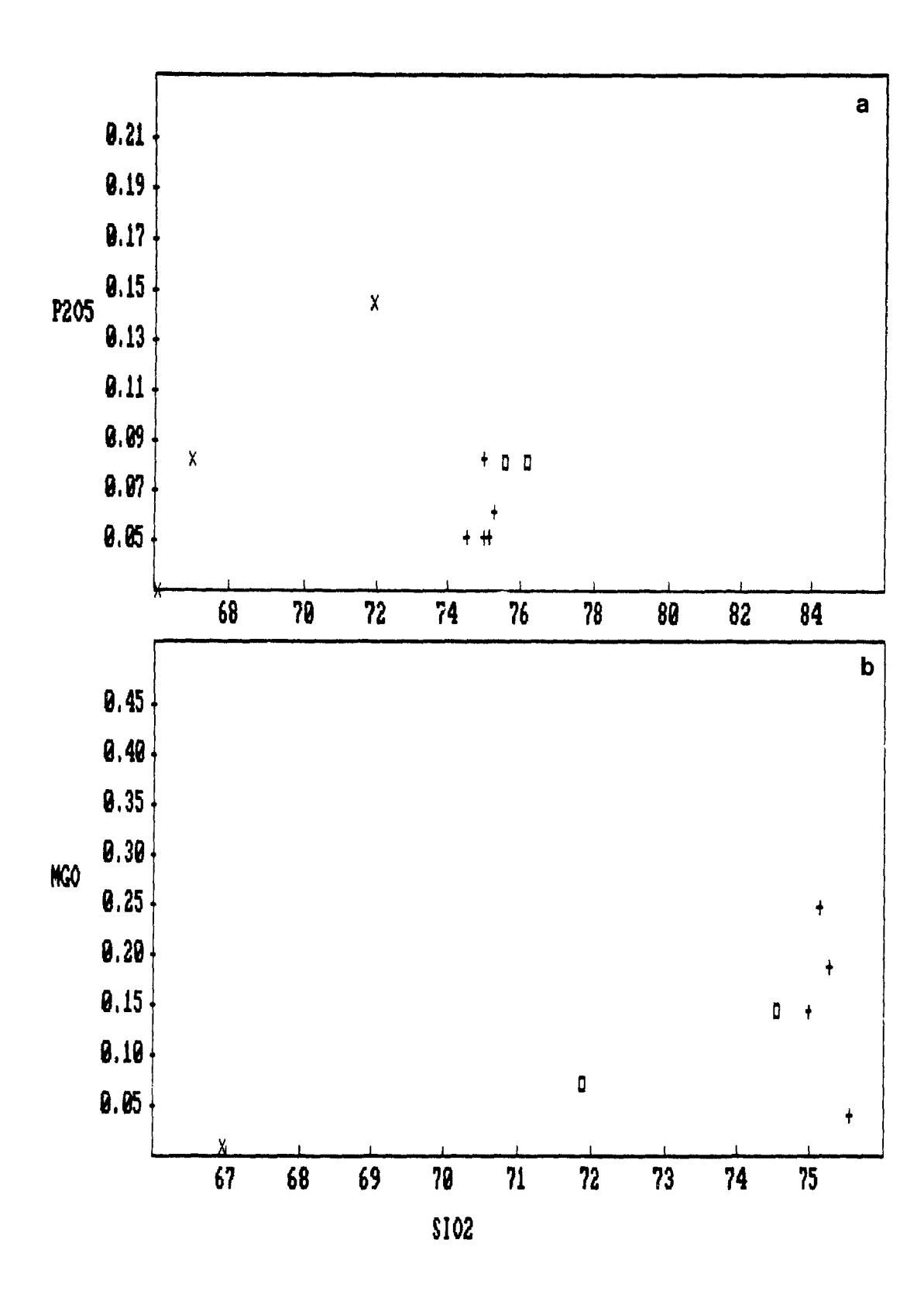


Figure 3.5 Plots of wt $% P_2O_5$ (a), MgO (b) versus SiO₂ diagram. Crosses represent unaltered granite, open boxes represent albitization, X's represent K-feldspathization.

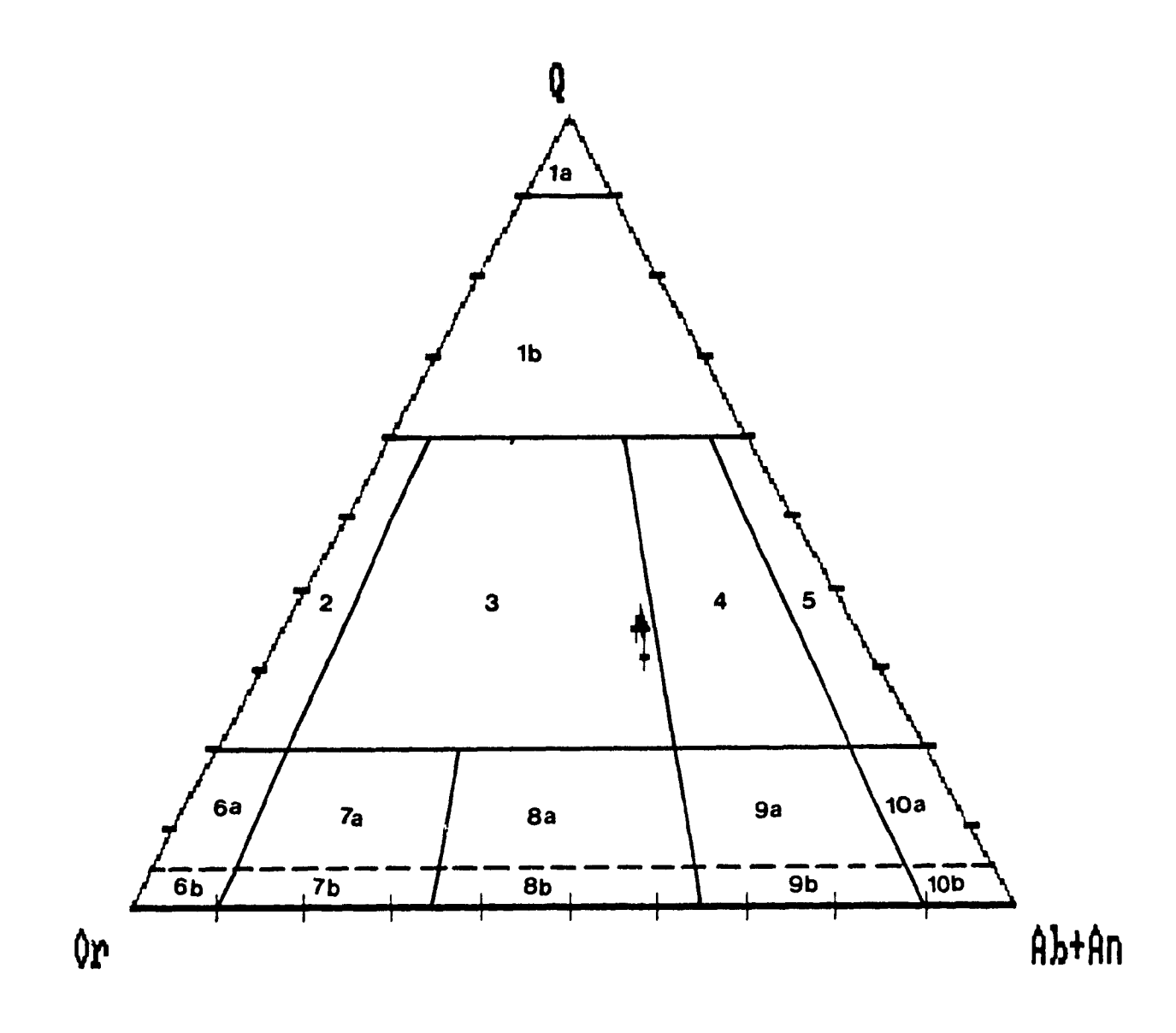


Figure 3.6 Q-Ab+An-Or diagram, showing the classification of intrusive rocks. The numbers mean as follow: 1a, quartzolite; 1b, quartz-rich granitoids; 2, alkalifeldspar granite; 3, granite; 4, granodiorite; 5, tonalite; 6a, quartz alkali-feldspar syenite; 6b, alkali-feldspar syenite; 7a, quartz syenite; 7b, syenite; 8a, quartz monzonite; 8b, monzonite; 9a, quartz-monzodiorite/quartz-monzogabro; 9b, monzodiorite/monzogabbro; 10a, quartz diorite/quartz gabbro/quartz anorthosite; 10b, diorite/gabbro/anorthosite. Dashed lines outline the field of spessartites and kersantites (After Streckeisen 1979). Crosses represent the host rock of the Cadillac molybdenum deposit.

Table 3.1 Whole rock analyses of leucoadamellite

					:	Sample 1	No: LC-	11			
	4A	4B	9 A	9B	5A	5B	26A	26B	29	30A	30B
SiO2	74.43	75.11	74.02	74.49	74.22	75.94	74.34	71.05	65.65	74.63	66.43
TiO2	0.15	0.03	0.13	0.13	0.14	0.02	0.12	0.06	0.02	0.14	0.03
A1203	14.53	14.70	14.72	12.79	15.06	14.38	14.87	16.23	19.93	14.40	18.71
Fe203	1.18	0.33	1.06	0.52	1.11	0.20	0.98	0.51	0.15	1.12	0.27
MnO	0.04	0.01	0.04	0.03	0.03	0.01	0.03	0.02	0.01	0.03	0.01
MgO	0.24	<0.01	0.14	0.04	0.15	<0.01	0.14	0.07	<0.01	0.18	0.01
CaO	1.08	0.58	1.16	1.09	0.96	0.47	1.07	0.92	1.29	1.06	0.63
Na20	3.63	5.20	3.93	1.47	3.58	4.88	3.74	4.58	6.08	3.63	4.39
K20	3.75	3.35	4.11	8.06	3.85	3.71	3.78	5.27	6.14	3.93	8.66
P205	0.05	0.08	0.05	0.03	0.05	0.08	0.08	0.14	0.03	0.06	0.08
V	<10	<10	<10	14	12	<10	<10	<10	<10	11	<10
Cr203	<15	<15	<15	<15	<15	<15	<15	<15	<15	<15	<15
Ni	13	17	<10	11	10	<10	<10	<10	<10	11	<10
BaO	691	386	676	1358	636	477	678	710	642	574	635
Li	123	26	65	38	129	24	118	52	<20	112	46
LOI	0.77	0.46	0.72	1.22	0.94	0.44	0.99	0.94	0.86	1.13	0.73
Total	99.93	99.89	100.14	100.02	100.15			99.86			100.04

In Table 3.1 samples with A represent unaltered rocks, and B altered rocks.

CHAPTER 4

FLUID INCLUSION STUDIES

4.1 INTRODUCTION

Forty-two doubly polished thin sections were prepared for fluid inclusion analyses from samples collected in the Cadillac and Preissac Molybdenum Deposits. Twenty-six of these are from the Cadillac deposit, and sixteen from the Preissac deposit. Microthermometric data were collected from fourteen doubly polished thin sections from the Cadillac deposit, and seven doubly polished thin sections from the Preissac deposit. All samples were from quartz veins with one exception, which was taken from a fluorite vein. Owing to the opaque nature of the fluorite, only a few of the inclusions contained in it could be studied.

Fluid inclusions are common in all quartz-bearing veins. The inclusions range from 5 μm to 40 μm in diameter. All inclusions were classified according to the criteria given by Roedder (1979). Most inclusions are either secondary (they are located along fracture planes and may cross several grains) or pseudosecondary (they occur in planes representing healed fractures and terminate within grain boundaries). Primary fluid inclusions are uncommon. These are isolated and generally have regular shapes. All samples contain more than

one type of fluid inclusion. Many fluid inclusion show evidence of necking down. This has resulted in variable phase ratios amongst some sets of inclusions. Fluid inclusions selected for microthermometric analyses come from sets in which the fluid inclusions had similar phase ratios.

4.2 METHODOLOGY

The doubly polished thin sections were studied with a petrographic microscope to locate fluid inclusions suitable for microthermometric analysis. The parts containing usable fluid inclusions were broken from the polished thin sections and analyzed using an S.G.E. model 3 heating/freezing stage. The stage was calibrated between -56.6° and 600°C using synthetic CO₂ an H₂O fluid inclusions and chemical compounds whose melting temperatures are known.

Each chip was frozen and gradually heated up to the temperature of homogenization. The temperatures of the various phase transitions were recorded and the nature of these transitions noted. Because fluorite is a soft mineral, inclusions in fluorite were heated first and later frozen to obtain the lcw temperature phase changes (if the internal pressure exceeds a certain finite limit due to the expansion of ice on freezing, permanent deformation of the host crystal around an inclusion results (Bodnar 1980). Some phase changes, notably ice melting, could not always be observed

because of the small size of some inclusions. The heating rate was held below 2°-3°C per minute to minimize problems with metastability. The first step in the microthermometric analysis of inclusions involved supercooling them (down to about -100°C for aqueous inclusions, and -135°C for carbonic inclusions). This was done with a flow of gas that had been passed through a copper coil immersed in liquid nitrogen. The inclusions were then warmed slowly by partially cutting off the flow of nitrogen gas, and subsequently by heating the nitrogen gas by passing it through a heating coil. The temperatures of the various phase changes observed during warming were measured with a chromel-alumel thermocouple connected to a digital indicator.

The homogenization of each inclusion was repeated to check the reproducibility of homogenization temperature measurements and to confirm that there had been no prior leakage.

4.3 CLASSIFICATION AND DESCRIPTION OF INCLUSIONS

Fluid inclusions were classified on the basis of general microscopic observation (plate 4.1-4.9), phase relations at room temperature and according to their compositions, which were determined from low temperature phase relationships. The fluid inclusions in quartz and fluorite from the Cadillac and Preissac Molybdenum deposits may be broadly divided into

three main types (1,2,3), and several subtypes.

1. Aqueous inclusions

- la. High to moderate salinity two phase aqueous inclusions, containing liquid H₂O and H₂O vapour.
- 1b. Moderate to low salinity one (liquid H₂O) and two phase (liquid H₂O and H₂O vapour) aqueous inclusions.
- 1c. Low salinity two phase aqueous inclusions, containing liquid H₂O and H₂O vapour.

2. Carbonic inclusions

- 2a. Two or three phase liquid-rich aqueous-carbonic inclusions containing liquid H₂O, liquid CO₂ and/or CO₂ gas.
- 2b. Non-aqueous carbonic inclusions containing liquid CO₂ and vapour CO₂.
- 2c. Two phase vapour-rich carbonic inclusions containing liquid H2O, and CO2 gas.

3. Solid-bearing aqueous inclusions

- 3a. Halite-bearing aqueous inclusions with or without a vapour phase.
- 3b. Aqueous inclusions containing solid trapped phases with or without vapour phase.

4.3.1 Type 1 Inclusions

Type 1 inclusions predominate in all types of material studied. Most are smaller than 30 μm in diameter. Those

analyzed microthermometrically generally ranged between 10 and 20 μm in diameter.

Type 1a inclusions contain two phases at room temperature, liquid H_2O , and vapour H_2O (Plate 4.1). The latter typically occupies 20 to 30 percent of an inclusion by volume (calculated using the equation given by Bodnar 1983). These high to moderate salinity inclusions generally have regular shapes and range up to 20 μ m in diameter. Type 1a inclusions do not contain any salt crystals, but hydrohalite sometimes formed during a freezing run.

Type 1b inclusions contain either liquid and vapour (Plate 4.2), or only liquid (Plate 4.3) at room temperature. In those inclusions which contain liquid and vapour, the vapour bubble occupies 3 to 25 percent of an inclusion by volume. Type 1b inclusions are most common along fracture planes and are clearly of secondary origin. They typically range from 5 μ m to 40 μ m in diameter, but they can be as large as 70 μ m in diameter, and are irregular in shape.

Type 1c inclusions have 10w salinity, and contain two phases at room temperature, an aqueous liquid and a vapour phase (Plate 4.4). Vapour bubbles typically occupy 40 percent of an inclusion by volume. They occur as isolated primary inclusions, are regular in shape, and are typically 15 μ m-20 μ m in diameter.

4.3.2 Type 2 Inclusions

Type 2a inclusions contain two phase (liquid H_2O and liquid CO_2) or three phase (liquid H_2O , liquid CO_2 , and CO_2 gas) at room temperature (Plate 4.5). The relative proportion by volume of CO_2 (liquid+vapour) to aqueous solution varies within the range of 1:4 to 3:2.

Type 2b inclusions contain either liquid CO₂ or liquid CO₂ and vapour CO₂ phases at room temperature (Plate 4.6), and in most cases are found with vapour rich Type 2c inclusions (Plate 4.7). Although they are generally found in clusters, it is not uncommon to see Type 2b inclusions along fracture planes and they are therefore clearly secondary.

Type 2c inclusions are of low density. They homogenize to a vapour phase which generally occupies 60 to 80 percent of the inclusion by volume at room temperature (Plate 4.7). Their shape varies from regular to irregular and their size is typically 25 μm to 7 μm .

Type 2c (Plate 4.7) and some Type 2a inclusions show variable carbonic fluid/ H_2O volume ratios at room temperature. They vary from a few μm to 30 μm in diameter and occur as primary, secondary or pseudosecondary inclusions in quartz veins. Primary inclusions have regular shapes and range from 10 to 20 μm in diameter, whereas secondary inclusions have irregular to regular shapes and are up to 30 μm in diameter.

Some Type 2a and 2b inclusions contain tabular solid

phases that are strongly anisotropic. They have variable phase ratios that are emphasized by the absence of one or more minerals between otherwise similar inclusions within the same plane or cluster of inclusions. This probably indicates accidental trapping of crystals. On heating none of the solids were observed to dissolve.

4.3.3 Type 3 Inclusions

Type 3a inclusions generally contain liquid ± vapour and a single colourless, isotropic crystal, generally of cubic shape, but in some cases with a round or imperfect squarish outline. This mineral is interpreted to be halite (plate 4.8). Type 3a inclusions (Plate 4.8) occur along healed fractures and are therefore secondary. They commonly do not contain vapour at room temperature. Where a bubble is present it is generally small at room temperature occupying 1 to 5 percent by volume of an inclusion. Type 3a inclusions may nucleate hydrohalite on freezing (Plate 4.10).

Type 3b inclusions contain solid trapped phases (as evidenced by variable solid-liquid ratios and by the failure of the solid phases to dissolve on heating) \pm vapour at room temperature (Plate 4.9), and are associated with Type 3a inclusions (Plate 4.9). They are very irregular and vary from a few μ m to about 45 μ m in diameter. Type 3b inclusions may also nucleate hydrohalite on freezing.

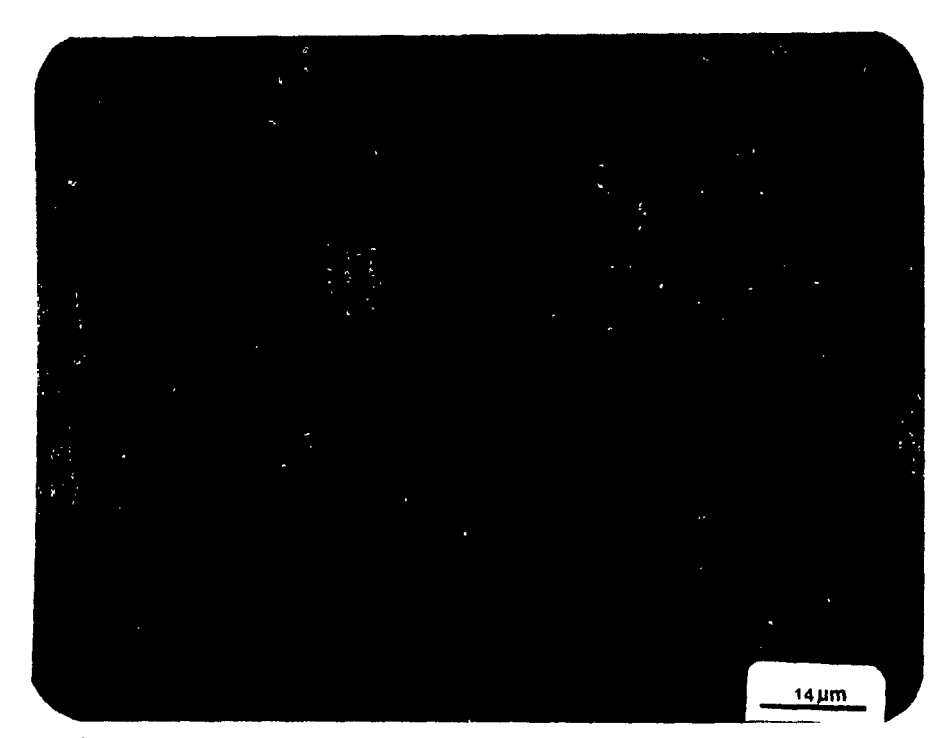


Plate 4.1 High to moderate salinity two phase Type 1a aqueous inclusions.

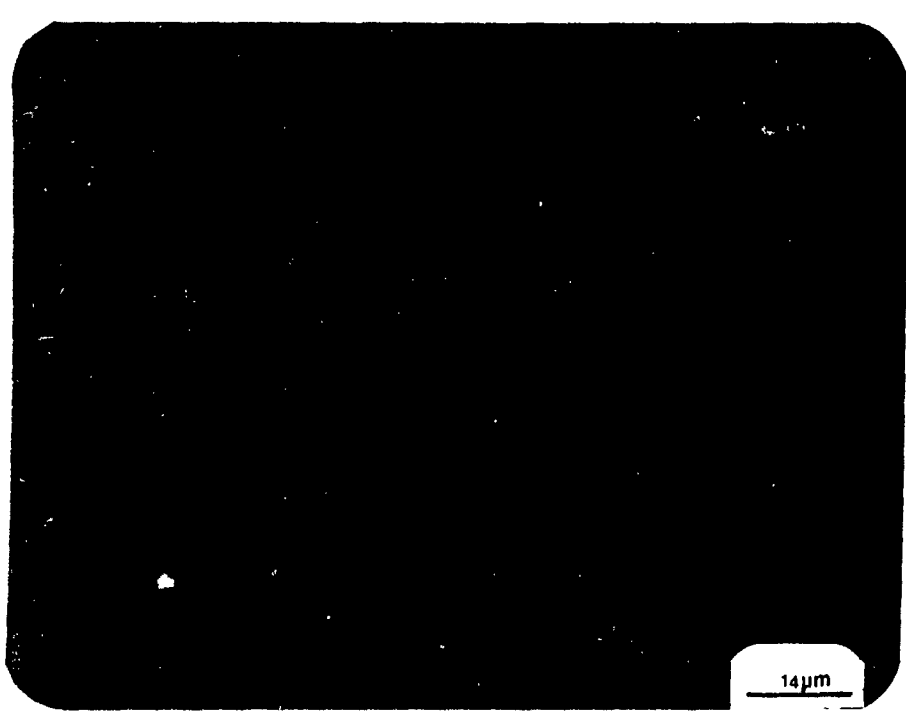


Plate 4.2 A moderate salinity two phase Type 1b aqueous inclusion.

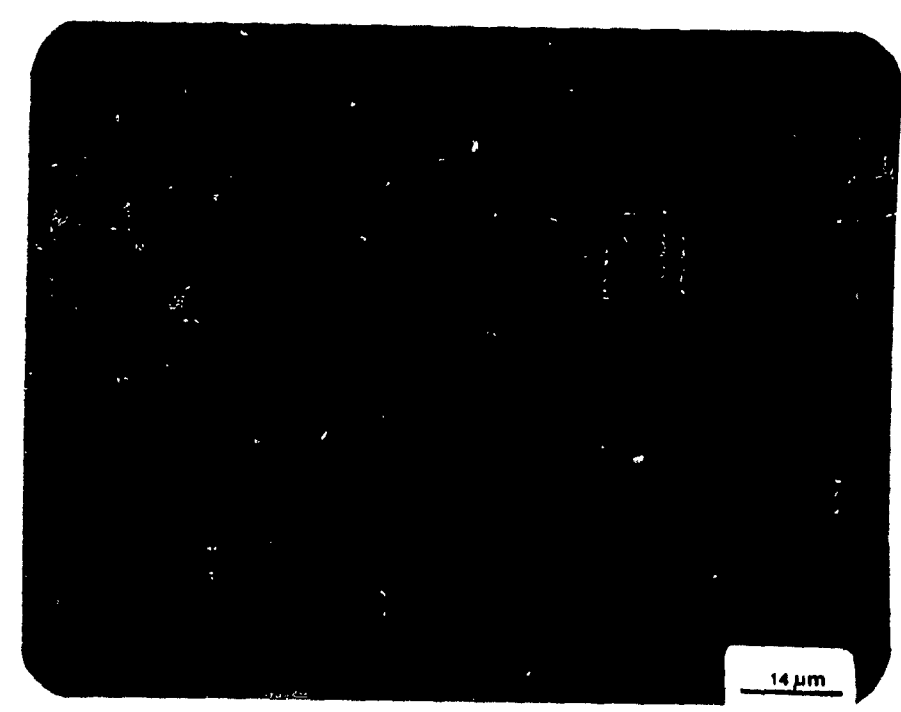


Plate 4.3 Moderate to low salinity one phase (liquid) Type 1b aqueous inclusions.



Plate 4.4 A low salinity two phase Type 1c inclusion.

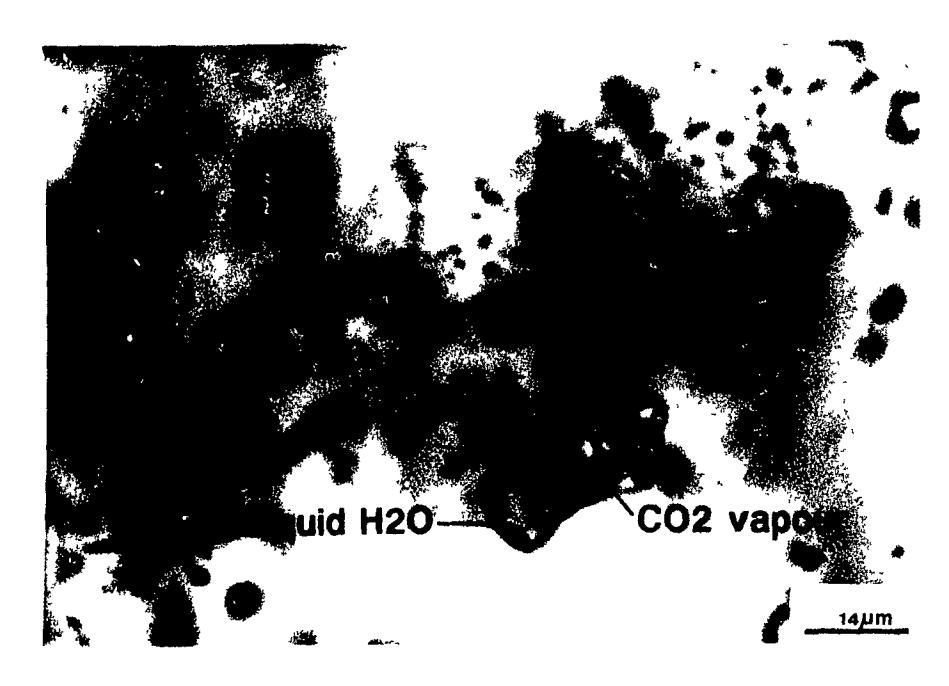


Plate 4.5 A three phase Type 2a aqueous-carbonic inclusion, containing liquid ${\rm H_2O}$, liquid ${\rm CO_2}$, and ${\rm CO_2}$ vapour.



Plate 4.6 One phase (liquid) Type 2b carbonic inclusions.



Plate 4.7 Vapour-rich, two phase Type 2c carbonic inclusions, and a single Type 1a aqueous inclusion.



Plate 4.3 Halite-bearing Type 3a aqueous inclusions.

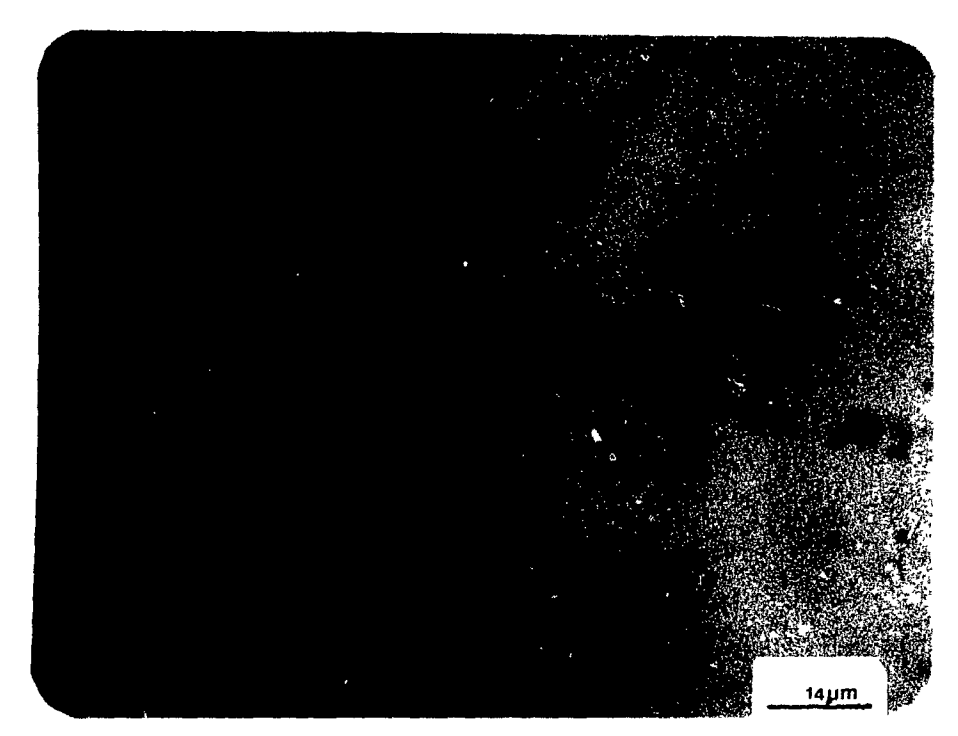


Plate 4.9 Trapped mineral-bearing Type 3b aqueous inclusions

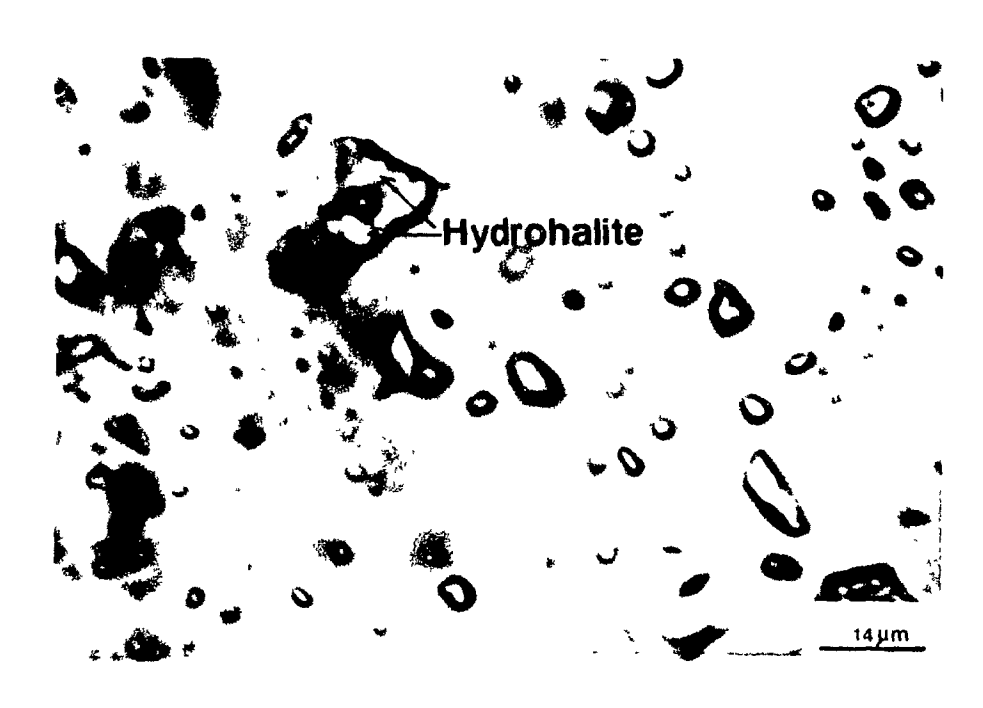


Plate 4.10 Formation of hydrohalite in Type 3a inclusions. The photo was taken after the sample had been frozen.

4.4 DISTRIBUTION OF FLUID INCLUSION TYPES

Type 1, 2, and 3 inclusions are present in each of the quartz vein classes described above. The majority of inclusions are Type 1, and in most cases they are secondary, but a few primary, low salinity (Type 1c) inclusions have been identified as isolated inclusions (Plate 4.4). High to moderate salinity (Type 1a) inclusions are pseudosecondary to secondary and are also found in most of the quartz veins. Carbonic (Type 2) inclusions are primary, pseudosecondary, or secondary and are the second most abundant inclusions after Type 1 inclusions in almost all samples. Type 3 inclusions are uncommon in all samples and are clearly secondary. Type 3b inclusions, as will be discussed later, are secondary and reflect the heterogenous trapping of solid phases suspended in the hydrothermal solution.

Only Type 1a, 1b, and Type 3b inclusions have been recognized in fluorite (sample LC-11-3). The reason for this may be that, as mentioned earlier, the fluorite is quite opaque and therefore very few inclusions were observed.

The distribution of the various inclusion types are indicated qualitatively in Table 4.1 for the Cadillac and the Preissac molybdenum deposits, with the corresponding vein and wallrock mineralogy. The distribution pattern shows the high abundance of Type 1 inclusions throughout all of the samples studied. Type 1b inclusions are more common than Type

la, and 1c inclusions. Type 1c inclusions are rare in all samples. Carbonic inclusions were observed in most of the samples in quartz. There is no obvious correlation between fluid inclusion types and alteration. But Type 2b inclusions are more common in K-reldspar alteration than albitic alteration. It is interesting to note that both albitic and potassic alteration are associated with low titanium (Table 4.1).

Table 4.1 Distribution of the inclusion types with the corresponding vein and wall rock mineralogy in the Cadillac and the Preissac molybdenum deposits.

		Sul.Min.	Oxid.Min.		71+							
Vein	Sil.Min.			Type 1 Incl.			Type 2 Inc.			Type 3 Inc.		Altera- tion
Туре				1a	1b	1c	2a	2b	2c	3a	3b	
d+m	q+pl+k.f +m+bi+ap zi+cc	Mo+py+ sp +cp	ilmenite+ rutile	С	VC	R	С	R	R	R	R	Albitic
q+m+ k.f	q+pl+k.f+ m+ti+cc+ zi	Mo+Bi	ilmenite	С	vc	R	С	vc	R	R	R	K-felds- par
q		ру			vc		С					
Fluo rite				С	С					R		

Sil.=Silicate, Sul.=Sulphide, Oxid.=Oxide, q=quartz, pl=plagioclase, k.f=K-feldspar, m=muscovite, cc=carbonate, zi=zircon, ap=apatite, bi=biotite, Mo=molybdenite, Bi=bismuthinite, cp=chalcopyrite, py=pyrite, sp=sphalerite, VC=very common, C=Common, R=rare.

4.5 LOW TEMPERATURE PHASE RELATIONSHIPS

4.5.1 Aqueous Inclusions

The following temperature measurements were made for aqueous (Type 1) inclusions: The first melting of ice, final melting of ice, and melting of hydrate which formed in high salinity (Type 1a) inclusions. During freezing, aqueous inclusions exhibited two kinds of behaviour; large inclusions showed a sudden appearance of a large number of crosscutting dark lines, indicating the multinucleated growth of ice. Other inclusions turned grey and remained relatively transparent, probably indicating the formation of a single ice crystal. On warming, the first liquid appeared in the temperature range -77° to -24°C for Type la, lb inclusions, and -45° to -24°C for Type 1c inclusions. The inclusions that exhibited multinucleated growth of ice showed the appearance of granular ice crystals and liquid on gradual warming. In such cases, it was easy to establish the final temperature of ice melting under reversible equilibrium conditions. In those inclusions that remained clear on freezing, a single ice crystal was generally seen on warming. When the ice crystal became very small during warming, it was more easily seen by dropping the temperature and observing shifts in the position of the vapour bubble. The ice crystal against the vapour bubble and distorted it. This phenomenon

was particularly helpful in obtaining freezing temperatures of some low density inclusions. Some single phase liquid inclusions nucleated small vapour bubbles on cooling. The final melting temperature of ice for Type 1a inclusions ranged about from -16° to -31.8°C, for Type 1b inclusions about from -15°C to almost 0°C, and for Type 1c inclusions from -1.2° to -3°C. The melting temperature of hydrate observed in some high salinity inclusions ranged from -9.6° to +8.3°C.

In fluorite the first melting temperature of ice ranges from -65° to -40° C, and last melting temperature of ice ranges from -15° to -28° C.

4.5.2 Carbonic Inclusions

Low temperature phase transition data measured for carbonic inclusions consisted of the initial melting temperature of carbonic ice, the final melting temperature of carbonic ice, the initial melting temperature of H₂O ice, and the final melting temperature of clathrate. On freezing clathrate forms at a temperature of between -25° and -27°C. Melting of the solid carbonic phase commenced at temperatures ranging between -110° and -59.5°C. The last melting of carbonic ice crystals occurred between -59.0° and -56.6°C with a mean of -56.7°C for the Cadillac deposit and -57.8 for the Preissac deposit, indicating that they consist

largely of CO_2 . The first visible change on further heating was the initial melting of H_2O ice, at temperatures ranging from -46.6° to -24.8°C. The last melting of ice could only be observed in a few cases because of the difficulty of distinguishing ice from clathrate; the observed range of final H_2O -ice melting is between -2° and -7.8°C. After the final melting of ice, the clathrate appeared to have an index of refraction less than that of the aqueous liquid but greater than that of the liquid CO_2 . The melting temperature of clathrate ranges from 6° to 10°C. The lack of clathrate melting temperatures above 10°C indicates that CH_4 is a insignificant component of the carbonic phase (Collins 1979, Burruss 1981).

4.5.3 Solid-Bearing Aqueous Inclusions

Low temperature data collected for Type 3a inclusions include the initial melting temperature of H₂O ice, which ranges from -64° to -40°C, the final melting temperature of H₂O ice, which ranges from -34° to -19°C, and the melting of hydrate, which ranges from -16.4 to 31°C. During the freezing runs some halite-bearing inclusions (Type 3a) nucleated a gas bubble. The explanation for the lack of a vapour bubble at room temperature is usually assumed to be metastability (Roedder 1984, p. 294). Formation of hydrohalite crystals in Type 3a inclusions provides a very good test for

distinguishing halite from sylvite, which forms no such hydrate (Roedder 1984, p.98). The presence of halite in these inclusions has been confirmed with the scanning electron microscope (see section 4.10).

Type 3b inclusions show similar behaviour to Type 3a inclusions in term of melting relationships. Hydrohalite may form during the freezing run. The following measurement were made for Type 3b inclusions: first melting temperature of ice, which ranges from -60° to -40°C, the final melting temperature of ice, which ranges from -15.5° to -22.6°C, and the melting temperature of hydrate which ranges from -9.6° to +9.2°C.

4.6 HIGH TEMPERATURE PHASE RELATIONSHIPS

4.6.1 Aqueous Inclusions

A total of 323 inclusions in 15 samples from the Cadillac and 62 inclusions in 7 samples from the Preissac Molybdenum Deposits were heated until homogenization occurred. About 60 percent of these inclusions were Type 1,30 percent were Type 2, 10 percent were Type 3. Figure 4.1 show the homogenization temperatures of Type 1 inclusions from the Cadillac and Preissac Molybdenum Deposits. Although the Cadillac molybdenum fluid inclusions apparently give higher maximum homogenization temperatures up to (650°C) (these high temperatures could reflect necking down) than the Preissac molybdenum inclusions

the mode of the homogenization temperature distribution is approximately the same (375°C) for both deposits. Therefore, statistically there is no significant difference homogenization temperature of the fluid inclusions in the two deposits. Figure 4.1 also shows the homogenization temperatures of Type 1 inclusions from veins with either albitic (Fig. 4.1c) or K-feldspar (Fig. 4.1d) alteration halos in the Cadillac molybdenum deposit. The peak homogenization temperature is the same for fluid inclusions in veins with albitic alteration haloes as that for veins with K-feldspar alteration haloes (375°C). The homogenization temperatures for subvertical and subhorizontal veins are similar (Fig. 4.2). The homogenization temperatures of Type 1 inclusions from fluorite range from 107.4° to 336°C with a peak between 225° and 300°C. They homogenize at somewhat lower temperature than in quartz (Fig. 4.2c).

Two types of behaviour were observed during the heating of aqueous inclusions: In some inclusions, the vapour bubble vibrated on heating, or changed direction rapidly when close to the homogenization temperature. In a few inclusions the vapour bubble became smaller on initial heating, then appeared to maintain constant volume through much of the heating process until finally the meniscus became hazy, and the boundary between vapour and liquid disappeared. This kind of behaviour is evidence that the fluid has a critical density (Roedder 1972).

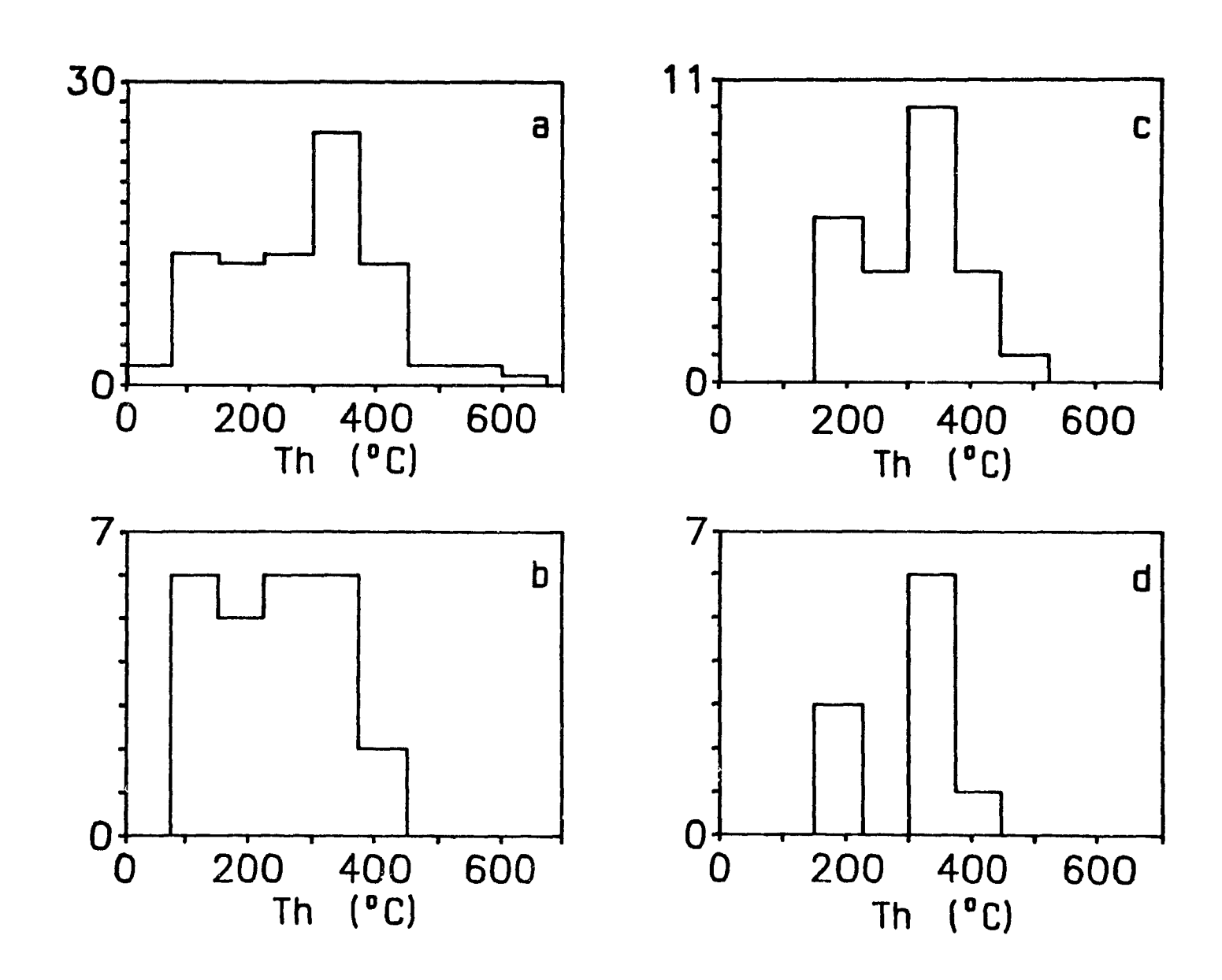
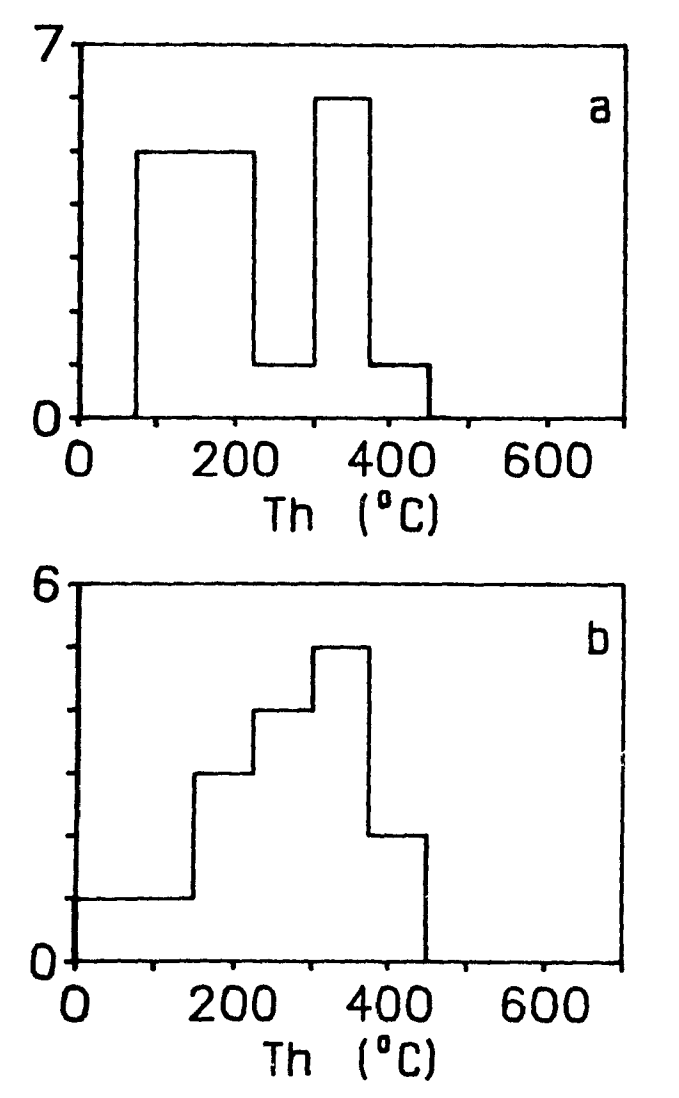


Figure 4.1 Histograms, showing homogenization temperatures versus frequency for aqueous Type 1 inclusions.

a) veins in the Cadillac deposit, b) veins in the Preissac deposit, c) veins with albitic alteration haloes in the Cadillac deposit, d) veins with K-feldspar alteration haloes in the Cadillac deposit.



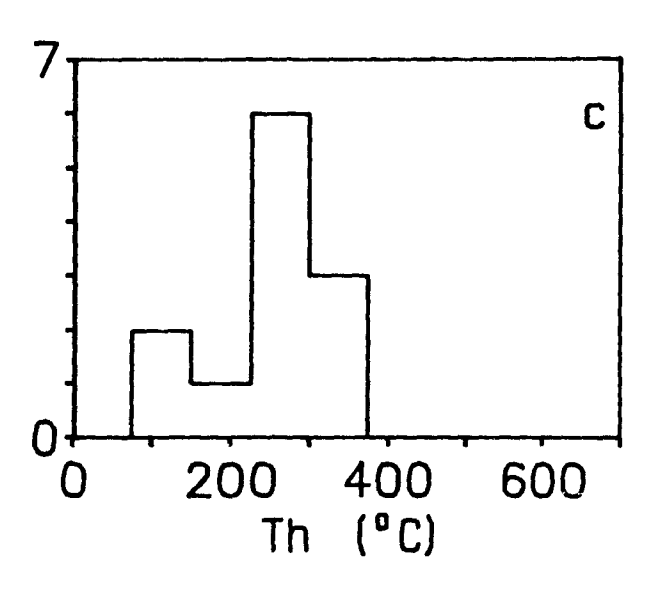


Figure 4.2 Histograms showing the frequency distribution of homogenization temperatures for Type 1 aqueous inclusions in a) subvertical veins, b) subhorizontal veins, c) fluorite.

4.6.2 Carbonic Inclusions

Most of the carbonic inclusions decrepitated prior to homogenization owing to the build up of high internal pressures (Burruss 1981). Those inclusions that did not decrepitate homogenized to the H₂O-rich phase, the CO₂-rich or exhibited critical phenomena. The frequency phase distribution of the homogenization/decrepitation temperatures for carbonic inclusions are shown in Figure 4.3 from the Cadillac and Preissac molybdenum deposits. The peak homogenization temperature is between 225° and 300°C in both deposits. The carbonic vapour homogenizes to carbonic liquid at temperatures between -21° and 31°C, with a peak between 29° and 31°C in the Cadillac deposit, and between 16° and 31°C, with a peak between 26°and 31°C in the Preissac deposit, indicating that carbonic fluid is composed largely of CO, with only minor amounts of dissolved species (e.g, CH,).

Homogenization temperatures obtained from Type 2c inclusions are variable because of the fact that small amounts of liquid were trapped with the vapour and small amounts of vapour with the liquid. Thus, vapour-rich inclusions homogenized from 281° to 525°C with a mean of 372.2°C. In some cases homogenization couldn't be observed even at temperatures of >600°C.

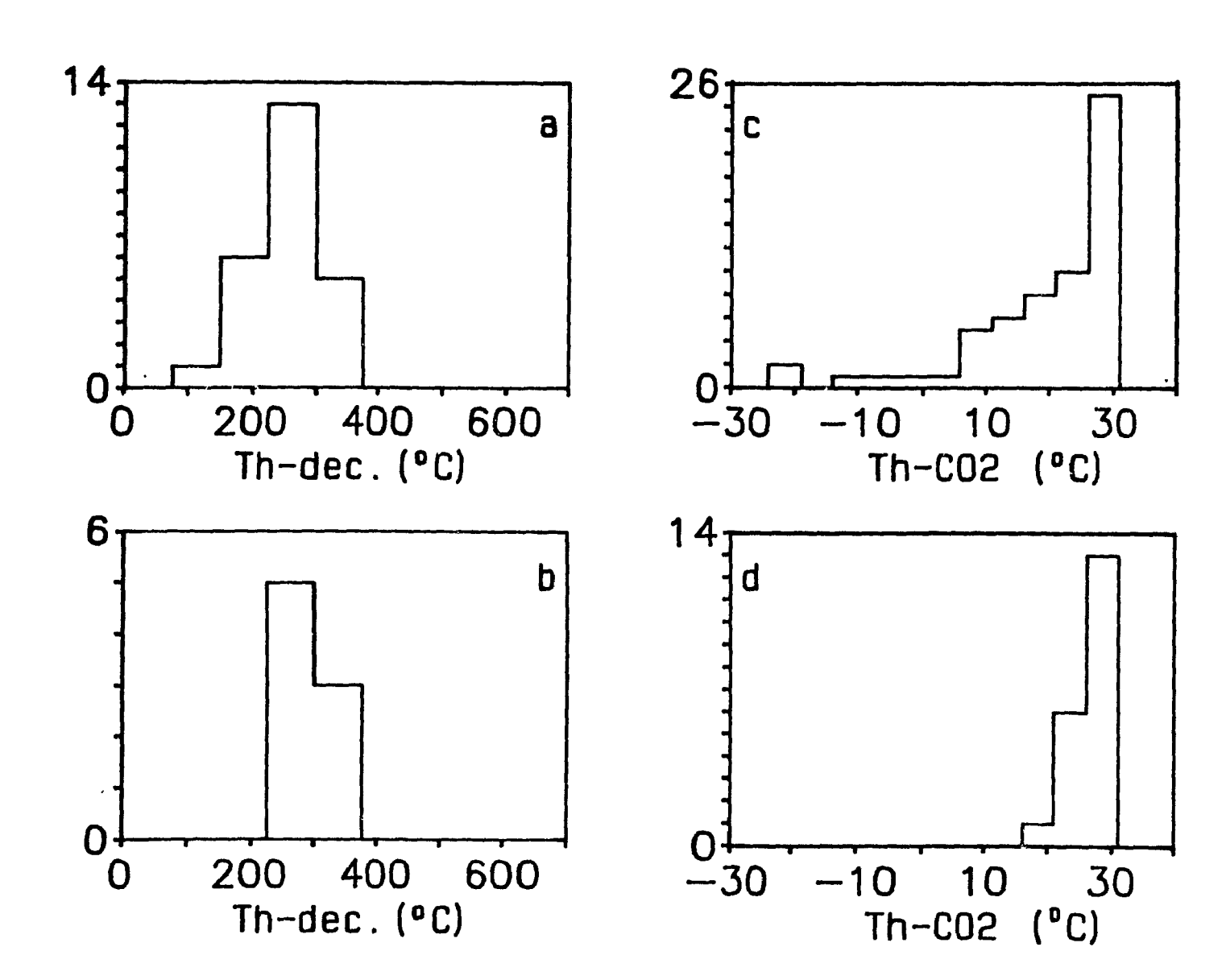


Figure 4.3 Histogram, showing homogenization/decrepitation temperature versus frequency (a- veins from the Cadillac deposit, b- veins from the Preissac deposit), and temperatures of homogenization of the carbonic phases of carbonic inclusions (c-veins from the Cadillac deposit, d- veins from the Preissac deposit).

4.6.3 Solid-Bearing Aqueous Inclusions

In Type 3a inclusions liquid-vapour homogenization generally occurs at temperatures lower than those of halite dissolution temperatures (Fig. 4.4). In a few cases the vapour bubble and halite disappeared at the same temperature. Figure 4.4 shows the homogenization temperature either by halite dissolution (ranges from 130° to 240°C) or vapour disappearance for Type 3a inclusions.

Type 3b inclusions show slightly higher homogenization temperatures than Type 3a inclusions (Fig. 4.4). Type 3b inclusions may or may not contain vapour at room temperature. The solid phases don't dissolve in Type 3b inclusions. The homogenization temperature is thus considered to be that of vapour disappearance temperature for Type 3b inclusions.

In one Type 3b inclusion, halite and a trapped mineral were found together. The halite homogenized at 146.3°C but the trapped mineral didn't dissolve. This may imply that Type 3a and 3b inclusions are related.

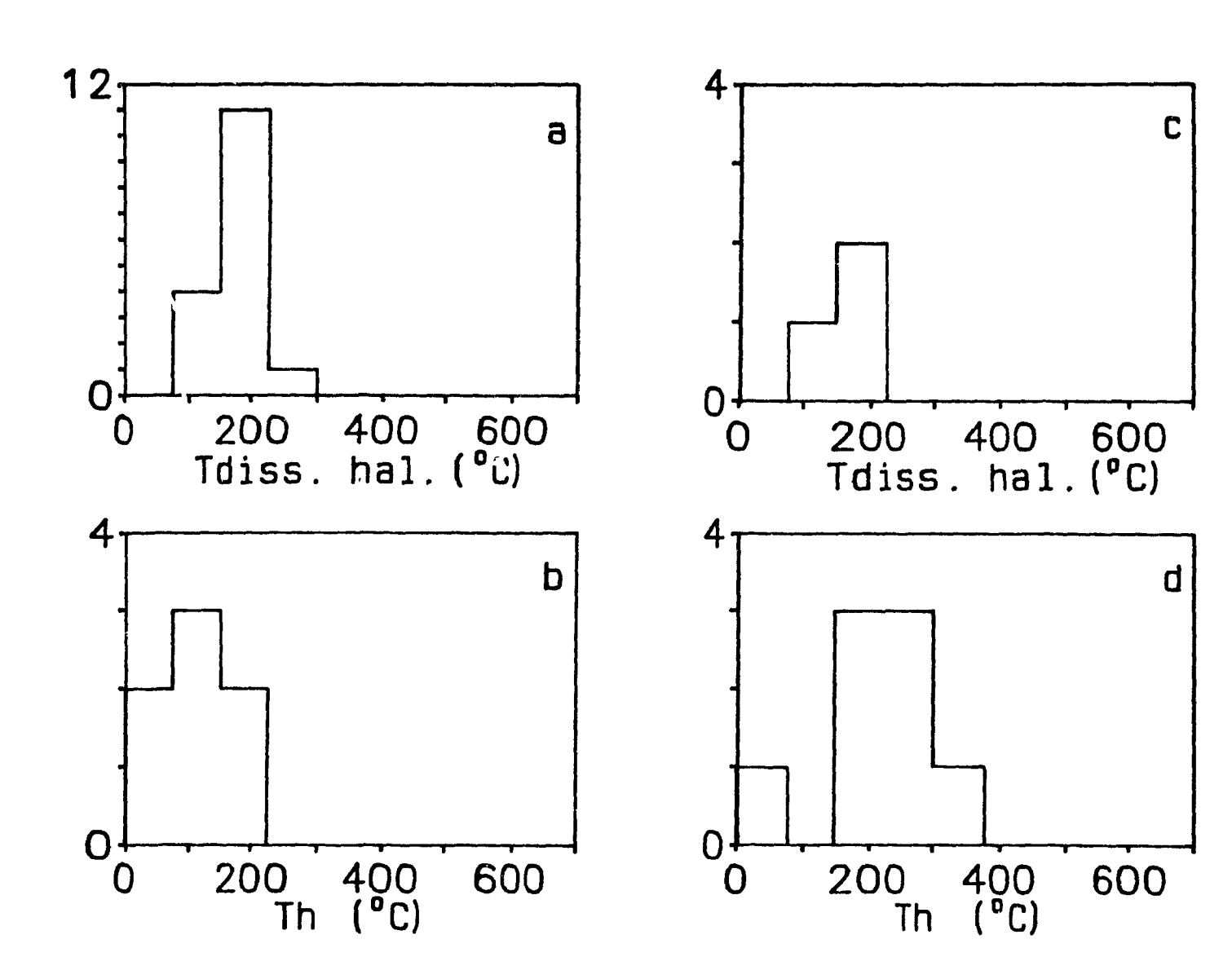


Figure 4.4 Distribution of halite dissolution temperatures in Type 3a inclusions (a- in veins from the Cadillac deposit, c- in veins from the Preissac deposit), and vapour disappearance temperatures in Type 3a inclusions (b-in veins from the Cadillac deposit), and vapour disappearance temperatures in Type 3b inclusions (d- in veins from the Cadillac deposit).

4.7 SALINITY ESTIMATES

4.7.1 Aqueous Inclusions (Type 1)

The final melting temperature of ice was used to determine salinities for Type 1 aqueous inclusions, using the following equation given below of Potter et al. (1978).

wt % NaCl eq. = $0.00-1.76958Tm_{1ce}-4.2384E-02Tm_{ice}^2-5.2778E-04Tm_{ice}^3\pm0.028$

where T_{mice} is the ice melting temperature in °C.

The salinities for Type 1 inclusions, thus calculated, range from 2.06 to 30.38 equivalent wt % NaCl. Figure 4.5 shows salinity data for Type 1 inclusions in quartz. The data show three distinct salinity groupings with peaks of 5, 18, and 26 wt % NaCl equivalent fluids in the Cadillac Molybdenum deposit and, two groupings with peaks of 5 and 17 wt % NaCl equivalent in the Preissac Molybdenum deposit. This suggests that similar low and moderate type 1 fluids were present in both hydrothermal systems but that high salinity Type 1 fluids were only present in the Cadillac hydrothermal system. Figure 4.6 also shows the salinity data for subvertical and subhorizontal veins from the Cadillac molybdenum deposit.

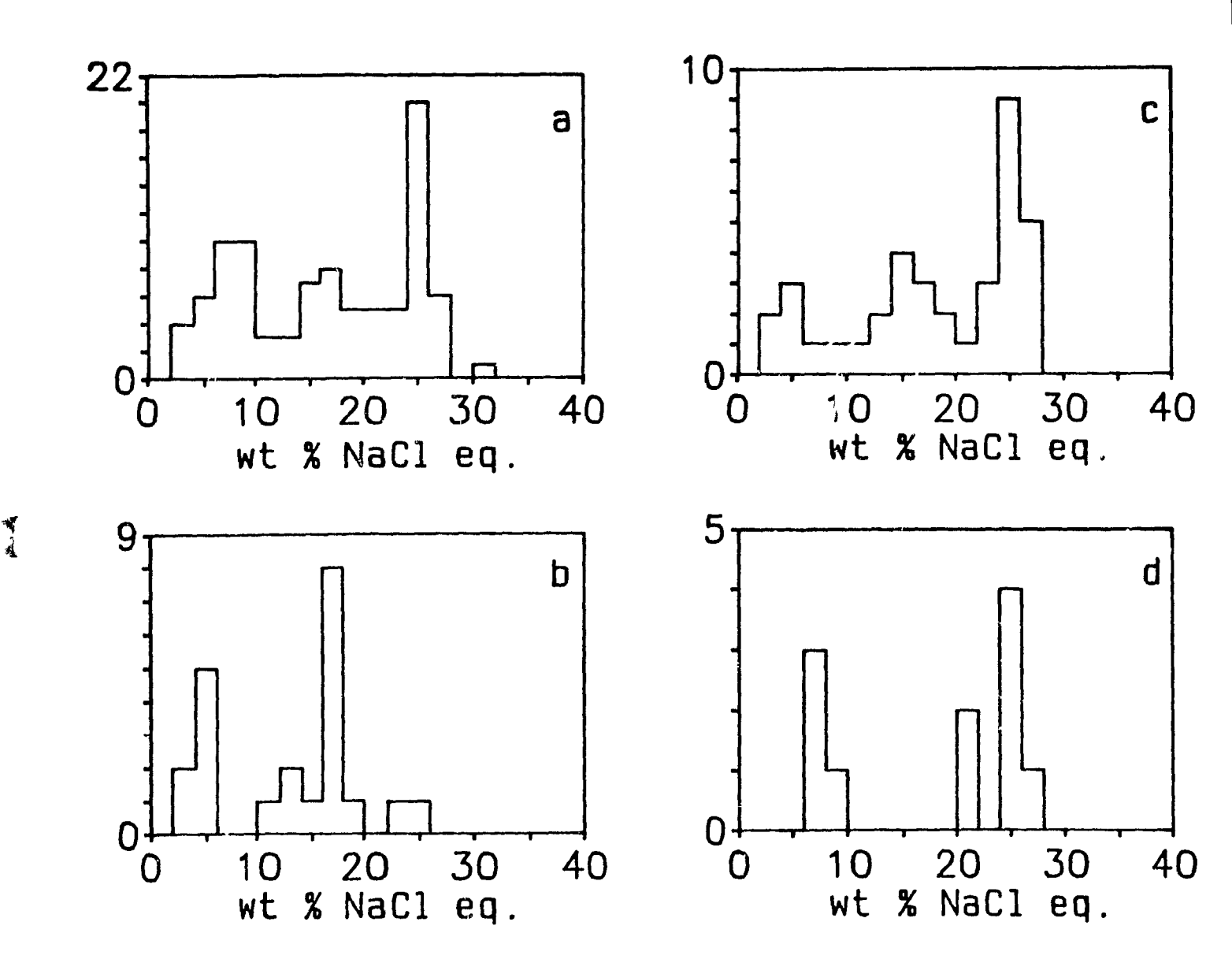
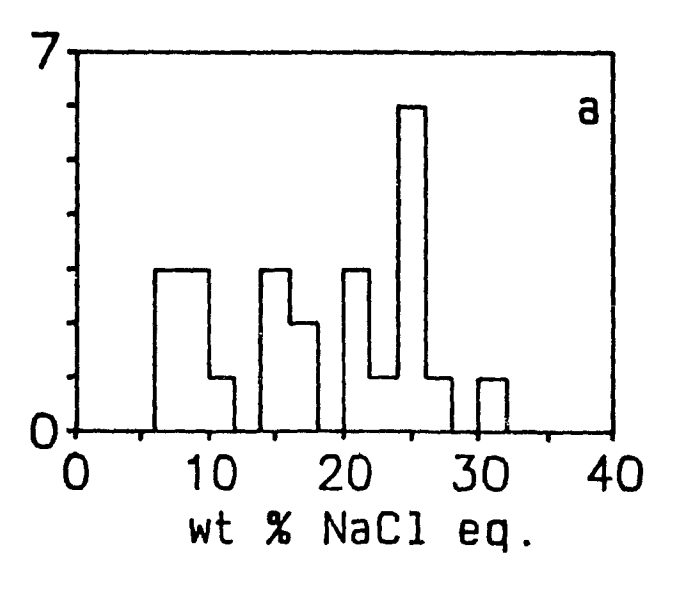
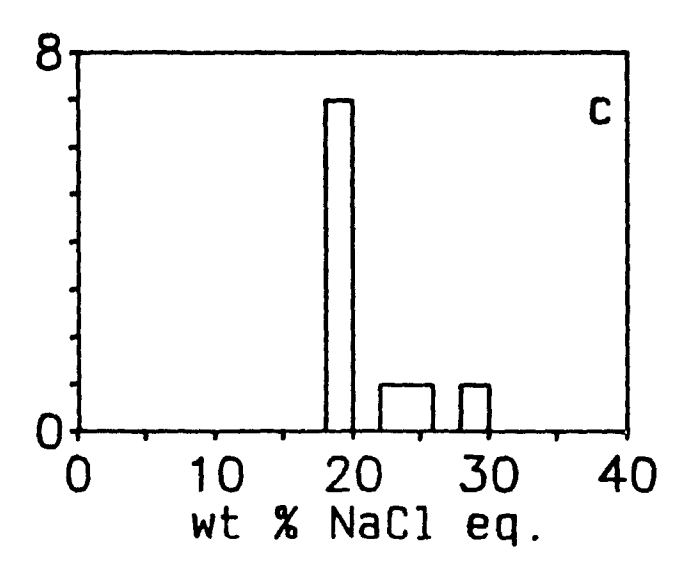


Figure 4.5 Salinity versus frequency histograms for Type 1 aqueous inclusions. a- veins from the Cadillac deposit, b- veins from the Preissac deposit, c-veins with albitic alteration haloes from the Cadillac deposit, d- veins with K-feldspar alteration haloes from the Cadillac deposit.





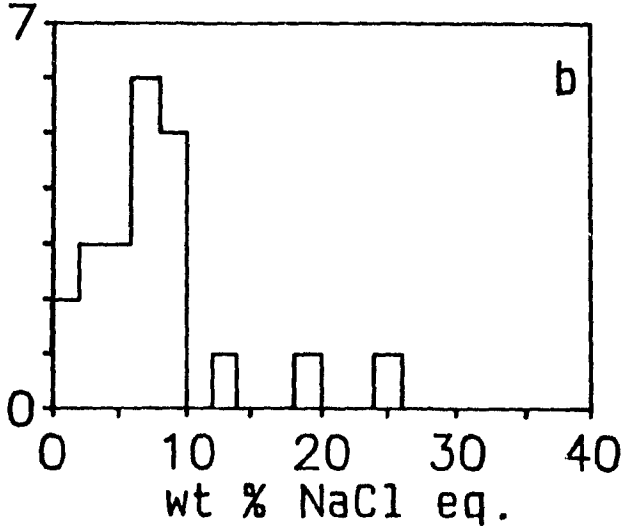


Figure 4.6 Salinity versus frequency histograms for Type 1 inclusions from the Cadillac deposit. a- in subvertical veins, b- in subhorizontal veins, c- in fluorite.

Inclusions from subhorizontal veins have mainly low salinity whereas those from subvertical veins show a broad range of salinities with higher values being more frequent.

The salinity of inclusions in fluorite ranges from 18 to 28 wt% NaCl equivalent with a peak of 18 wt% NaCl equivalent (Fig. 4.6c).

4.7.2 Carbonic Inclusions (Type 2)

Salinities for Type 2a and c carbonic inclusions were calculated using the equation given by Bozzo et al. (1975), in which the clathrate melting temperature is related to the salt content of the fluid inclusion.

wt % NaCl =
$$0.05286 (10-Tm_{clath}) (Tm_{clath}+29.361)$$

Calculated salinities for carbonic inclusions range from 0.41 to 8.29 equivalent wt % NaCl, with a peak of 6 equivalent wt % NaCl (Fig. 4.7).

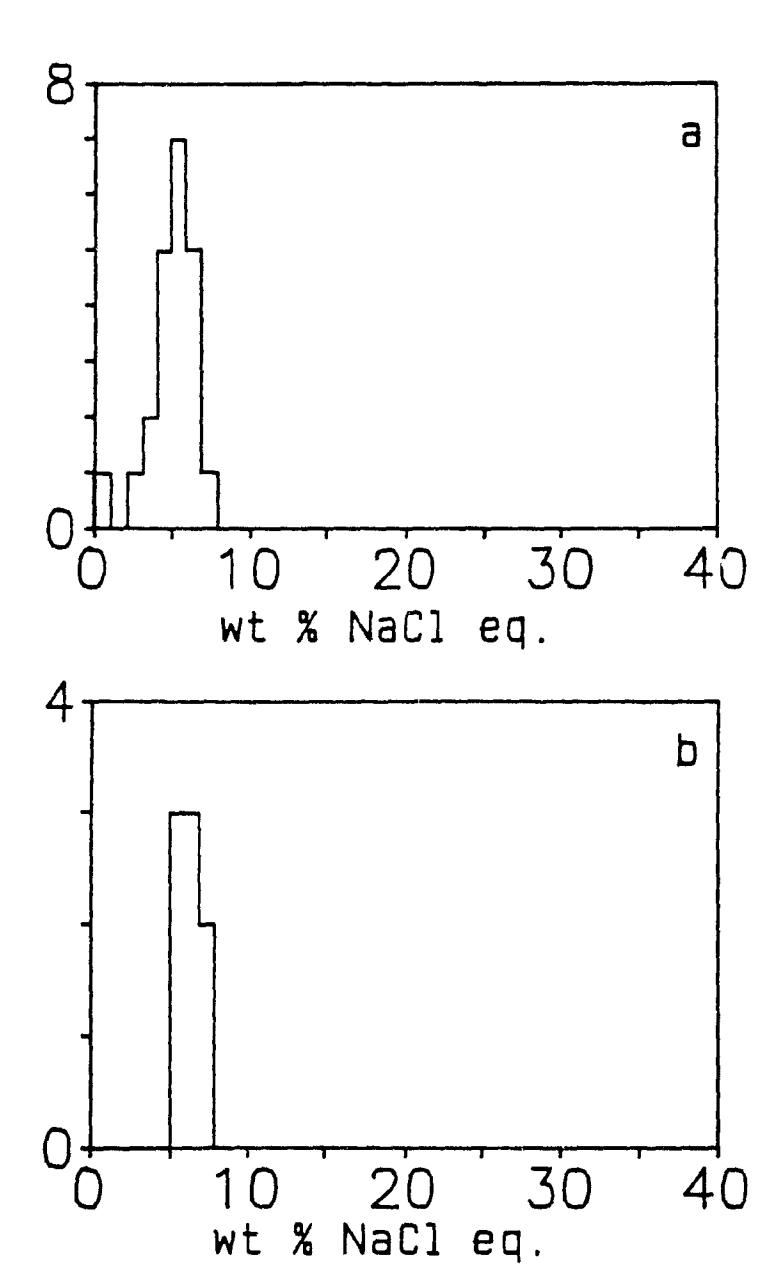


Figure 4.7 Salinity histograms for carbonic inclusions. aveins from the Cadillac deposit, b- veins from the Preissac deposit.

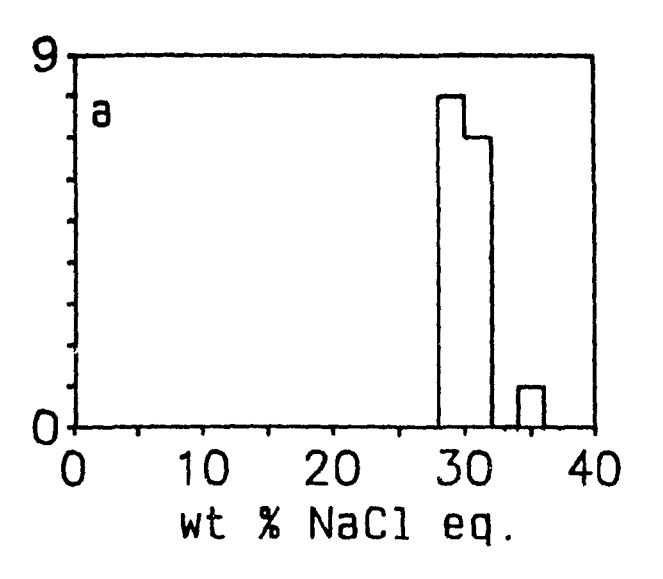
4.7.3 Solid-Bearing Aqueous Inclusions (Type 3)

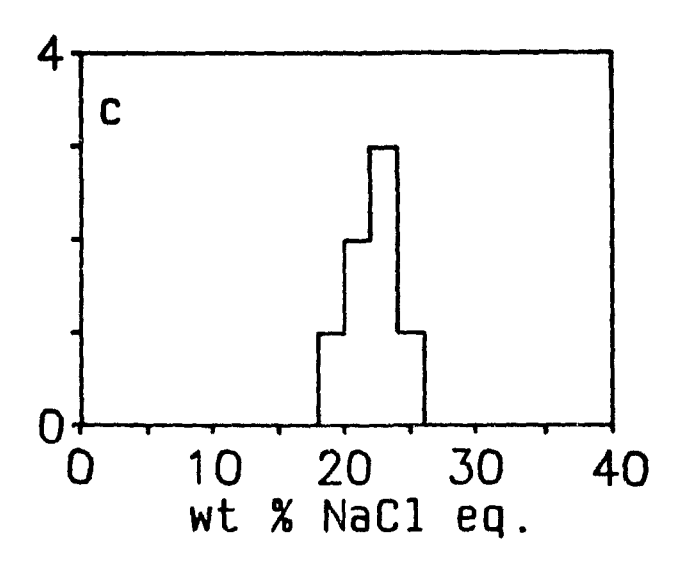
The salinities of halite-bearing aqueous inclusions were calculated using the halite dissolution temperature in conjunction with the formula given by Potter et al. (1977);

wt percent NaCl =
$$26.218 + 0.0072Tm_{halite} +$$

 $0.000106Tm_{halite}^2 \pm 0.05$

The calculated salinities for halite-bearing aqueous inclusions range from 28.95 to 34 wt percent equivalent NaCl in the Cadillac molybdenum deposit, and from 28 to 30 wt percent equivalent NaCl in the Preissac molybdenum deposit (Fig. 4.8). The salinities of Type 3b inclusions were calculated using the final melting temperature of ice, and the equation of Potter et al.(1978) see section 4.7.1. They range from 20 to 24 wt percent equivalent NaCl (Fig. 4.8).





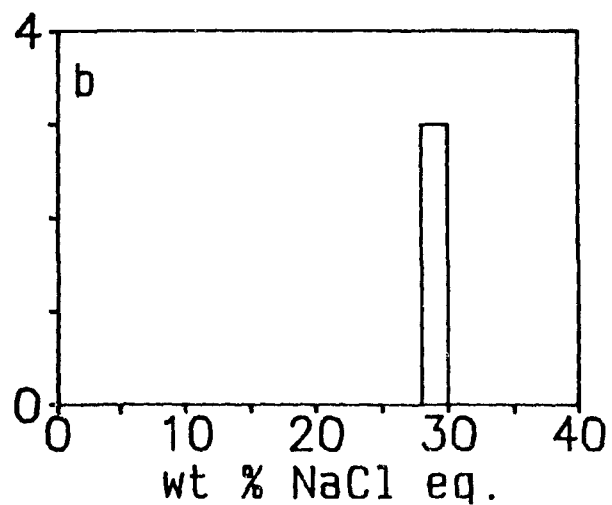


Figure 4.8 Salinity histogram for Type 3 aqueous inclusions.

a- halite-bearing inclusions from the Cadillac deposit, b- halite-bearing inclusions from the Preissac deposit, c- trapped mineral-bearing inclusions from the Cadillac deposit.

4.8. COMPOSITION OF THE FLUIDS

4.8.1 Nature of the species dissolved in the Aqueous Type 1 and Type 3 Inclusions

The very low eutectic temperatures observed in Type 1a, 1b, and Type 3 inclusions (<<-20.8, the eutectic temperature of the system NaCl-H₂O) indicate the presence of salts other than NaCl in the inclusion fluids. Most of the initial melting temperatures were less than -30°C and some were as low as -77°C. The most likely cause of these extremely low melting points is the presence of CaCl₂ in solution (Crawford 1981). However, other additional salts may be required to explain an initial melting point as low as -77°C (the eutectic temperature in the system NaCl-CaCl₂-H₂O is -52°C). LiCl can lower the eutectic melting temperature down to about -75°C (Roedder 1984). AlCl₃ and FeCl₃ are other species that also significantly lower the eutectic temperature of brines (Roedder 1984, p.249).

Type 3a inclusions can be modelled in the system NaCl- $CaCl_2$ - H_2O using T_mice and T_d halite following the method of Williams-Jones and Samson (in press), which involves the intersection of tie lines drawn between the composition of the fluid at final ice melting, hydrohalite and halite with isotherms of halite saturation.

Figure 4.9 Diagram, showing the composition of Type 3a halitebearing aqueous inclusions (the diagram is from Williams-Jones and Samson, in press).

So, the compositions of the halite-bearing aqueous inclusions determined and are shown in Figure 4.9. From this Figure we can see that these inclusions have compositions between 15 and 26 % NaCl, and 11 and 22 % CaCl₂. The corresponding Ca/Na ratios are 0.73 and 0.84. This suggests that CaCl₂ is a major additional component of the fluids.

4.8.2 FLUID INCLUSION LEACHATE ANALYSES

4.8.2.1 Introduction

Inclusion leachate analyses were performed on 20 quartz samples from the Cadillac and Preissac Molybdenum deposits to investigate the compositions of the aqueous inclusions. As shown earlier, the quartz veins in the Cadillac and Preissac molybdenum deposits contain three types of fluid inclusions: aqueous inclusions, carbonic inclusions, and solid-bearing aqueous inclusions. The halite and trapped mineral-bearing aqueous inclusions are relatively rare in the deposits. The CO2-rich inclusions are nonsaline; the H2O-CO2 inclusions have low salinity and are not as abundant as the aqueous inclusions. Therefore the results of leachate analyses largely represent the average composition of the aqueous Type 1 inclusions with minor contamination by H2O-CO2 inclusions, halite bearing aqueous inclusions, and trapped mineral-bearing aqueous inclusions.

4.8.2.2 Method

Initially, several hundred grams of crushed quartz were separated by naked eye from each sample, using tweezers, and sieved to a size of 9 and 12 mesh. For each sample, 10 g. of quartz were handpicked under the binocular microscope. Four additional lots, each containing 2 g. of quartz, were also handpicked from the same samples to test the reproducibility of the leachate analyses. The various quartz samples were then boiled in concentrated HNO3 acid for half an hour, rinsed numerous times with doubly distilled water, and dried in an oven at 100°C. Each sample was thereafter ultrasonically cleaned three times, each cleaning lasting 10 minutes, and rinsed between each washing with doubly distilled water. All beakers and the agate mortar used in the crushing were cleaned by soaking in Chromosulphuric acid for an hour and then were rinsed with doubly distilled water.

The cleaned samples were put in an agate mortar and a few ml of doubly distilled water were added to avoid the ejection of quartz grains during crushing. The crushed samples were then leached with 14 ml of doubly distilled water. Two types of blank samples were used: uncrushed quartz samples from the veins and commercially available quartz samples, which are free of fluid inclusions. The leachates were centrifuged to remove any fine solids in suspension.

The leachates were analyzed for Na, K, Ca, and Mg, using

flame atomic absorption spectroscopy, and for Fe, Li and Ni atomic using Zeeman graphite absorption furnace spectrophotometry. A Perkin Elmer model 5100 atomic absorption spectrometer was used in the analyses. Molybdenum analysis was done by Induchvely Coupled Plasma-Atomic Spetrometry (ICP-AES). The Cl concentrations of the leachates were determined using a chloride sensitive ion electrode. In all cases except for Fe, and Ni, the concentrations of the elements in the blank samples were below the detection limit: Na=0.06ppm; K=<0.04ppm;Ca=<0.05ppm; Mq = < 0.004ppm;Mo=<0.025ppm; Li=<0.002 ppm. The analyses of samples and blanks are given in Appendix II, Table 1.

4.8.2.3 Results

The compositions of 20 leachates from fifteen samples and blanks are given in Appendix II, Table 1. The results show that Na and Ca are the major cations in the fluid inclusions. K is significantly less abundant than Na and Ca. The Li content of the fluid is low, despite the occurrence of Li minerals in the granites of the area. There are minor amounts of Mg, Fe and Ni in the leachates. A few samples contain significant concentrations of Mo, but, in general the concentration of Mo is very low. All samples contain significant concentrations of Cl. The reproducibility of the leachate analysis was confirmed by four replicate analyses of

the 2g. splits from the same samples as the 10g. splits were previously taken (see Appendix II, Table 1). The K/Na ratio ranges from 0.12 to 0.36 with a mean of 0.21. The Ca/Na ratio ranges from 0.02 to 0.22 with a mean of 0.08.

If the concentrations of the elements (in Appendix II, Table 1) are recalculated in terms of atomic proportions, it is chloride ion concentration apparent that the is considerably higher than predicted by the combined charge of the measured cations. This indicates that there is another cation that has not been considered or that the results are in error. Because, HCl occurs predominantly as an associated species at high temperature, but is completely disassociated at room temperature (Barnes and Ernst 1963), it was thought possible that the cation deficiency could be accounted for by an excess of H ions.

4.3.2.4 pH calculation

In order to test the hypothesis that H ions may account for the difference between the sum of the cations and the chloride concentration, two independent pH calculations were undertaken. Both calculations of pH were performed at 425°C and 700 bars, the conditions of formation of the molybdenum mineralization as inferred from fluid inclusion microthermometry and oxygen isotope analysis (see below).

The first calculation was carried out assuming that the

Na/K ratio measured in the leachate analysis is representative of the composition of the fluids. The actual K⁺ concentration of the fluid was calculated by combining the leachate data with the bulk salinity determined from ice melting temperatures,. The data of Bowers et al. (1984) were then used to calculate the high temperature pH assuming equilibrium between K-feldspar, muscovite and quartz.

The second pH calculation was executed assuming that the difference between the Cl ion concentration and the sums of the charges of all the anions could be entirely attributed to H at room temperature. Then, the high temperature pH was determined by calculating the distribution among the various species in the H - Na - K - Ca²⁺ - Mg²⁺ - Cl system. The species assumed to exist were H, Na , K, Ca²⁺, Mg²⁺, NaCl , HCl , KCl , CaCl , CaCl , MgCl . A series of mass action and mass balance equations and one charge balance equation were solved iteratively using the equilibrium solver algorithm developed by Crerar (1975), and the B-dot expression of Helgeson (1969) for the activity of the charged species. If the hypothesis that H is the "missing" cation is correct, then the two independent pH calculations should arrive at the same final valve.

The pH, resulting from the K-feldspar-muscovite boundary calculation was approximately 5 whereas, that calculated using the speciation model was only 2 or less. Therefore, H⁺ cannot account for the excess of chloride ion. An example of the

calculation and the result is given in Appendix III.

Subsequent to the execution of these calculations a publication was discovered, which suggested that if the leaching is done with doubly distilled water, Ca and sometimes Mg precipitate and are introduced in disproportionally low quantities in the leachate (Bottrell et al. 1988). This could explain the cation gap, and indicates that the actual Ca and Mg contents of the fluids is much higher than that obtained by leaching with double distilled water. Bottrell et al. (1988) used a 0.13MHNO, + 200µg/ml LaCl, solution to leach their inclusions which resulted in an improved Ca+Mg recovery. Leaching experiments were therefore repeated for five samples (Appendix II, Table 2b) using the method of Bottrell et al. (1988). The improved leaching method resulted in higher Ca and concentrations, but little change in concentrations as Bottrell et al. (1988) have also shown. The sum of the newly obtained cation concentrations in the leachates equals that of the anions within the limit of experimental error. Since, the bulk of the missing cations was Ca, the other ion analyses were corrected by balancing the charges and attributing the cation charge deficiency to Ca. The corrected values for Ca are given in Appendix II, Table 2a. The Ca/Na ratio is higher than that reported above ranging from 0.02 to 2.78 with a mean of 0.88 (Appendix II, Table 2), which is similar to that determined for Type 3 inclusions (see section 4.8.1) using the method of Williams-Jones and Samsor.

4.8.3 Composition of the Carbonic Inclusions

The mole fraction of CH, in the carbonic phase was calculated using the method of Burruss (1981), which is based on the final melting temperature of carbonic ice and the homogenization temperature of the carbonic phase. However, the high final melting temperature of the carbonic ice (Xcadillac =-56.7, X_{preissar}=-57.8) and low clathrate melting temperature <10°C suggest that the carbonic phases consist almost entirely of CO2. The values determined for XH2 range from 0.008 to 0.02. The high homogenization temperature of the carbonic phases 31°C (Fig. 4.10), with a peak between 29° and homogenization of the carbonic phase to the liquid phase are additional indications of the low concentration of components such as CH, and N, in the system.

The mole fractions of H₂O and the carbonic components were calculated using the density of the aqueous phase (Bodnar 1983), the density of the CO₂ phase at the homogenization temperature of the carbonic phase (Lowry and Erickson 1927), and the visually estimated volumes of the carbonic and aqueous phases. It was assumed that the carbonic phases consisted only of CO₂ since XCH₄ is very small. A sample calculation is given in Appendix IV. The XCO₂ ranges from 0.0343 to 0.172 for the Preissac and from 0.0212 to 1 for the Cadillac fluid inclusions.

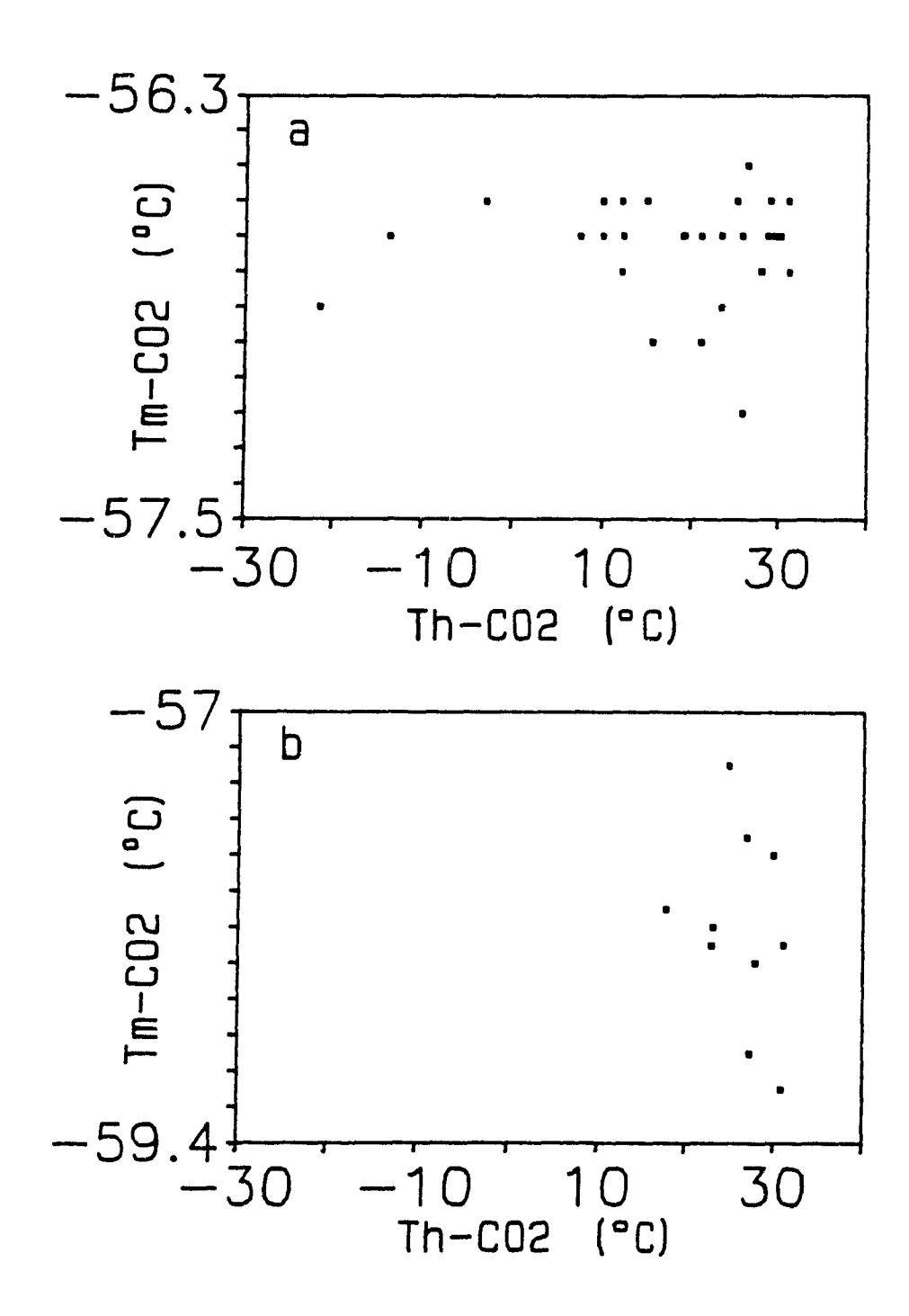


Figure 4.10 Diagrams, showing the homogenization temperature versus final melting temperature of carbonic ice in Type 2 inclusions. a- in veins from the Cadillac deposit, b- in veins from the Preissac deposit.

4.8.4 SCANNING ELECTRON MICROSCOPY OF MINERALS IN FLUID INCLUSIONS

Scanning electron microscopy-energy dispersive analysis (SEM-EDS) was performed on opened fluid inclusions to identify the trapped minerals in Type 3 inclusions. Same inclusions contain as many as four to five minerals but more commonly one or two minerals.

4.8.4.1 Method

Pieces of the samples previously used for microthermometric analysis of fluid inclusions were broken and frozen in liquid nitrogen. After the pieces were removed from the liquid nitrogen they were broken into smaller chips that could easily be inserted into the SEM. The pieces were attached to carbon mounts using carbon cement with the freshly broken surface up and coated with carbon.

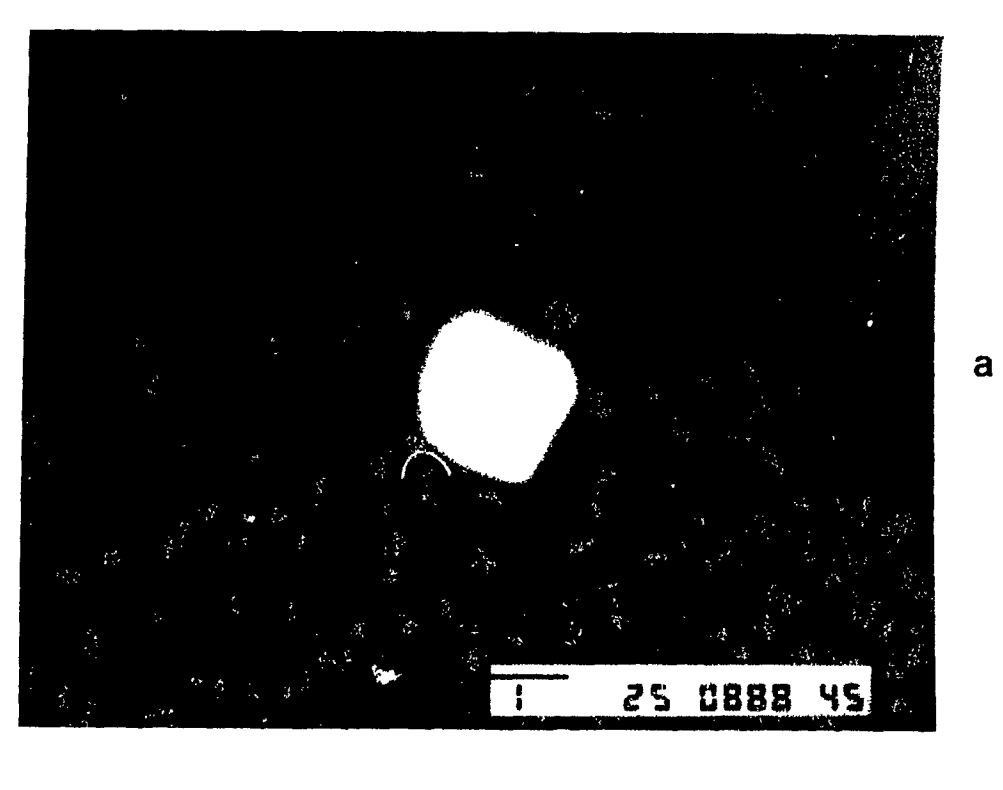
The accelerating voltage used in this study was between 15 and 25V. After analysis of each trapped mineral, the background was also analyzed by moving the electron beam off the trapped mineral onto the quartz host.

4.8.4.2 Results

Peaks corresponding to the following elements were

recognized during SEM-EDS analyses of the solid phases in fluid inclusions: Si, Cl, Ca, Na, K, Al, Ni, S, Ba, Fe, and Cu. Ca and Cl were the elements most commonly detected. Peaks for Si, Fe and Cu were also observed in the background. The Si peak which is present in all analysis simply reflects the host quartz. The Fe and Cu, on the other hand, are interpreted as contamination from the SEM column.

Halite is the only daughter mineral recognized under the optical microscope. Its identity was confirmed by SEM analysis which yielded a spectrum containing Na and Cl peaks (Fig. 4.11). The most common mineral spectra was one that only contained a peak for Ca in addition to those making up the background. This mineral is tentatively identified as calcite CaCO, (Fig. 4.12 and 4.13). Another common mineral is one with a spectrum containing K and Al peaks. This mineral on the basis of its morphology and composition, is thought to be mineral muscovite (Fig. 4.13). Another with peaks corresponding to Ca and Cl, interpreted to be hydrophilite, CaCl, or antarctcite, CaCl, 6H,0 (Fig. 4.14). This mineral was probably formed when the samples were frozen in the liquid nitrogen. An unexpected spectrum was one containing peaks of and S (Fig. 4.15) elements corresponding either to millerite (NiS) or one of several other Ni sulphide minerals that occurred in nature. The only other mineral identified was barite which occur in a single inclusion (4.16).



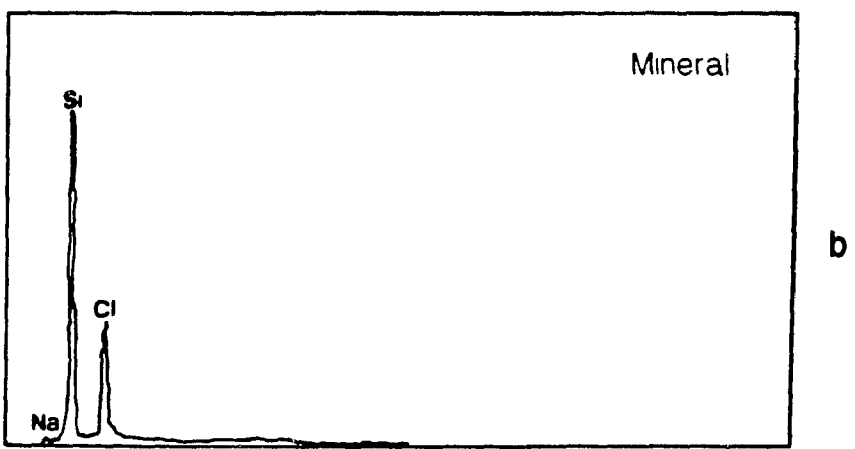
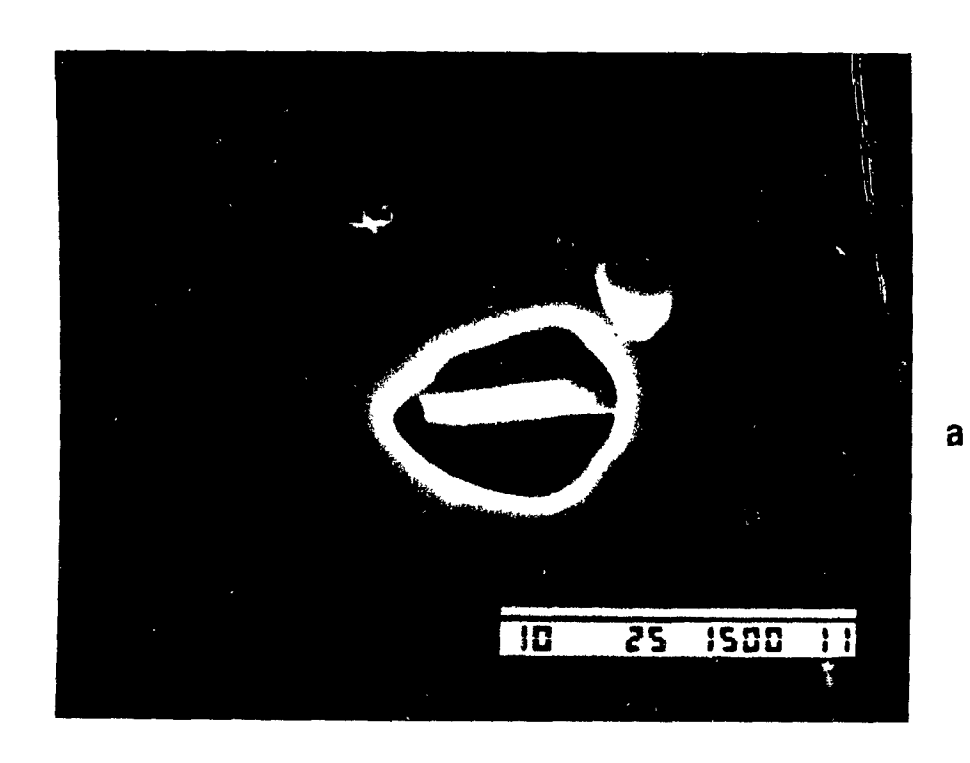


Figure 4.11 a) an inclusion cavity, containing halite, b) The X-ray spectra of the mineral.



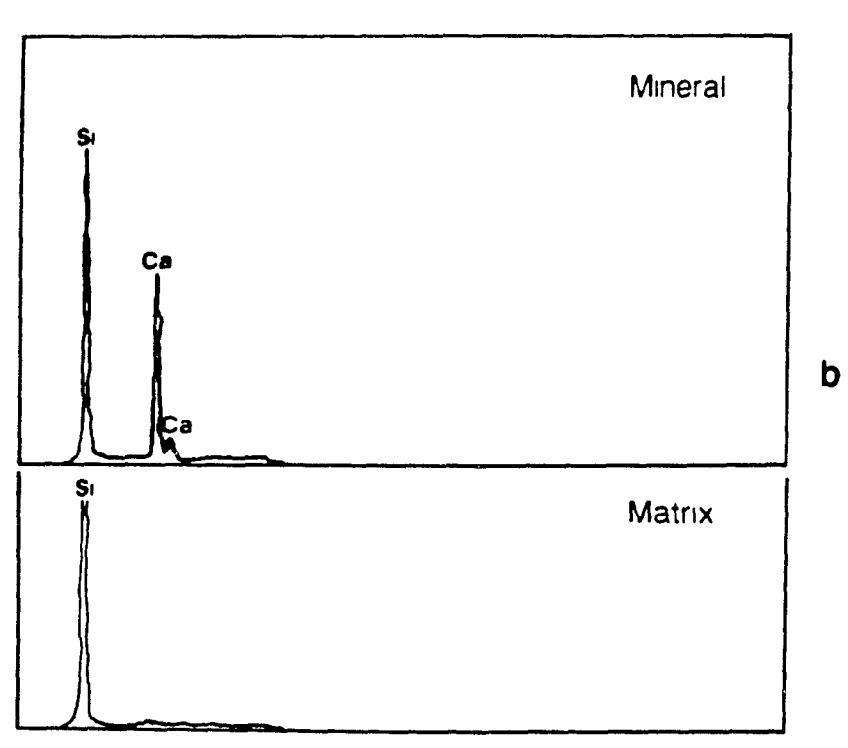
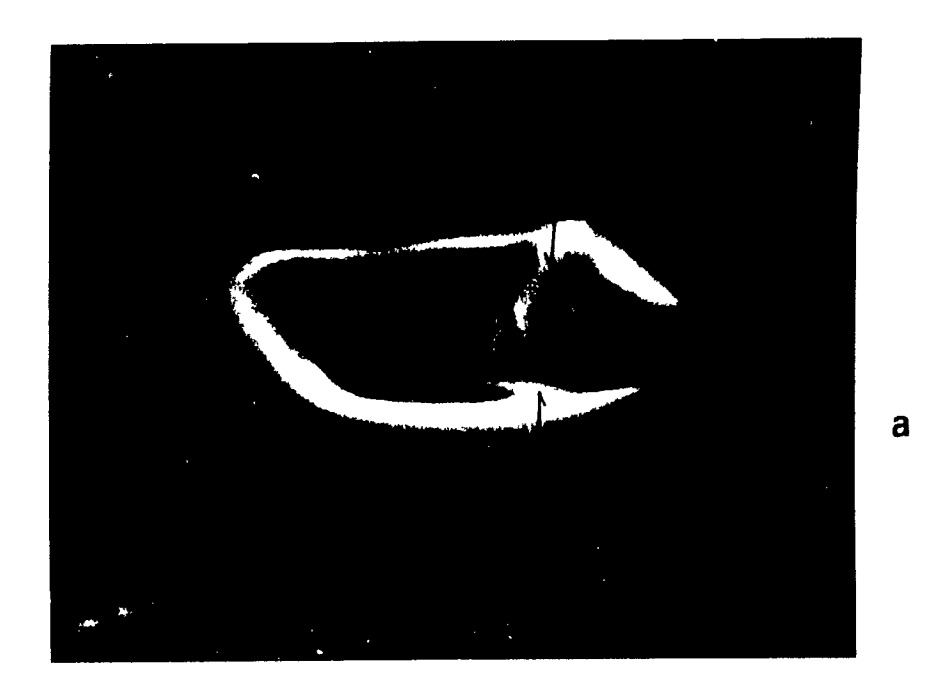


Figure 4.12 a) an inclusion cavity, containing calcite, and b) X-ray spectra of the mineral and its matrix.



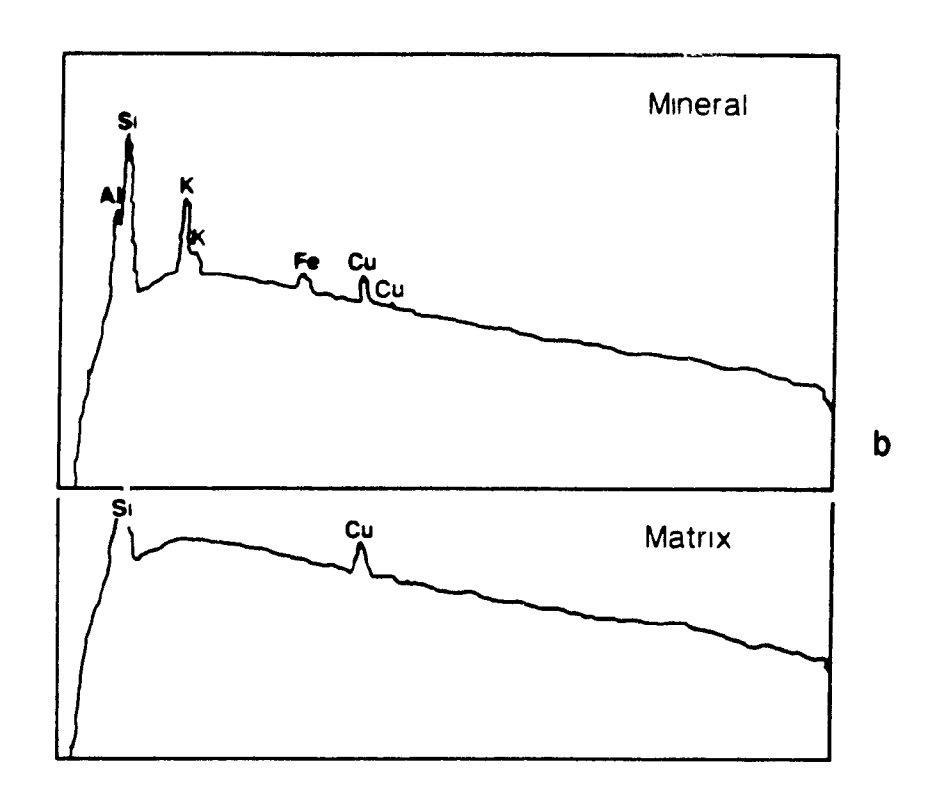


Figure 4.13 a) an inclusion cavity, containing calcite (1) and muscovite (2), and b) X-ray spectra of muscovite and its matrix.



а

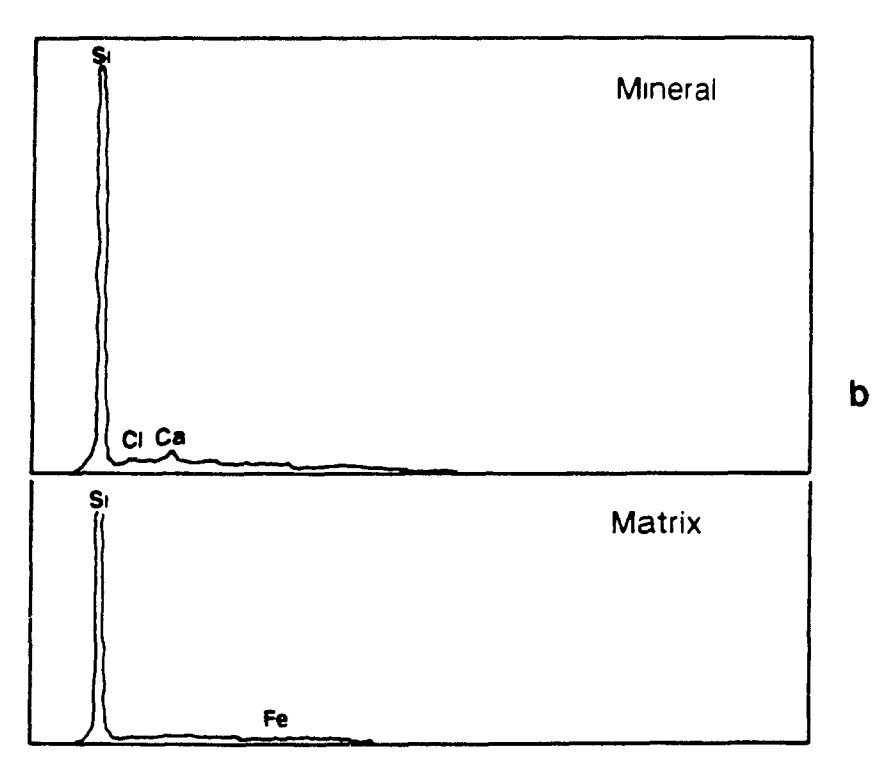


Figure 4.14 a) an inclusion cavity, containing a Calcium chloride mineral, and b) X-ray spectra of the mineral and its matrix.



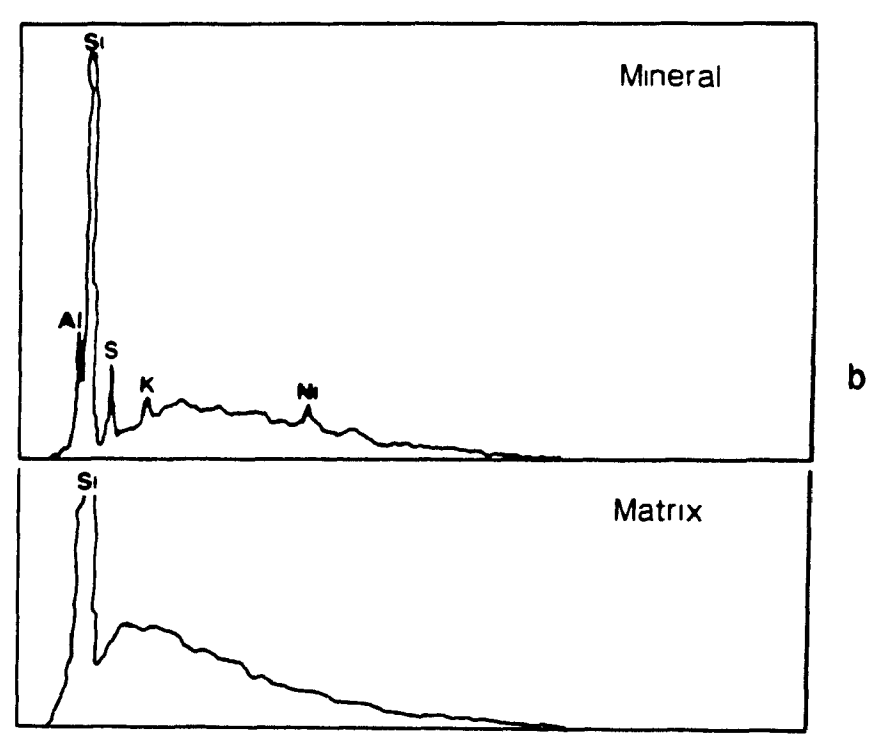


Figure 4.15 a) an inclusion cavity, containing a nickel mineral, and b) X-ray spectra of the mineral and its matrix.

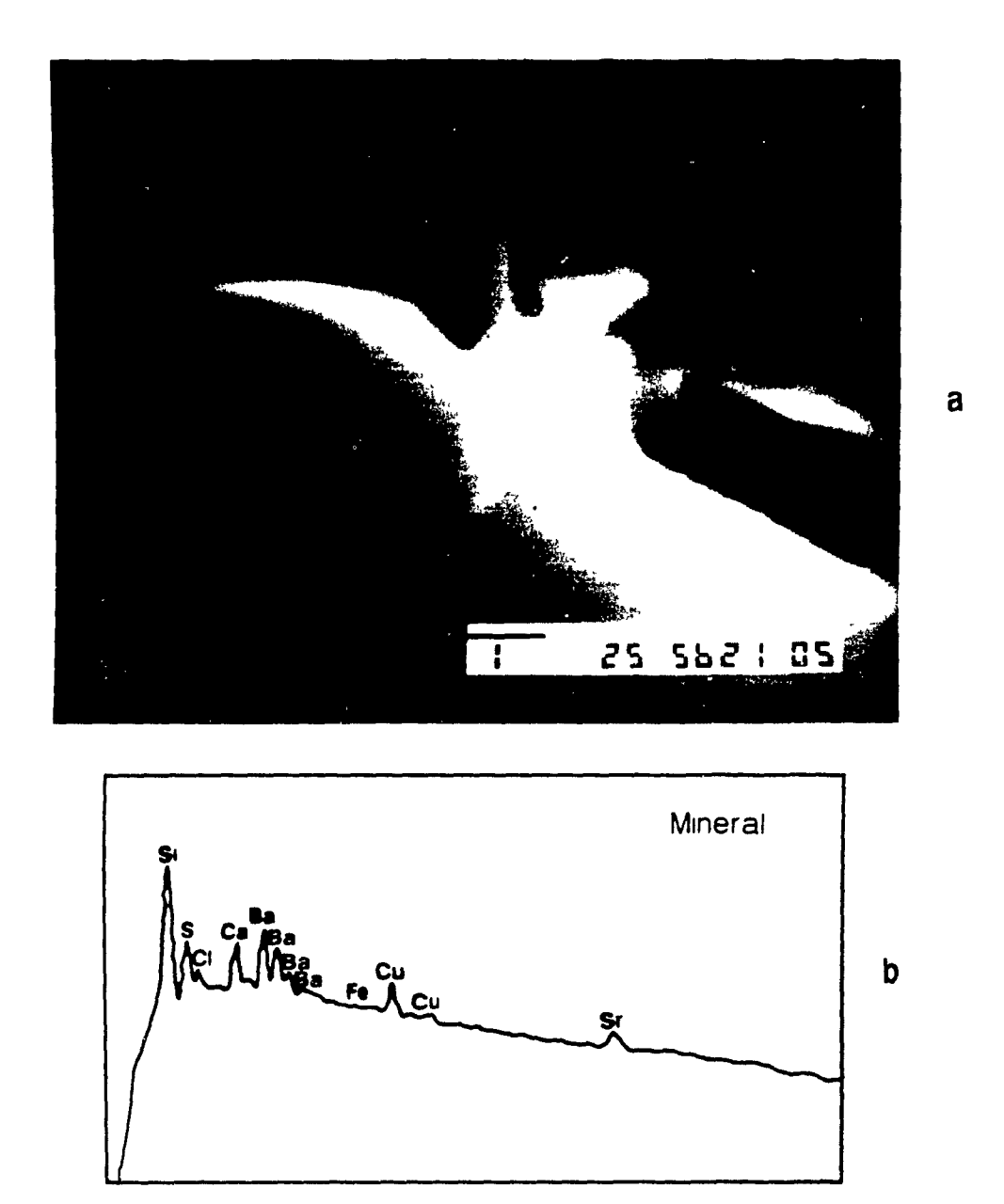


Figure 4.16 a) an inclusion cavity, containing barite, and b) X-ray spectra of the mineral.

CHAPTER 5

STABLE ISOTOPE STUDY

5.1 Introduction

If two mineral have isotopically equilibrated with the hydrothermal fluid from which they formed, the isotopic fractionation between the two phases can be used to estimate their formation temperature. The isotopic compositions of the minerals can in turn be used to estimate the isotopic composition of the related hydrothermal fluid. The most suitable mineral pair for isotopic geothermometry in the Cadillac and the Preissac Molybdenum Deposits is muscovite and quartz.

Four pairs of quartz and muscovite samples from four mineralized veins were separated by hand picking from crushed material with the aid of a binocular microscope, and analyzed for their oxygen isotopic compositions at McMaster University by Dr. H. P. Schwarcz. The precision of the analyses is about 0.1 per mil, based on replicates of the NBS28 quartz standard. Duplicate analyses were carried out to check the reproducibility of the analyses.

5.2 Results

The temperatures of formation from quartz and muscovite pairs were calculated using equations of Clayton et al. (1972) for quartz and O'Neil (1969) for muscovite. The temperatures of formation so calculated range from 342° to 584°C with a mean of 463°C for the Cadillac deposit, and from 383° to 428°C with a mean of 400°C for the Preissac deposit. For both deposits the temperatures of formation range from 584° to 342°C with a mean of 425°C. These temperatures agree remarkably well with estimates of entrapment temperatures based on fluid inclusions microthermometry.

The oxygen isotopic compositions of quartz and muscovite, are given in Table 5.1. The calculated isotopic composition of waters in equilibrium with quartz and muscovite and the temperature of formation from quartz and muscovite pairs are also given in Table 5.1. The oxygen isotope values of muscovite range from 6.49 to 8.07 per mil with a mean of 7.28 per mil for the Cadillac deposit, and from 6.73 to 7.50 per mil for the Preissac deposit with a mean of 7.15 per mil. The oxygen isotope values for quartz range from 9.62 to 9.92 per mil with a mean of 9.77 per mil for the Cadillac deposit, and from 9.54 to 10.02 per mil with a mean of 9.85 per mil for the Preissac molybdenum deposit.

The oxygen isotopic composition of the fluids was calculated using the equations for quartz-water fractionation

from Clayton et al. (1972), and for the muscovite-water fractionation from O'Neil (1969) at the temperatures of formation. The corresponding oxygen isotopic composition of the aqueous fluid in equilibrium with these minerals ranges from 1.2 to 5.5 per mil with a mean of 3.35 per mil for quartz, and -0.6 to 2.3 with a mean of 0.85 for from muscovite for the Cadillac molybdenum deposit. For the Preissac deposit the corresponding values are as follows; from 3.4 to 4.2 with a mean of 4.0 for quartz, and 0.9 to 1.6 with a mean of 1.3 for muscovite. Using the mean temperature of formation (425°C) the mean oxygen isotopic composition of the aqueous fluid is 3.53 per mil for quartz, and 0.99 per mil for muscovite for both deposits.

Table 5.1 Oxygen isotopic analyses of selected quartz+muscovite samples and calculated fractionation factors and temperatures

Sample	Analyses	$(\delta^{18}$ O per mil)	δ ¹⁸ O _{fluid}	δ ¹⁸ O _{fluid}	
	Qtz.	Mus.	Qtz	Mus	Temp.(°C)
LC-11-29	9.92	8.07	1.2	-0.6	584.34
LC-11-6	9.62	6.49	5.5	2.3	342.30
LC-10-3	10.02,	7.50,	3.4	0.9	428.71
	9.99	7.23	4.2	1.5	390.57
LC-10-6	9.54	6.73	4.4	1.6	383.38
			X=3.53	0.99	425

CHAPTER 6

INTERPRETATIONS

6.1 P-T CONDITIONS OF MINERALIZATION

Isochores for the aqueous inclusions were calculated using the P-V-T data presented in Potter and Brown (1975). 6.1 shows an isochore representing the and salinity of the Type 1 homogenization temperature inclusions. Figure 6.1 also shows isochores for non-aqueous carbonic inclusions computed using the equation of state of Kerrick and Jacobs (1981). The aqueous-carbonic inclusions proved unsuitable for P-T determination because of the large errors associated with the volume estimates (estimation of the bulk density of aqueous and carbonic inclusions requires that the relative volumes of the aqueous and carbonic phases be visually estimated. This is not necessary for aqueous or nonaqueous carbonic inclusions). Isochores for the non-aqueous carbonic inclusions intersect the modal isochore for aqueous fluid inclusions at a temperature of approximately 425°C, and pressures between 680 and 740 bars.

An independent estimate of temperature was provided by the oxygen isotopic compositions reported in Chapter 5. The mean oxygen isotopic temperature of 425°C is the same as that derived from the intersection of the aqueous and carbonic

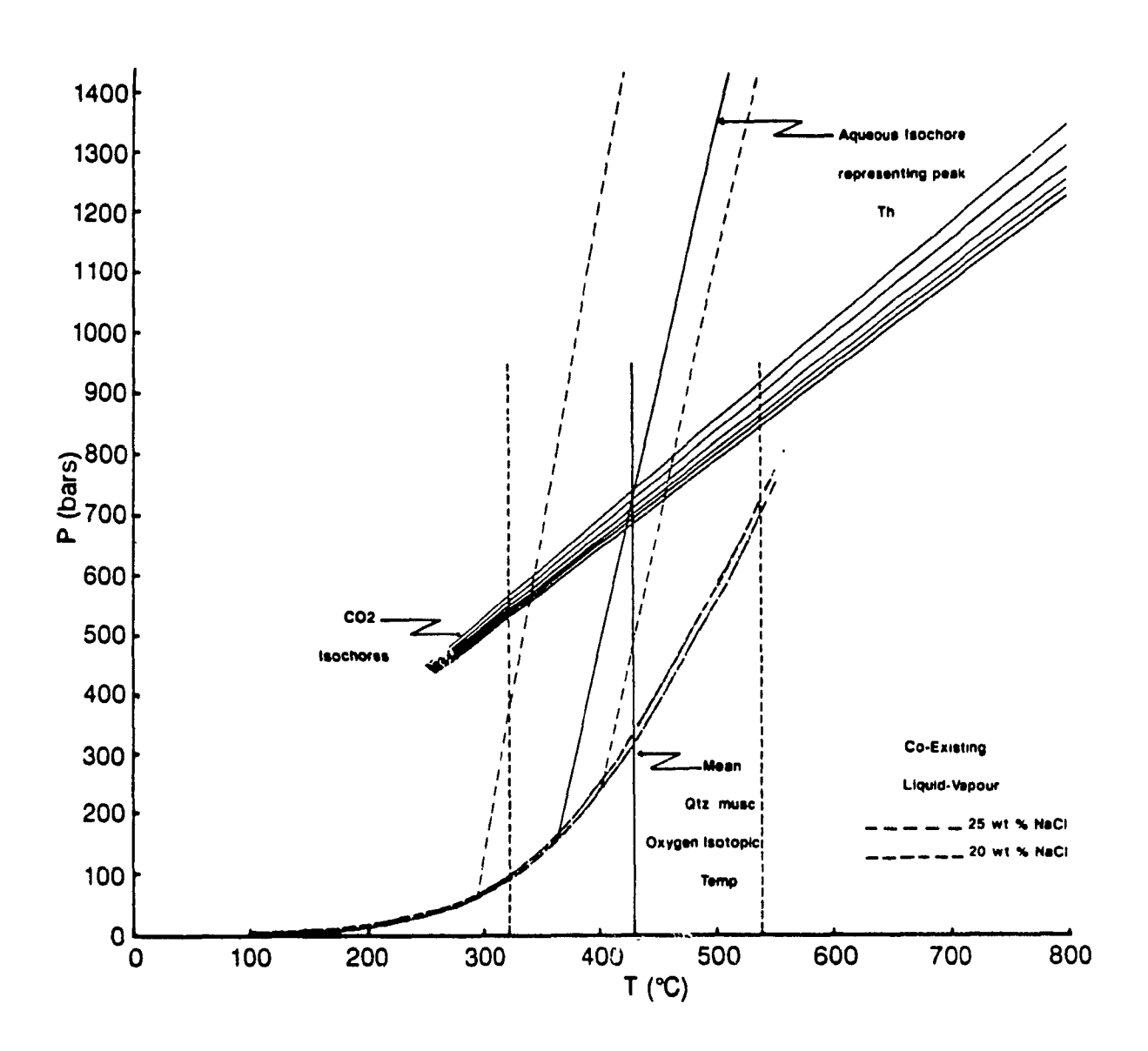


Figure 6.1 P-T diagram, showing isochores for non aqueous carbonic inclusions intersecting the isochore for the modal homogenization temperature and salinity of Type 1 aqueous inclusions, at a temperature of approximately 425°C, and pressure between 680 and 740 bars. A line representing the mean temperature based on oxygen isotopic fractionation between quartz and muscovite in mineralized quartz veins is also shown. The dashed and dot-dashed lines represent standard deviations of the aqueous Type 1 isochores and oxygen isotopic temperatures, respectively.

isochores. The excellent agrement between the two temperature estimates provides strong evidence for a mean pressure of entrapment of about 700 bars.

In summary the available evidence strongly suggests that the mineralization was emplaced at a temperature of approximately 425°C and a pressure of 700 bars.

6.2 SOURCE OF HYDROTHERMAL FLUIDS

The presence of multiple generations of fluid inclusions in specimens of vein quartz from the Cadillac and Preissac molybdenum deposits is interpreted to represent fluid entrapment during repeated fracturing of the veins.

Insight into the nature and number of aqueous fluids involved in the hydrothermal activity can be obtained by plotting the salinity of the aqueous fluid inclusions against their homogenization temperatures. Homogenization temperature versus salinity data are plotted in Figure 6.2 for Type 1 aqueous and Type 3 solid-bearing aqueous inclusions. The high temperature inclusions correspond to the high to moderate salinity Type 1a and low salinity Type 1c inclusions. Neither of these inclusion types contain halite or trapped minerals. The low temperature, high and moderate salinity inclusions correspond to the halite-bearing Type 3a and trapped mineral-bearing Type 3b secondary inclusions. Moderate to low

salinity, two and one phase secondary inclusions correspond to the low temperature Type 1b inclusions. Examination of Figure 6.2 suggests that there may be two populations of Type 1 inclusions: 1) a high temperature population with moderate to high salinity; and 2) a population ranging from low temperature and low to moderate salinity to high temperature-low salinity.

The high temperature, high to moderate salinity (Type la) inclusions could have been derived from the magma. It has been shown that felsic and intermediate magmas dissolve large quantities of water which is exsolved to form an orthomagmatic hydrothermal fluid when the magma crystallizes (Whitney 1975, Burnham 1979). Any chloride dissolved in the magma is partitioned almost entirely into the fluid together with Na and K (Kilinc and Burnham 1972, Burnham 1979). The exsolved fluid can be a vapour with low salinity (1 to 10 % NaCl), a saline liquid with tens of percent NaCl, or a mixture of these two fluids (Sourirajan and Kennedy 1962). Evidence that the fluids are, at least in part, ortho-magmatic is provided by the observation of micrographic textures in thin sections of the rocks from the Preissac batholith. commonly developed in water-rich textures generally in the presence of a separate aqueous phase (Jahns and Burnham 1969). The comparatively low homogenization temperatures and their high Ca content indicate, however, that, if the Type la fluids were initially orthomagmatic, they had evolved considerably by the time of their entrapment. Magmatic waters in equilibrium with igneous rocks at high temperatures have oxygen isotopic values between 6 and 8. The oxygen isotopic composition of the fluids of the Cadillac and the Preissac Molybdenum Deposits ranges from -0.6 to 5.5 which is well below the range of magmatic water. These low oxygen isotopic values suggest evolution of early fluids through mixing with meteoric water.

The other possibility for the origin of Type 1a inclusions is that they may be heated formation waters from the surrounding meta-sediments. Boiling doesn't appear to be a likely explanation for the high salinity Type 1a fluids, since there is no evidence of an aqueous vapour ever having been present.

The high temperature low salinity Type 1c fluids could be magmatic in origin. Their rarity, isolated occurrences and the high homogenization temperature suggest that they may represent fluids exsolved from the magma. It is, however, more likely from their relatively low salinity, that they represent trapped meteoric waters that were close to the intrusion and were heated early in the emplacement history of the intrusion.

Type 3 inclusions are the least abundant and are clearly secondary in origin. The Type 3 inclusions, are of a comparatively low temperature, and appear to comprise a high salinity halite-bearing subtype (Type 3a) and a slightly lower salinity trapped mineral-bearing, halite absent subtype (Type

3b). The general absence of trapped minerals from the first subtype and of halite from the second suggest that the two subtypes had different origins or at least largely separate histories.

The majority of the halite-bearing aqueous inclusions (Type 3a) homogenized by halite dissolution, and in a few cases by both halite dissolution and vapour disappearance. Although these inclusions may have been saturated with halite at the time of entrapment, it is more likely, given the narrow halite dissolution temperatures, that precipitated on cooling. The most likely source for the Type 3a inclusion fluids is deep, saline groundwaters which are reported to be widespread across the present day Canadian Shield (Frape et al. 1984) and may also have been present during the formation of the molybdenum deposits in the Preissac-Lacorne batholith. These ground waters according to Frape et al. (1984) can contain up to 32.5 wt % dissolved salts and are generally calcium-rich, a feature of the Type 3a inclusions. Other alternative sources for the Type 3a inclusions are the residual of boiling or waters that have interacted with evaporates. There is no evidence of boiling nor are there any reports of evaporates or their metamorphosed equivalents in the surrounding metasediments.

The origin of low temperature, high to moderate salinity

Type 3b inclusions is not clear. The occurrence of trapped

minerals in Type 3b and Type 2 inclusions suggest that these

fluids had a common origin. An attractive explanation, which is discussed in more detail below, is that the Type 3b inclusions were derived from an aqueous-carbonic fluid which unmixed at a low temperatures to yield a high salinity fluid and a high XCO₂ carbonic fluid.

Figure 6.2 suggests that high temperature low salinity (Type 1c), low temperature moderate to low salinity (Type 1b) and/or low temperature high to moderate salinity fluid inclusions (Type 3a, 3b) may be linked by a mixing line. Type inclusions are the most abundant inclusions and may represent mixing of low salinity heated meteoric waters with high salinity, low temperature fluids. The common occurrences of calcite and the identification of trapped nickel minerals in the Type 3b inclusions, and the high nickel and calcium contents of fluid inclusions leachates (the concentration of Ni calculated to be present in the original fluid is about 200 ppm. This is much higher than the Ni content of granitic rocks. See section 6.4.1), which largely represent the Type 1b inclusions, support the interpretation that fluid Types 1c and 3b mixed to yield fluid Type 1b. The high nickel and calcium content of the inclusions also strongly suggest that fluids circulated through and interacted with the surrounding carbonatized volcanic (komatiitic) rocks in which there is nickel mineralization.

Some understanding of the evolution of the Type 2 inclusions can be obtained by examining T-XCO2 relationships.

Figure 6.3 plots homogenization-decrepitation temperature versus XCO, for carbonic (Type 2) inclusions. The fairly constant H2O/CO, ratios in some aqueous-carbonic inclusions imply trapping of a homogeneous one-phase fluid (Fig. 6.3). On the other hand, the existence of pure CO, inclusions and the coexistence of two phase vapour-rich and liquid-rich carbonic inclusions with variable H,O/CO, ratios suggest fluid immiscibility during entrapment. Bowers and Helgeson (1983) have shown that at high pressures and temperatures NaCl-H2O-CO, solutions are homogeneous fluids. If pressure and/or temperature decreases, this results in fluid unmixing to give an NaCl-rich liquid and an H2O-CO2-rich fluid. Zhang and Frantz (1989) have studied the CaCl2-H2O-CO2 system and have shown that the region of immiscibility extends to much higher pressure and temperature than that of the NaCl-H2O system. It is thus likely, given the high CaCl2 content of the Cadillac and Preissac fluids that although carbonic and low salinity aqueous fluids may have been miscible during the early history of these deposits, they became immiscible when temperature and pressure decreased, to produce separate high to moderate salinity aqueous (Type 3b) and carbonic fluids. The occurrence of vapour-rich carbonic inclusions (Type 2c) may indicate CO, effervescence. Some of the variation in H2O-CO2 ratios in Figure 6.3 may also have been caused by necking down, and leakage, but the occurrence of vapour-rich, and pure CO, inclusions cannot be explained by these mechanisms.

The two most likely sources for the carbonic fluids are the magma and the carbonatized volcanic rocks into which the Preissac massif intruded.

The molybdenum mineralization is hosted by a S-Type, two mica granite and it is thus possible that the corresponding magma, if produced by anatexis of sedimentary rocks, may have been saturated with CO2. Burnham (1979) has summarized experimental data indicating that CO, is less readily dissolved than H,0 in aluminosilicate melts. It therefore, follows that a fluid phase, exsolved at relatively pressures by magmas containing both H2O and CO2, will be CO2rich. Kay and Strong (1983) have described low salinity CO,-bearing inclusions in As-Sb-Au veins in Newfoundland which they conclude were exsolved from felsic magmas at pressures of 900 to 1,500 bars. A magmatic origin is also postulated for the fluid that deposited molybdenite at Boss Mountain, B.C. It is interpreted to have separated into aqueous and carbonic phases at pressures of less than 350 bars (MacDonald and Spooner 1982).

The close proximity of the deposits to metasedimentary and carbonatized volcanic country rocks is an attractive alternative source for the carbonic fluids. Part of the hydrothermal system undoubtedly interacted with these country rocks as evidenced by the high Ca (which could come from calcite in the carbonatized volcanics) and the high Ni contents of the fluids. Early hot fluids could have released

CO₂ either as a separate immiscible phase, or dissolved it and then later exsolved it in response to decreasing pressure, temperature or both.

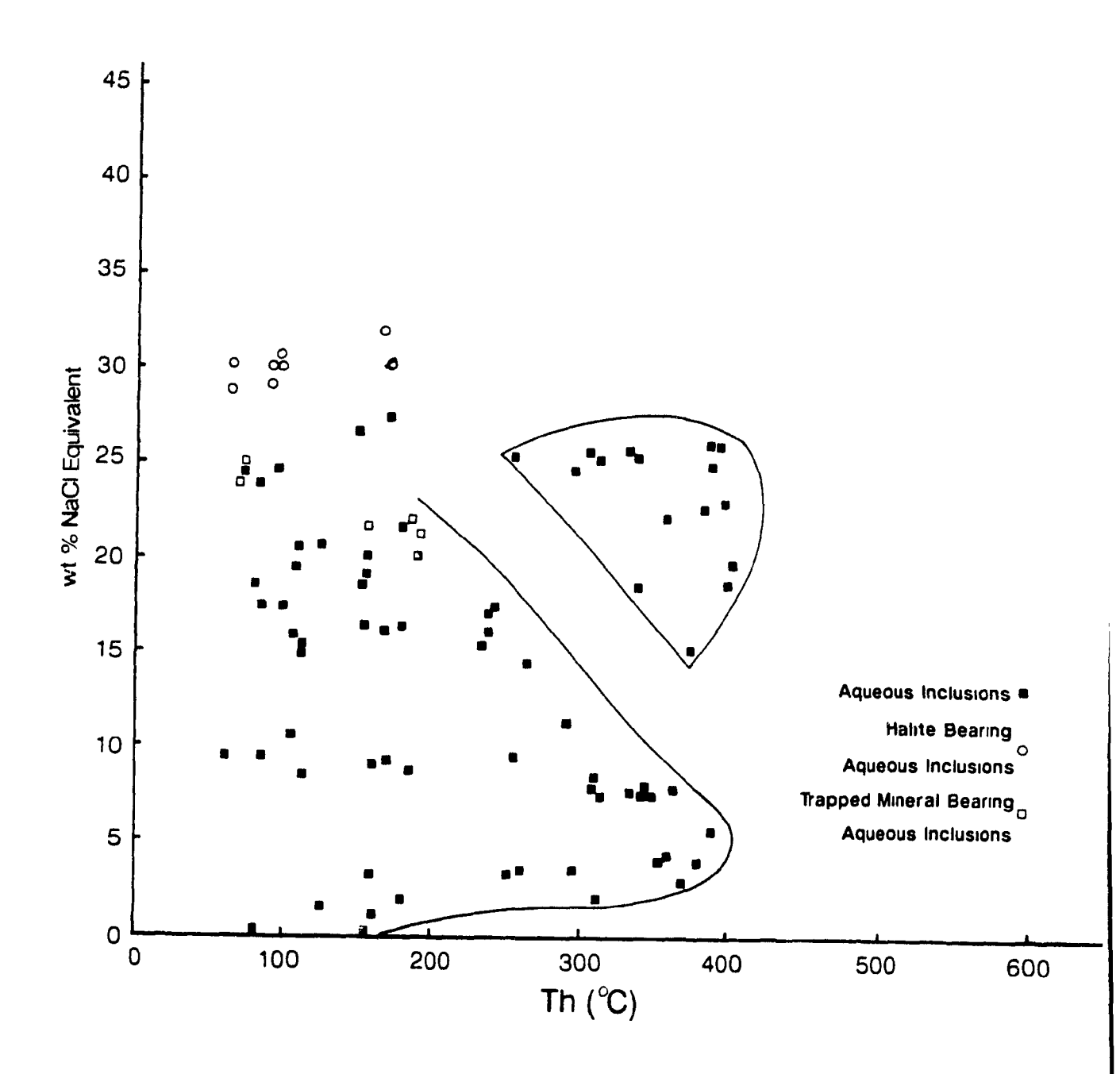


Figure 6.2 A plot of salinity versus homogenization temperature diagram of Type 1 and Type 3 inclusions from the Cadillac deposit.

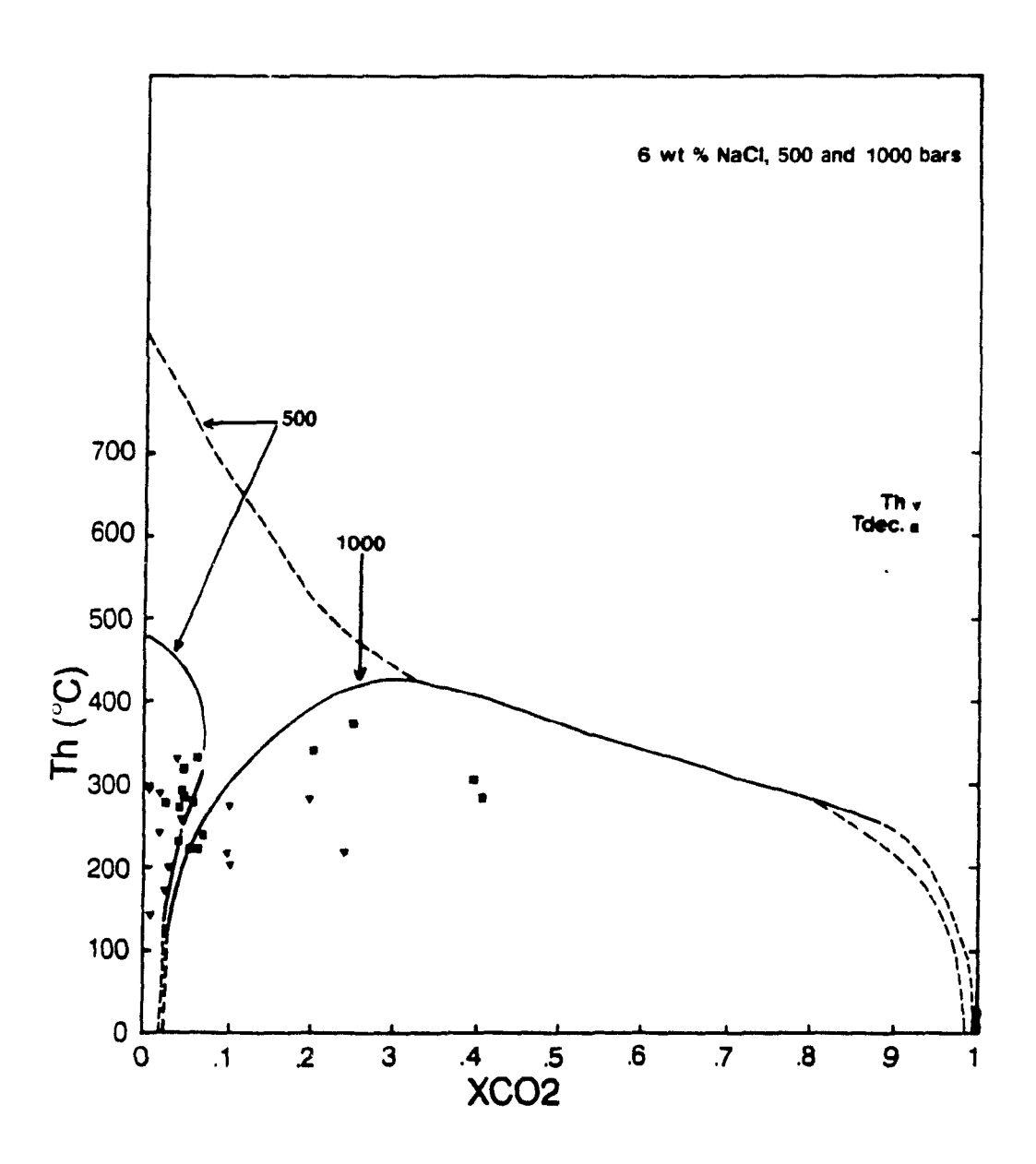


Figure 6.3 Homogenization/decrepitation temperature versus mole fraction of ${\rm CO_2}$ for carbonic inclusions (the solvi are from Bowers and Helgeson 1983).

6.3 FLUIDS AND ALTERATION

In the Cadillac molybdenum deposit there are two main types of alteration: early albitic and later K-feldspar alteration.

It has been shown experimentally that the distribution of alkalis between a homogeneous fluid and alkali feldspar is strongly temperature dependent, and essentially independent of pressure and chloride molality in the fluid (e.g., Orville 1962, Lagache and Weisbrod 1977). Lagache and Weisbrod (1977) showed that if, at a given temperature and K/Na ratio, a fluid is in equilibrium with two feldspars, increasing temperature tends to cause albitization and decreasing temperature, K-feldspathization for the same K/Na ratio.

Lagache and Weisbrod (1977) proposed two models for moderate and high temperature K-feldspar alteration:

1- One obvious mechanism for promoting K-feldspathization is to sharply decrease pressure by opening up a fracture to the surface, thereby changing the conditions from lithostatic to hydrostatic. Such pressure changes commonly cause adiabatic expansion of the fluid and consequent drops in temperature.

2- Another mechanism for promoting K-feldspathization is lowering temperature through mixing of early hot solutions with later cool solutions.

The mixing trend shown in Figure 6.2 linking high temperature low salinity Type 1c to low temperature, moderate

to low salinity Type 1b and Type 3b inclusions tends to support the second mechanism for K-feldspathization.

6.4 Solubility of molybdenite

Several experimental studies on the solubility and transport of Mo in hydrothermal solutions have been described in the literature. A summary of the results of some of the more important of these studies is given below.

Khitarov et al. (1965) studied the effect of hydrogen sulphide on the migration of molybdenum and showed that, at elevated temperatures and pressures, molybdenum and silica can be transported in the form of a silicomolybdate complex. However, if the concentration of hydrogen sulphide in the solution exceeds 0.01 mole/litre, molybdenum is transported as a molybdenite suspension in silica-rich solutions.

Isuk and Carmen (1981) studied the solubility of molybdenite at 450°to 850°C and 340 bars to 1.36 kb. They found that the solubility of molybdenite is temperature dependent and reaches a maximum around 650°C with retrograde solubility at higher temperatures.

Khitarov et al. (1982) studied the distribution of Zn, Cu, Pb, and Mo between a fluid phase and a silicate melt of granitic composition at temperatures between 700° and 900°C and a pressure of 2000 bars. Their results showed that the extraction of molybdenum from the melt is low for NaCl

solutions but very high for NaHCO₃ solutions. These authors therefore proposed carbonate complexes as a possible means of Mo transport. However, their results could also reflect a pH effect.

Tingle et al. (1982) studied the transport of molybdenum in magmatic systems and found that if an aqueous vapour phase is present, molybdenum and sulphur are strongly partitioned into it. K, Na, Al, and Si were also transported and deposited by the vapour. Molybdenite transport was not, however, affected by Cl, S, or F activities, suggesting that none of these are important ligands in the transport of molybdenite.

Smith (1983) theoretically evaluated the solubility of molybdenite in slightly acidic aqueous solutions at 250°, 300° and 350°C and concluded that molybdenite solubilities range up to several thousand ppm at 350°C, and decrease with decreasing temperature. He suggested that molybdenum is predominantly transported as HMOO₄ or MoO₃F and that chloride and sulphide complexes are not significant.

candela and Holland (1984) also suggest that molybdenum is probably transported as a molybdate species and fluoride and chloride complexes are not important, based on measurements of the partitioning of molybdenum between a hydrothermal fluid and a felsic silicate melt.

Kudrin (1985) studied the solubility of MoO₂ in aqueous solutions at various concentrations at temperatures between 250° and 450°C and pressures between 500 and 1000 bars. He

concluded that molybdenum hydroxy complexes $H_2MoO_4^{\circ}$, $HMoO_4^{\circ}$, and $MoO_4^{\circ 2}$ are the predominant species in hydrothermal solutions of low salinity in the range of 10^{-1} m HCl to 10^{-3} m K (Na)OH between 250°and 450°C, the latter species occurring below 300°C. He used his data to calculate the solubility of molybdenite as a function of temperature, pH and chloride content. He also concluded that MoS_2 solubility falls sharply with temperature.

Wood et al. (1987) studied the solubility of pyrite-pyrrhotite-magnetite-sphalerite-galena-gold-stibnite-bismuthinite-argentite-molybdenite in H₂O-NaCl-CO₂ solutions containing 0 to 5 m NaCl between 200°and 350°C at saturated vapour pressure plus 0.69 to 172 bars excess CO₂ pressures. Their study showed that molybdenite solubility is essentially independent of NaCl concentration below 350°C. They noted that the hard-soft rule of Pearson (1963) is consistent with their results in that the hard Mo⁺⁶ ion binds only with the hard anions OH and O⁻⁶. They concluded that molybdenum is probably transported as an oxyacid.

CaO et al. (1988) investigated the solubility of MoO_3 in NaCl solutions at 300° to 450°C under vapour saturated conditions and a pH between 4 and 5. Their result indicates that there is a strong dependency of MoO_3 solubility on NaCl concentration, at temperatures above 350°C, suggesting the existence of Mo-oxychloro complexes. They also found, however, that, in the presence of S_2 , the concentration of Mo decreases

sharply. They concluded that at 400°C MoO2Cl° and MoO4Cl24 are the dominant species. At lower temperatures, HMoO3° may be important. Subsequently these workers have reappraised their data and found it to be consistent with Na-molybdate ion pairs than chloride complexes (CaO 1989, personal rather communication). It has similarly been demonstrated that, in the case of molybdenum's cogener in the periodic table, tungsten, increases in solubility with NaCl concentrations are more likely due to Na ion pairing than Cl complexing (Wood and Vlassopoular 1989).

Although the conclusions of the various studies summarized above are somewhat disparate with one another, it appears that the bulk of the studies suggest that neither Cl , F, or S complexes are likely to be important for Mo transport. Although there is less evidence for or against carbonate complexation of Mo, it is considered unlikely that carbonate complexing was an important means of Mo transport in the Preissac-Lacorne batholith in spite of the presence of elevated CO, in the fluids. This conclusion is based on the fact that CO_3^{2-} and HCO_3^{-} are very weak ligands which would have difficulty displacing OH and O2 from the Mo6 ion. Also, carbonate complexes are generally more important under near neutral to basic conditions, where the species HCO3 and CO32 occur in greater concentration relative to CO2. The Mobearing solutions at the Cadillac and Preissac molybdenum deposits were at least slightly acidic as indicated by the results of this investigation. Furthermore, based on the studies described above, carbonate complexing is not necessary to effect sufficient Mo transport because significant solubilities can be attained through the oxyacid species (H₂MoO₄, HMoO₄ and MoO₄²⁻). Sodium or potassium ion pairing would slightly increase the solubility of MoS₂ as the oxyacid species at the temperature and pressure of formation of the molybdenum deposits studied here without greatly changing the depositional mechanisms required.

The temperature and pressure at the time of approximately 425°C, and 700 deposition were bars respectively. The presence of the assemblages quartz + Kfeldspar + muscovite in veins suggest that the a_r/a_u ratio of the hydrothermal solution was buffered. A value of 5 was calculated for the corresponding pH using the K concentration obtained from leachate and salinity data at 425°C and 700 bars. Fluid inclusion leachate results show that the mean K/Na ratio = 0.21, Ca/Na = 0.88, and K/Ca = 0.30, suggesting a Naand Ca rich system. The occurrence of pyrite throughout all of the stages of veining, the low iron content of the sphalerite, the existence of barite as a trapped mineral in fluid inclusions and the low XCH, of carbonic inclusions all suggest that the fluids were comparatively oxidizing during the formation of these deposits. Under these conditions the most likely species are HMoO, and/or H2MoO, or ion paired equivalents.

The close association of molybdenite with muscovite (the two minerals are commonly intergrown) in veins containing K-feldspar suggest that the following equations may be written to represent the deposition of molybdenite in the Cadillac and Preissac molybdenum deposits:

 $3KAlSi_3O_8+2H^++2H_2MOO_4+4H_2S_{(aq)}=KAl_2(AlSi_3O_{10})$ (OH) $_2+2K^++6SiO_2+2MoS_2+6H_2O+O_2$

or

 $3KAlSi_3O_8 + 4H^+ + 2HMoO_4^- + 4H_2S_{(aq)} = KAl_2(AlSi_3O_{10}) (OH)_2 + 2K^+ + 6SiO_2 + 2MoS_2 + 6H_2O + O_2$

equations indicate that the deposition molybdenite may have been caused by a decrease in pH or f0, or an increase in aH2S. In addition, most of the studies mentioned above indicate that MoS, solubility is a strong function of temperature. Given the fact that both deposition of MoS2 and the formation of muscovite from K-feldspar are favoured by decreasing temperature, a drop in temperature due to mixing or adiabatic cooling may represent the most likely mechanism of MoS, deposition. A decrease in pH is also a possible depositional mechanism according to the equations above. An increase in acidity could come about as follows. If the Mo was originally transported in a fluid temperatures greater than about 425°C, then most of the H ion in the fluid could be tied up as HCl due to the increased association constant of this species at supercritical temperatures. Upon cooling, HCl will begin to dissociate,

generating acidity which may then both cause the precipitation of MoS₂ and drive the fluid from the K-feldspar field in to the muscovite field. As muscovite and molybdenite begin to form, pH will once again increase but by that time the temperature will have dropped too far for the redissolution of MoS₂ to occur.

Thus, it is likely that both a temperature drop and an increase in acidity contributed to the deposition of molybdenite and its frequent association with muscovite. However, the temperature effect would appear to be dominant, because a temperature drop controls the initial decrease in pH as well.

6.4.1 Solubility of Nickel

Because of the high nickel content of the solution the solubility of nickel in hydrothermal solutions was also of interest. The actual nickel content of the fluids was calculated by combining the leachate data with the bulk salinity determined from ice melting temperatures, and found to be about 200 ppm. Lin and Popp (1984) have measured the solubility and complexing of Ni in the system NiO-H₂O-HCl in the range of 450° to 700°C, and 1 to 2 kb. Their work showed that, over the entire temperature range, the solubility of Ni is relatively low and the NiCl₂° complex is the dominant Ni species in the fluid.

Fahlguist and Popp (1989) studied the solubility of NiO in NaCl solutions. They found that under these conditions NiCl₃ was the dominant species. More importantly they concluded that, of the divalent cations (Ca, Fe, Mg, Mn, Ni), only Mg is less soluble in chloride solutions under supercritical conditions than Ni. This suggests that the high Ni content (200 ppm) relative to Fe and Mn measured in the fluid inclusion leachate analyses is very unusual indeed and that a very Ni-rich source is required. This is consistent with the suggestion that the nearby komatiites, which are known to contain Ni deposits, have interacted with the oreforming fluids.

6.5 Comparison of the Cadillac and Preissac Molybdenum Deposits to Other Molybdenum Deposits

Westra and Keith have subdivided molybdenum deposits into two major classes: 1) Calc-alkaline molybdenum deposits, and 2) Alkali-calcic and alkalic molybdenum deposits. Alkali-calcic and alkalic molybdenum deposits are hosted by metaluminous to peraluminous granitic rocks and have molybdenite grades above 0.3 wt percent. They are enriched in fluorine and tin. The associated fluid inclusions are dominantly aqueous (cf., Climax: Roedder 1971, Henderson: Kamilli 1978). Hypersaline fluid inclusions are common as are vapour-rich aqueous inclusions. However, carbonic inclusions

are conspicuously absent. The homogenization temperatures are high, in many cases exceeding 600°C. Calc-alkaline molybdenum deposits are hosted by peraluminous rocks ranging in composition from quartz-diorite to granite with granodiorite and quartz monzonite being the most common. Molybdenite grades rarely exceed 0.25 percent and they are fluorine poor. Tin is absent. The principal fluid inclusions are aqueous-carbonic with low salinity and homogenization temperatures lower than 400°C and there is no evidence of boiling (e.g., Trout Lake: Linnen and Williams-Jones, in press).

The following features of the Cadillac and Preissac deposits are pertinent to the present discussion:

- 1- The host rock is a peraluminous S-Type leucoadamellite (muscovite+biotite granite).
- 2- The principal fluid inclusions associated with mineralization are aqueous. But, H_2O-CO_2 inclusions are also common. There is no evidence of boiling.
- 3- The grade of molybdenum mineralization is relatively low (in the Cadillac 0.11% Mo and 0.030% Bi, in the Preissac 0.19% Mo and 0.024% Bi).
- 4- There is a close association between K-feldspar alteration and mineralization and molybdenite is commonly intergrown with muscovite.
 - 5- The deposits formed at shallow depth.
- 6- The fluorine content is low (Bourne and Danis, 1986; the average F content of the Lacorne batholith is 3 ppm).

However, fluorite does occur as late stage fracture fillings.

The nature of the host rocks would seem to place the Cadillac and Preissac molybdenum deposits in the Alkali-Calcic-Alkali class. However, most of the features listed above, their low grade, low emplacement temperatures, abundance of CO₂ inclusions, lack of hypersaline or vapourrich aqueous inclusions appear to put them in the calcalkaline class of molybdenum deposits.

6.6 Genetic Model

Based on the results of fluid inclusions, stable isotopes and the petrography of the granitic rocks in the batholith a genetic model may be presented. After the emplacement of a granodiorite magma at depth in Archean time, a late, watersaturated, differentiated two-mica granite was emplaced into the Preissac massif. Solidified roof rocks fractured, either as a result of tectonic forces or due to the volatile pressure exceeding confining pressure or a combination of the two. The shallow emplacement of the magma chamber suggests that these structures may have vented to the surface. A moderate to high salinity and possibly CO2-rich aqueous fluid separated from This crystallizing magma. fluid the evolved through interaction with the carbonatized volcanic country rocks to give Ca, Ni and CO2 enriched fluids. Albitization occurred early in the evolution of the hydrothermal system. Deposition

of molybdenite occurred later and was accompanied by a change from albitization to K-feldspathization. The principal cause of mineralization and K-feldspathization was a drop in temperature and possible CO, effervescence due to pressure release. The association of muscovite and molybdenite suggest that decreasing pH also may have contributed to molybdenite deposition. During the later stages of hydrothermal activity salinity heated meteoric waters mixed with temperature-high salinity fluids that had interacted extensively with volcanic (komatiitic) and sedimentary country rocks.

CHAPTER 7

CONCLUSIONS

The principal conclusions of this study are:

- 1- The Cadillac and Preissac molybdenum deposits are hosted by a two mica granite which intruded into carbonatized komatiitic volcanic country rocks.
- 2- Hydrothermal activity involved four principal fluid types: 1) a high temperature-moderate to high salinity fluid of possible magmatic origin; 2) a high temperature-low salinity fluid; 3) a low temperature-high salinity fluid; and 4) a low and high density CO₂ and CO₂-H₂O fluid with low XCH₄.
- 3- Peak hydrothermal activity occurred at a temperature of about 425°C, and a pressure of about 700 bars.
- 4- The early stages of hydrothermal activity were marked by high temperature fluids that produced albitic alteration.
- 5- Molybdenite mineralization was associated with later lower temperature fluids that were in equilibrium with K-feldspar and/or muscovite and produced K-feldspathization of the host rocks. The latter was accompanied by leaching of SiO₂ which created a porous host for the infiltrating fluids.
- 6- The ore-forming fluids exsolved from crystallizing magmas (as evidenced by micrographic textures), and evolved through interaction with carbonatized volcanic (komatiitic), and sedimentary country rocks which yielded moderately high

Ca/Na ratios, and relatively high Ni in the aqueous fluids.

7- Molybdenum was probably transported as HMoO4 or related species and molybdenite was deposited in response to decreasing temperature, and/or pH.

REFERENCES

- AMBROSE, J.W., 1941, Clericy and La Pause map-area, Quebec: Geol. Surv. Can., Mem. 233, 61 pages.
- BAILEY, E.H., and STEVENS, R.E., 1960, Selective staining of K-feldspar and plagioclase on rock slabs and thinsections: Amer. Mineral., 45, 1020-1025.
- BAKER, B.H., and McBIRNEY, A.R., 1985, Liquid fractionation. Part III. Geochemistry of zoned magmas and the effects of crystal fractionation. Jour. Volcan. Geother. Research, 24, 55-81.
- BARNES, H.L., and EARNST, W.G., 1963, Ideality and ionization in hydrothermal fluids: the system MgO-H₂O-NaOH: Am. J. Sci., 262, 129-150.
- BARTON, P.B., and SKINNER, B.J., 1979, Sulfide mineral stabilities: in Barnes, H.L., Geochemistry of Hydrothermal ore deposits, 2nd ed., 71-136, New York, Wiley Interscience.
- BODNAR, R.J., 1983, A method of calculating fluid inclusion volumes based on vapour bubble diameters and P-V-T-X properties of inclusion fluids: Econ. Geol., 78, 535-542.
- BODNAR, R.J., and BETHKE, P.M., 1980, Systematics of "stretching" of fluid inclusions as a result of overheating (abstr.). EOS, Trans. Am. Geophys. Union, 61, 393.
- BOILY, M., WILLIAMS-JONES, A.E., and PILOTE, P. 1989, Metallogeny and petrology of the Li, Ta, Be bearing pegmatites associated with the monzogranites of the Preissac-Lacorne complex, Abitibi, Canada: Geol. Assoc. Can. Annual Meeting, Montreal 89, in Program with abstract, vol.14 p. A1 (abst.).
- BOTTRELL, S.H., YARDLEY, B. and BUCLEY, F., 1988, A modified crush-leach method for the analysis of fluid inclusion electrolytes: Bull. Mineral., 111, 279-290.
- BOURNE, J., and DANIS, D., 1987, A proposed model for the formation of reversely zoned plutons based on a study of the Lacorne complex, Superior Province, Quebec: Can. Jour. Earth Sci., 24, 2506-2520.
- BOWERS, T.S., and HELGESON, H.C., 1983a, Calculation of thermodynamic and geochemical consequences of nonideal mixing in the system H₂O-CO₂-NaCl on phase relations in geologic systems: Equation of state for H₂O-CO₂-NaCl

- fluids at high pressures and temperatures. Geochim. Cosmochim. Acta, 47, 1247-1275.
- BOWERS, T.S., and HELGESON, H.C., 1983b, Calculation of the thermodynamic and geochemical consequences of nonideal mixing in the system H₂O-CO₂-NaCl on phase relations in geologic systems: metamorphic equilibria of high pressures and temperatures. Amer. Mineral., 68, 1059-1075.
- BOWERS, T.S., JACKSON, K.J., and HELGESON, H.C., 1984, Equilibrium Activity Diagrams for coexisting minerals and aqueous solutions at pressures and temperatures to 5 kb and 600°C. Springer-Verlag, Berlin Heidelberg New York Tokyo
- BOZZO, A.T., CHEN, H.-S., KASS, J.R. and BARDUHN, A.J., 1975, The properties of hydrates of chlorine and carbon dioxide: Desalination, 16, 303-320.
- BURNHAM, C.W., 1979, Magmas and hydrothermal fluids. In: Barnes, H.L., Geochemistry of Hydrothermal Ore Deposits, 2nd ed., 71-136, New York, Wiley Interscience.
- BURRUS, R.C., 1981, Analysis of Phase Equilibria in C-O-H-S Fluid Inclusions: In: Mineral. Assoc. Can, Short Course in Fluid Inclusions: Application to petrology, vol 6, L.S. Hollister and M.L. Crawford eds., 39-74.
- CAMERON, E.N., JAHNS, R.H., McNAIR, A.H., and PAGE, L.R., 1949, Internal structure of granitic pegmatite: Econ. Geol. Mon.2.
- CANDELA, P.A., and HOLLAND, H.D., 1984, The partitioning of copper and molybdenum between silicate melts and aqueous fluids: Geochim. Cosmochim. Acta, v. 48, p. 373-380.
- CAO, X., RICHARDSON, S.M., and RICHARDSON, C.K., 1988, Dissolution and speciation of MoO₃ in NaCl solutions at elevated temperatures and pressures: EOS vol. 69, No. 16, p.528.
- CARD, K.D., 1982, Progress report on regional geological synthesis, central Superior Province. In Current Research, Part A,: Geol. Surv. Can., paper 82-1A, 23-28.
- CLAYTON, R.N., O'NEIL, J.R. and MAYEDA, T.K., 1972, Oxygen isotope exchange between quartz and water: Journal of Geophysical Research, 77, 3057-3067.
- COLLINS, P.L.F., 1979, Gas hydrates in CO₂-bearing fluid inclusions and the use of freezing data for estimation

- of salinity: Econ. Geol., 74, 1435-1444.
- CRERAR, D.A., 1975, A method for computing multi-component chemical equilibria based on equilibrium constants. Geochim. Cosmochim. Acta 39, 1375-1384.
- CRAWFORD, M.L., 1981, Phase in aqueous fluid inclusions: In: Mineral. Assoc. Can. Short Course in Fluid Inclusions: Application to Petrology, vol. 6, L.S. Hollister and M.L. Crawford eds., 75-100.
- DANIS, D., 1985, Pétrologie et géochimie du batholite de Lacorne, Québec: Mémoire de M.Sci. Université du Québec à Montreal, 199 pages.
- DAWSON, K.R., 1966, A comprehensive study of the Preissac-Lacorne batholith, Abitibi county, Quebec: Geol. Surv. Can: Bull. 142, 76 pages.
- DIMROTH, E., IMREH, L., ROCHELEAU, M., and GOULET, N., 1982, Evolution of the south-central part of the Archean Abitibi belt, Quebec. Part I: Stratigraphy and paleogeographic model: Can. Jour. Earth Sci., 19, 1729-1758.
- DIMROTH, E., IMREH, L., GOULET, N., and ROCHELEAU, M., 1983a, Evolution of the south-central segment of the Archean Abitibi belt, Quebec. Part II: Tectonic evolution and geomechanical model: Can. Jour. Earth Sci., 20, 1355-1373.
- DIMROTH, E., IMREH, L., GOULET, N. and ROCHELEAU, M., 1983b, Evolution of the south-central segment of the Archean Abitibi belt, Quebec. Part III. Plutonic and metamorphic evolution and geotectonic model: Can. Jour. Earth Sci., 20, 1374-1388.
- FRAPE, S.K., FRITZ, P., and McNUTTR.H., 1984, Water-rock interaction and chemistry of groundwaters from the Canadian Shield: Geochimica et Cosmochimica Acta, v. 48, p. 1617-1627.
- FAHLQUIST, L.S., and POpp, R.K., 1989, The effect of NaCl on bunsenite solubility and Ni-complexing in supercritical aqueous fluids: Geochim. et Cosmochim. Acta, v. 53, p. 389-995.
- GARIEPY, C., and ALLEGRE, C.J., 1985, The lead isotope geochemistry and geochronology of late-kinematic intrusives from the Abitibi greenstone belt, and the implications for late Archean crustal evolution: Geochimica et Cosmochimica Acta, 49, 2371-2383.

- GOODWIN, A.M., and RIDLER, R.H., 1970, The Abitibi orogenic belt: Geol. Surv. Can. Paper 70, 40 pages.
- HAAS, J.L., 1971, The effect of salinity on the maximum thermal gradient of a hydrothermal system at hydrostatic pressure: Econ. Geol., 66, 940-946.
- HAAS, J.L., 1976, Thermodynamic properties of the coexisting phases and thermochemical properties of the NaCl component in boiling NaCl solutions: U.S. Geol. Surv. Bull. 1421-B, 71 pages.
- HELGESON, H.C., 1969, Thermodynamics of hydrothermal systems at elevated temperatures and pressures: American Journal of Science, v. 267, p. 729-804.
- ISUK, E.E., 1981, The system Na₂Si₂O₅-K₂Si₂O₅-MoS₂-H₂O with implications for molybdenum transport in silicate melts: Econ. Geol., v. 76, p. 2222-2235.
- ISUK, E.E., 1982, Behaviour of molybdenum in alkali silicate melts: effects of excess SiO₂ and CO₂: Lithos, 16, 17-22.
- JAHNS, R.H., and BURNHAM, C.W., 1969, Experimental studies of pegmatite genesis: I. A model for derivation and crystallization of granitic pegmatite: Econ. Geol., 64, 843-864.
- KAMILLI, R.J., 1978, The genesis of stockwork molybdenite deposits: implications from fluid inclusion studies at the Henderson mine. Geol. Soc. Am. Abstr. Programs, 10, 431, 276-277.
- KAY, A., and STRONG, D.F., 1983, Geologic and fluid controls on As-Sb-Au mineralization in the Moretons Harbour in Newfoundland: Econ. Geol., 78, 1590-1604.
- KERRICH, R. and JACOBS, G.K., 1981, A modified Redlich-Kwong equation for H₂O, CO₂, and H₂O-CO₂ mixtures at elevated pressures and temperatures. Am. J. Sci., 281, 735-767.
- KHITAROV, N.I., ARUTYUNYAN, L.A., and RYZHENKO, B.N., 1965, The effect of hydrogen sulphide on the migration of molybdenum in the form of a silicomolybdate complex under elevated temperatures: Geochem. Internat. v. 2, p. 192-195.
- KHITAROV, N.I., MALININ, S.P., LEBEDEV, YE.B., and SHIBAYEVA, N.P., 1982, The distribution of Zn, Cu, Pb, and Mo between a fluid phase and a silicate melt of granitic

- composition at high temperatures and pressures: Geochem. Internat. v. 19, p. 123-136.
- KILINC, I.A., and BURNHAM, C.W., 1972, Portioning of chloride between a silicate melt and coexisting aqueous phase from 2 to 8 kilobars: Econ Geol., 67, 231-235.
- KUDRIN, A.V., 1985, The solubility of tugarinovite MoO₂ in aqueous solutions at elevated temperatures: Geochem. Internat. v. 23, p. 126-138.
- LAGACHE, M. and WEISBROD, A., 1977, The system two alkali feldspar- KCl-NaCl-H₂O at moderate to high temperatures and low pressures: Contr. Mineral. Petrol. 62, 77-101.
- LATULIPPE, M., 1953, Map showing the geology of the northwestern quarter of Lacorne Township, Quebec: Quebec Bur. Mines.
- LEDUC, M., 1980, Géologie et lithogéochimie des masses batholitiques de la région de Preissac: Ministère de l'Energie et des Ressources du Québec, DPV-779.
- LIN, S. and POPP, R.K., 1984, Solubility and complexing of Ni in the system NiO-H2O-HCl: Geochimica et Cosmochimica Acta, v. 48, p. 2713-2722.
- LINNEN, R.L., and WILLIAMS-JONES, A.E., 1989, Aqueous-carbonic fluid evolution at the Trout Lake deposit, British Colombia: The role of cooling as a control of mineralization for molybdenum deposits: Econ. Geol., 84, (in press).
- LOWRY, H.H., and ERICKSON, W.R., 1927, The densities of coexisting liquid and gaseous carbon dioxide and the solubility of water in liquid carbon dioxide: Amer. Chem. Soc. Jour., 49, 2729-2734.
- LUDDEN, J., and HUBERT, C., 1986, Geological evolution of the late Archean Abitibi greenstone belt of Canada: Geology, 14, 707-711.
- MacDONALD, A.J., and SPOONER, E.T.C., 1982, Carbonate complexing of molybdenum in hydrothermal solutions: Evidence from Boss Mountain, British Colombia (abst.): Geol. Soc. Amer., Abstract with programs, v. 14, p 552.
- MURPHY, J.B., and HYNES, A.J., 1986, Contrasting secondary mobility of Ti, P, Zr, Nb, and Y in two metabasaltic suites in the Appalachians: Can J. Earth Sci. v. 23, p. 1138-1144.

- O'NEIL, J.R., and TAYLOR, H.P., 1969, Oxygen isotope equilibrium between muscovite and water: Journal of Geophysical Research, 74, 6012-6022.
- ORVILLE, P.M., 1962, Alkali-metasomatism and feldspars: Norsk. Geol. Tidsskr., 42, 283-316.
- POTTER, R.W., and BROWN, D.L., 1975, The volumetric properties of aqueous sodium chloride solutions from 0° to 500°C at pressures up to 2000 bars based on a regression of the available literature data U.S. Geol. Survey open file rept., No. 75-636, 31 p.(234-263)
- POTTER, R.W., BABCOCK, R.S., and BROWN, D.L., 1977, A method for determining the solubility of salts in aqueous solutions at elevated temperatures: Jour. Research U.S. Geol. Surv., vol. 5, No. 3, p. 389-395.
- POTTER, R.W., CLYNNE, M.A., and BROWN, D.L., 1978, Freezing point depression of aqueous sodium chloride solutions: Econ. Geol., 73, 284-285.
- ROEDDER, E., 1971, Fluid inclusions studies on the porphyrytype ore deposits at Bingham, Utah, Butte, Montana, and Climax, Colorado. Econ. Geol.., 66, 98-120.
- ROEDDER, E., 1972, Composition of fluid inclusions. U.S. Geol. Surv. Prof. Paper 440-jj, 164 pages.
- ROEDDER, E., 1979, Fluid inclusions as samples of ore fluids: In Geochemistry of Hydrothermal Ore Deposits, H.L. Barnes ed., p.684-737.
- ROEDDER, E., 1984, Fluid inclusions. Mineral. Soc. Amer., Review in Mineralogy, vol. 12, 644 pages.
- ROSE, A.V., and BURT, D.M., 1969,, Hydrothermal alteration: In Geochemistry of Hydrothermal Ore Deposits, H.L. Barnes, ed.,p. 173-227.
- ROWE, R.B., 1953, Pegmatitic beryllium and lithium deposits, Preissac-Lacorne region, Abitibi County, Quebec: Geol. Surv. Can., paper 53-3.
- SIROONIAN, H.A., 1958, Distribution of lithium in granitic rocks of the Preissac-Lacorne area, Quebec, University McMaster, M. Sc. thesis (unpubl.).
- SMITH, R.W., 1983, Aqueous chemistry of molybdenum at elevated temperatures and pressures with applications to porphyry molybdenum deposits: New Mexico Institute of Mining and

- Technology, Socorro, New Mexico, Ph.D. thesis, 311 pages.
- SOURIRAJAN, S., and KENNEDY, G.C., 1962, The system H₂O-NaCl at elevated temperatures and pressures: Amer. Jour. Sci,. 260, 115-141.
- SWANENBERG, H.E.C., 1979, Phase equilibria in carbonic systems, and their application to freezing studies of fluid inclusions: Contrib. Mineral. Petrol. 68, 303-306.
- THOMPSON, T.B., 1982, Classification and genesis of stockwork molybdenum deposits- a discussion. Econ. Geol., 77, 709-714.
- TINGLE, T.N., DAVIS, CA., AND FENN, P.M., 1982, The concentration and transport of molybdenum in magmatic systems, experimental evidence: Geol. Soc. Amer. Abstracts with programs, v. 14, p. 240.
- TREMBLAY, L.P., 1950, Fiedmont map-area, Abitibi County, Quebec: Geol. Sur. Can., Mem., 253.
- TRUDEL, P., 1980, Métallogénie et prospection du molybdenite au Québec: Ministère de l'Energie et des Ressources du Quebec, DPV-733.
- URUSOVA, M.A., 1975, Volume properties of aqueous solutions of sodium chloride at elevated temperatures and pressures. Zh. Neorg. Khim., 20, 3103-3110 (in Russian; translated in Russian J. Inorg. Chem., 20, (11), 1717-1721).
- WEISBROD, A., 1981, Fluid inclusions in shallow intrusives: In Mineral Assoc. Can. Short Course in Fluid Inclusions:: Application to Petrology, vol. 6, L.S. Hollister and M.L. Crawford eds., p 241-271.
- WESTRA, G., and KEITH, S.B., 1981, Classification and genesis of stockwork molybdenum deposits: Econ. Geol., 76, 844-873.
- WHITNEY, J.A., 1975, Vapour generation in a quartz monzonite magma: a synthetic model with application to porphyry copper deposits. Econ. Geol., 70, 346-358.
- WILLIAMS-JONES, A.E., 1982, Patapedia: an Appalachian calcsilicate hosted copper prospect of porphyry affinity: Can. Jour. Earth Sci., 19, 438-455.
- WILLIAMS-JONES, A.E., and LINNEN, R.L., 1987, A short course on the application of fluid inclusion techniques to the study of hydrothermal ore deposits: IREM/MERI publ.,

Montreal, Canada.

- WOOD, S.A., CRERAR, D.A., and BORCSIK, M.P., 1987, Solubility of the assemblage pyrite-pyrrhotite-magnetite-sphalerite-galena-gold-stibnite-bismuthinite-argentite-molybdenite in H2O-NaCl-CO2 solutions from 200° to 350° C: Econ. Geol., v. 82, p. 1864-1887
- WOOD, S.A., and VLASSOPOULOS DIMITRIOS, 1989, Experimental determination of the hydrothermal solubility and speciation of tungsten at 500°C and 1 kbar: Geochim. Cosmochim. Acta v.53, p. 303-312
- ZHANG, Y.G, and FRANTZ, J.D., 1989, Experimental determination of the compositional limits of immiscibility in the system CaCl₂-H₂O-CO₂ at high temperatures and pressures using synthetic fluid inclusions: Chemical Geology, 74, 289-308.

APPENDIX I Table 1

COMPOSITIONS OF FELDSPARS FROM THE CADILLAC MOLYBDENUM DEPOSIT

Sample no LC-11-2 (host rock from non mineralized vein)

CaŌ Na ₂ O	19.92 0.44 11.65 0.06 99.35	2 66.62 20.53 0.75 11.41 0.75 99.40	20.52 1.53 10.65 0.07 98.55	66.02 20.60 1.65 10.70 0.11 99.08	1 64.42 21.44 2.54 10.40 0.10 98.89	2 64.97 21.72 2.73 10.26 0.13 99.80	63.92 18.24
. .					asis of		
Si Al Ca Na K	1.034 0.021 0.995	2.936 1.066 0.035 0.975 0.006	1.076 0.073 0.919	1.075 0.078 0.918	2.868 1.125 0.121 0.898 0.005	1.129 0.129 0.878	1.002 0.001 0.081
		М	ol perc	ents			
AB AN OR	97.61 2.04 0.35	95.96 3.47 0.57	92.30 7.32 0.38	91.59 7.79 0.62	11.84	12.73	7.63 0.12 92.26
Sample			lteration		unaltere		rock) igoclase
SiO ₂ Al ₂ O ₃ CaO Na ₂ O K ₂ O	0.94 11.20	2 67.55 19.59 0.51 10.65 0.05	68.1 19.3 0.4	82 1 67 41	0.01 0.29	21.54 2.79 10.01	64.92 21.62 2.70
Total	98.42	98.35	100.	25 9	9.87	100.03	99.54
		Number	of ions	on the	basis o	of 8(0)	
Al 1.0 Ca 0.0 Na 0.9	0.02	21 24 13	2.977 1.018 0.031 0.964 0.002	2.994 0.993 0.026 1.007	1.1 0.1 0.8	.15 .31 .32	2.870 1.126 0.128 0.873 0.007

Table 1 (continued)

Mol percent

AB	94.97	97.11	96.63	2.51	86.04
AN	4.41	2.59	3.13	0.06	13.25
OR	0.63	0.30	0.23	97.43	0.71

Sample no LC-11-29 (K-feldspar alteration)

	Albite	Ortho	clase
	1	1	2
SiO ₂	68.24	64.84	64.89
$A1_2\bar{O_3}$	19.92	18.39	18.16
CaŌ	0.42		
Na ₂ 0	11.17	0.39	0.45
K ₂ Õ Total	0.30	16.87	16.89
Total	100.05	100.49	100.39

Number of ions on the basis of 8(0)

Si	2.978	2.989	2.998
Al	1.025	0.999	0.998
Ca	1.98		
Na	0.945	0.034	0.040
K	0.016	0.992	0.994

Mol percent

AB	96.27	3.36	3.92
AN	2.02	0.01	
OR	1.71	96.64	96.08

COMPOSITIONS OF MUSCOVITES IN VEINS FROM THE CADILLAC

Table 2

	LC-	11-1	LC-11-	31	L	C-10-6			
	(1	non mine	eralized)		(min	eralized))		
	1	2	1		1	2		3	
sio,	50.19	48.12	49.16	46	04	46.80		46.41	
TiO_2	1.02	0.85	0.70	0	.71	0.54		0.70	
Al_2O_3	30.71	29.81	31.23 5.31	30	.21	29.30		29.86	
Feo	5.59	5.71	5.31	5	. 24	5.14		5.67	
MnO	0.12	0.14	0.10		. 18			0.17	
		1.52	1.55	1	. 45	1.38		1.17	
CaO	0.01	0.07	0.02	0	. 02	0.01			
SnO ₂	0.03		0.01			0.01			
Na ₂ O	0.19	0.31	0.32	0	. 22	0.24		0.27	
K ₂ O	5.76	7.05 1.13	6.66	11.	. 12	11.14		11.05	
		1.13	0.03	0	. 45	0.19		0.19	
	0.01					0.02		0.01	
H ₂ O	4.55	4.42	4.52	4.	. 37	4.36		4.38	
			99.61					99.89	
			0.01	0 .	. 19	0.09		0.08	
Tot	99.95	98.65	99.59	99.	.81	99.23		99.81	
			Number of	ions on	the	basis of	22	(0)	
Si ^{iv}	6.606	6.525	6.515	6.304		6.430	6.3	354	

Si ^{iv}	6.606	6.525	6.515	6.304	6.430	6.354
Al.	1.394	1.475	1.485	1.696	1.57	1.646
	8.000	8.000	8.000	8.000	8.000	8.000
Al ^{vi}	3.370	3.288	3.392	3.179	3.174	3.173
Ti	0.101	0.086	0.069	0.073	0.056	0.071
Fe	0.615	0.648	0.588	0.600	0.591	0.650
Mn	0.014	0.016	0.011	0.021	0.022	0.020
Mg	0.296	0.307	0.306	0.295	0.281	0.239
Sn	0.001					
	4.397	4.345	4.366	4.168	4.124	4.153
. vii						
Na ^{xii}	0.049	0.080	0.082	0.058	0.064	0.073
K	0.967	1.219	1.126	1.941	1.953	1.929
	1.016	1.299	1.208	1.999	2.017	2.002
F	0.170	0.485	0.013	0.194	0.083	0.083
Cl	0.003				0.005	0.003
XMg ⁽²⁾	0.32	0.31	0 24	0 22	0 21	0 26
MIG	0.32	0.31	0.34	0.32	0.31	0.26

^{(1):} Fe tot. expressed as FeO
(2): XMg = Mg/(Mg+Fe+Mn)

MOLYBDENUM DEPOSIT

Table 3

COMPOSITION OF RUTILE

LC-11-5

Numbers of ions on the basis of 2 (0)

	1		1
TiO,	99.65	Ti	0.998
SnO ₂	0.03	Sn	0.0004
Al_2O_3	0.09	Al	0.0003
FeÖ	0.014	Fe ⁺²	0.0002
ZnO	0.07	Zn ⁺²	0.0007
Na ₂ O	0.02	Na	0.0001
Total	100.01		0.9997

COMPOSITIONS OF ORE MINERALS

LC-11-9

			Bis	muthinite		
	1		2		3	
		Atom. C		Atom. C		Atom. C
Bi	81.64	0.4033	82.37	0.4218	82.28	0.4105
S	18.29	0.5890	17.19	0.5738	17.89	0.5819
Cu	0.28	0.0046	0.14	0.0023	0.24	0.0039
Nb	0.04	0.0005			0.03	0.0004
Pb	0.22	0.0011			0.26	0.0013
Mo	0.14	0.0015	0.14	0.0016	0.12	0.0013
Tot	100.61		99.84		100.82	
Comp	osition:	Bi ₂ S ₃		Bi ₂ S3		Bi_2S_3
Pyrr	hotite					
_		Atom. C				
Fe	46.65	0.3392				
S	51.87	0.6571				
Ag	0.10	0.0004				
Bi	0.22	0.0004				
Mo	0.57	0.0024				
As	0.04	0.0002				
Co	0.01	0.0001				
Tot	99.46					
Comp	osition:	Fe ₄ S ₃				

Table 3 (continued)

LC-10-3

	Chalcopyrite			Sph	Sphalerite			Gladite	
		Atom. C			Atom. C			Atom. C	
Fe	30.06	0.2493	Zn	58.98	0.4665	Вi	66.12	0.3050	
Cu	34.15	0.2488	Fe	0.99	0.0092	Cu	4.81	0.0730	
S	34.53	0.4986	Cu	0.69	0.0057	Pb	12.80	0.0596	
Zn	0.13	0.0009	S	31.97	0.5156	Fe	0.62	0.0108	
Ag	0.02	0.0001	Bi	0.12	0.0003	Zn	1.67	0.0246	
Βi	0.08	0.0002	Mo	0.46	0.0025	Mo	0.16	0.0016	
Mo	0.42	0.0020	Ag	0.03	0.0001	S	17.48	0.5255	
Tot	99.39			93.12			103.66		
Com	pos.:	FeCuS ₂			ZnS		Bi _{5.2} Cu _{1.}	3PbFe _{0.2} S ₉	

	Molybo	lenite	Bi	smuthinite		Native Bismuth
			1	2		
		Atom.C		Atom.C	Atom.C	Atom.C
Mo	56.88	0.3378	Bi 81.91	0.4002 80.75	0.4029	100.19
S	36.57	0.6499	S 18.40	0.5861 17.90	0.5822	0.01
Bi	3.28	0.0089	Cu 0.44	0.0071 0.45	0.0075	
Аg	0.49	0.0026	Pb 0.89	0.0044 0.93	0.0047	
			Mo 0.17	0.0019 0.25	0.0028	
Tot	97.22		101.81	100.28		100.20
Comp	osition	: MoS ₂	Bi_2S_3	Bi_2S_3		Bi

Mineral X						
		Atom. C				
Bi	42.93	0.1340				
Fe	34.84	0.4070				
S	22.45	0.4569				
Pb	0.12	J.0004				
Mo	0.18	0.0012				
Ag	0.02	0.0001				
Zn	0.01	0.0002				
Cu	0.01	0.0002				

Tot 100.56

Composition: Fe_{4.4}Bi_{1.4}S₅

APPENDIX II

Table 1

FLUID INCLUSIONS LEACHATE ANALYSES (with DDW)

Concentration(ppm)							Atomic ratios		ios			
Samp	ole Na LO	K	Ca	Mg	Fe	Ni	Мо	Li	Cl-	K/Na	Ca/Na	K/Ca
3	1.31	0.48	0.18	0.011	0.122	0.094	0.003	0.01	4.0	0.36	0.08	2.2
6	4.18	0.50	0.82	0.010	0.283	0.014	0.049	0.07	12.6	0.12	0.11	0.6
4	0.56	0.30	0.14	0.009	0.124	0.009	0.012	0.00	3.8	0.53	0.14	2.2
16	0.73	0.16	0.23	0.011	0.138	0.019	0.008	0.00	3.5	0.22	0.18	6.2
14	2.71	0.63	0.30	0.013	0.034	0.003	0.050	0.037	6.5	0.23	0.06	2.1
Blk	0.05	0.04	<0.05	<0.004	0.127	<0.005	<0.025	<0.002	1.3			
LC-1	11											
9	4.64	0.59	0.21	0.016	0.022	0.012	0.016	0.01		0.12	0.02	2.9
4	2.99	0.55	0.34	0.013	0.057	0.011	0.009	0.011		0.18	0.06	1.6
5	2.69	0.61	0.35	0.014	0.125	0.017	0.006	0.008	7.0	0.22	0.07	1.8
26	5.22	0.90	2.02	0.019	0.171	0.029	0.005	0.035	15.8	0.17	0.22	0.4
29	4.07	0.68	0.58	0.014	0.028	0.001	0.005	0.025		0.16	0.08	1.2
Blk		<0.04			<0.001	0.036	<0.025		1.4			
7	3.26	0.45	0.56	0.014	0.031	0.003	0.195	0.022	8.7	0.13	0.09	0.8
30	2.26	0.53	0.30	0.021	0.021	0.005	0.006	0.007	6.0	0.23	0.07	1.8
18	5.60	0.63	0.65	0.013	0.033	0.005	0.008	0.027		0.11	0.06	1.0
22	1.02	0.22	0.10	0.005	0.171	0.070	0.001	0.001	3.4	0.21	0.05	2.2
19	1.40	0.23	0.11	0.004	0.045	0.072	0.091	0.006	4.0	0.16	0.04	2.1
6	3.32	0.94	0.16	<0.004	0.066	<0.005	<0.025	<0.002		0.28	0.04	5.8
	ole of	2g.										
LC-												
4	0.59	0.18		<0.004				0.002	2.6	0.30	0.10	1.7
5	0.45	0.12	0.10	<0.004	:			0.043	2.0	0.26	0.12	1.2
26	0.92	0.22	0.18	0.004				0.018	4.2	0.23	0.11	1.2
29	0.69	0.13		<0.004	0.007			0.00	2.8	0.18	0.11	1.0
Blk	0.03	<0.04	<0.05	<0.004	0.154			0.00	1.3			
									X	=0.21	0.08	1.97

1 3

APPENDIX II
Table 2a (calcium corrected)

FLUID INCLUSIONS LEACHATE ANALYSES

Concentrations(ppm)								Atomic ratios				
	ole Na	a K	Ca	Mg	Fe	Ni	Mo	Li	Cl-	K/Na	Ca/Na	K/Ca
LC-												
3	1.31	0.48	0.9	0.011	0.122	0.094	0.003	0.01	4.0	0.36	0.68	0.53
6	4.18	0.50	2.86	0.010	0.283	0.014	0.049	0.07	12.6	0.12	0.68	0.17
4	0.56	0.30	1.56	0.009	0.124	0.009	0.012	0.00	3.8	0.53	2.78	0.19
16	0.73	0.16	1.29	0.011	0.138	0.019	0.008	0.00	3.5	0.22	1.76	0.12
14	2.71	0.63	1.02	0.013	0.034	0.003	0.050	0.037	6.5	0.23	0.37	0.61
Blk	0.05	0.04	<0.05	<0.004	0.127	<0.005	<0.025	<0.002	1.3			
LC-	11											
9	4.64	0.59	0.21	0.016	0.022	0.012	0.016	0.01		0.12	0.02	2.9
4	2.99	0.55	0.34	0.013	0.057	0.011	0.009	0.011		0.18	0.06	1.6
5	2.69	0.61	1.33	0.014	0.125	0.017	0.006	0.008	7.0	0.22	0.49	0.46
26	5.22	0.90	3.9	0.019	0.171	0.029	0.005	0.035	15.8	0.17	0.74	0.23
29	4.07	0.68	4.3	0.014	0.028	0.001	0.005	0.025	14.5	0.16	1.05	0.15
Blk	0.06	<0.04	<0.05	<0.004	<0.001	0.036	<0.025	<0.002	1.4			
7	3.26	0.45	1.9	0.014	0.031	0.003	0.195	0.022	8.7	0.13	0.58	0.23
30	2.26	0.53	1.18	0.021	0.021	0.005	0.006	0.007	6.0	0.23	0.52	0.45
18	5.60	0.63	1.59	0.013	0.033	0.005	0.008	0.027	12.0	0.11	0.28	0.39
22	1.02	0.22	0.94	0.005	0.171	0.070	0.001	0.001	3.4	0.21	1.92	0.23
19	1.40	0.23	0.97	0.004	0.045	0.072	0.091	0.006	4.0	0.16	0.69	0.23
6	3.32	0.94	0.16	<0.004	0.066	<0.005	<0.025	<0.002				
Samı	ole of	£ 2q.							2	x=0.21	0.88	0.30
LC-11												
4	0.59	0.18	0.91	<0.004				0.002	2.6	0.30	1.54	0.2
5	0.45	0.12	0.7	<0.004				0.043	2.0	0.26	1.55	0.17
26	0.92	0.22	1.48	0.004				0.018	4.2	0.23	1.60	0.15
29	0.69	0.13	0.92		0.007			0.00	2.8	0.18	1.33	0.14
Blk		<0.04		<0.004	0.154			0.00	1.3			
DIR	J. UJ							-	_			

Table 2b

LEACHATE USING 0.13MHNO $_3$ +200 μ m/ml La

Concentrations (ppm)					Aton	Atomic ratios				
	Na	K	Ca	Mg	K/Na		K/Ca			
Blk	<0.016	<0.022	<0.01	<0.005	Ly IIu	cu) na	10,00			
LC-11										
5	2.80	0.44	1.33	0.163	0.15	0.48	0.33			
29	5.48	0.72	4.11	0.059	0.14	0.75	0.17			
7	3.83	0.44	2.71	0.042	0.14		0.16			
Sample	of 2g.				3123	31.0	0.20			
4	1.0	0.24	0.55	0.012	0.24	0.55	0.43			
26	2.47	0.42	3.46	0.009	0.17	1.4	0.12			

In Appendix II (Blk) represent blank samples.

APPENDIX III

Sample No: LC-11-5

 $3KALSi_3O_8 + 2H^+ = KAl_2(AlSi_3O_1O)(OH)_2 + 2K^+ + 6SiO_2$

 $K=(K^{\dagger})/(H^{\dagger})$, at 425°C, and 700 bars logK=3.72

 $logK=2log(a_{K}^{+}/a_{H}^{+}), log(a_{K}^{+}/a_{H}^{+})=3.72$

 $\log(a_{\kappa}^{+} - a_{\mu}^{+}) = 3.72$

 $pH=3.72-loga_{r}^{+}$

Salinity wt% NaCl, X=-11.31=3.1 molal, standard deviation=9.12

 $X_1 = -2.194 = 0.658 \text{ molal}$

 $X_2 = -20.43 = 5.1 \text{ molal}$

 m_{cl} = Freezing data x leachate result=3.1x0.000197

 $m_{cl} = 0.0006107$

 $m_{r}^{+} = X_{r}^{+}x3.1, m_{r}^{+}=0.231$

-log $_{K}^{+}=(A_{ZK}^{+2}I^{1/4}/1+a^{\circ}_{K}^{+}BI^{1/4})+bI$

 $I=1/2\Sigma m_i Z_i^2$, I=0.5(0.0006107+0.231), I=0.1153

A=2.05, B=0.42 at 425°C, 700 bars, $a_{K}^{+}=3.0$

κ⁺=0.248

 $a_{K}^{+} = {}_{K}^{+}xm_{K}^{+} = (0.248)(0.231), a_{K}^{+} = 0.057$

pH=3.72-(-1.24), PH=4.96

First guesses

HCl°=H*+Cl' LOGK=-2.85, PH=LOGCl - LOGK - LOGHCl°

 $\Sigma HCl = \Sigma CL - \Sigma Cations = (0.000197 - 0.000148/0.000197) \times 3.1$

 Σ HCl=0.771

 $HCl^{=\Sigma}HCl^{-}(KxHCl^{\circ})^{\frac{1}{2}}, HCl^{=0.738}$

pH=0.49+2.85+0.131

pH=3.47

 $H^{+}=3.38\times10^{-4}$

To get the concentration of each element, the leachate result of each cation divided by the leachate result of Cl and multiplied by the salinity, obtained from the freezing measurements of the inclusions.

Example:

 $X_{Na}^{+}=0.000117/0.000197=0.59$, $m_{Na}^{+}=3.1x0.59$

 $m_{Na}^{+}=1.84$

NaCl, KCl, CaCl, CaCl, MgCl concentrations were calculated using mass action equations.

Example:

 $NaCl=Na^{+} + Cl^{-}, logK=-2.08$

x=NaCl

Na=1.84-x

Cl=3.1-x

NaCl=1.82

So, the obtained H value is:

For 3.1 molal salinity=1.465x10⁻² mean value

So, using these H value the cations and chlorite can not be balanced.

APPENDIX IV

Calculation of the bulk composition and bulk densities of inclusions

Since the pressure and temperature conditions in a fluid inclusion related to its density, it is important to determine the density of an inclusion to obtain the true formation temperature and pressure. The determination of bulk density is based on the measurement of the volumes of all phases and their individual densities.

The volume of aqueous inclusions was calculated using the following equation given by Bodnar (1983).

$$V_1 = V_2^{\dagger 1} (d_2^{\dagger 1} - d_1^{\dagger 1}) / (D_1 - d_1^{\dagger 1})$$

where V_1 =volume of the inclusion, V_2 =the volume of the vapour phase within the inclusion, D_1 is the density of the homogenous fluid inclusion contents, d_2 represents the density of the vapour phase and d_1 represents the density of the aqueous salt solution and T1 represents room temperature, respectively. The vapour bubble volume at room temperature was obtained using the following equation:

$$V_2 = 4/3\pi x r^3$$

where r is the estimated radius of the bubble. The volumes of the non-aqueous carbonic inclusions were determined in the same way. The volume of carbonic inclusions was calculated as follows: Each inclusion was drawn on paper as it appears at room temperature using a camera lucida projection tube. The inclusions are irregular in shape and thus, the volume of the whole inclusion was determined by measuring the area of the drawn inclusion with a transparent millimetre grid, multiplying this result by an estimate of the third dimension from the diameter of the CO₂ phase, and subtracting the volume of the spherical CO₂ phase.

Sample Calculation

The mole fraction of CO_2 was calculated using the densities of the CO_2 phase at the homogenization temperatures (Lowry and Erickson 1927) by the following equations:

 $nco_2 = (dco_2/44) \times vol.$ percent CO_2 $nco_2 = (1/18) \times vol.$ percent H_2O $Xco_2 = nco_2/(nco_2 + nH_2O)$

The mole fraction of CH_4 was calculated using the method of Burruss (1981), and ranges from 0.008 to 0.02 with a peak 0.007 (this method is based on the final melting temperature of carbonic phase and homogenization temperature).

If the relative volume of the aqueous and carbonic phases are known at room temperature (section 8.3) and if the salinities are known from freezing data the density of the original fluid can be estimated.

The density of the ${\rm H_2O}$ phase was calculated from the clathrate melting temperature, using the equation given by Potter (1978).

The determination of bulk density is based on the measurement of the volumes of all phases and their individual densities. Each inclusion was drawn on a paper using a camera lucida projection tube at room temperature. The inclusions are irregular in shape and thus, the volume of the H₂O phase was determined by measuring the area of the drawn inclusion with a transparent millimetre grid, multiplying this result by an estimate of the third dimension from the diameter of the CO₂ phase, and subtracting the volume of the CO₂ phase. Thus, the bulk composition was calculated using the following equation:

Dbulk=(vol. percent $H_2O \times dH_2O$)+(vol. percent $CO_2 \times dCO_2$ (at the homogenization temperature).